



UvA-DARE (Digital Academic Repository)

Non-contact spectroscopic age determination of bloodstains

Bremmer, R.H.

Publication date

2011

Document Version

Final published version

[Link to publication](#)

Citation for published version (APA):

Bremmer, R. H. (2011). *Non-contact spectroscopic age determination of bloodstains*. [Thesis, fully internal, Universiteit van Amsterdam].

General rights

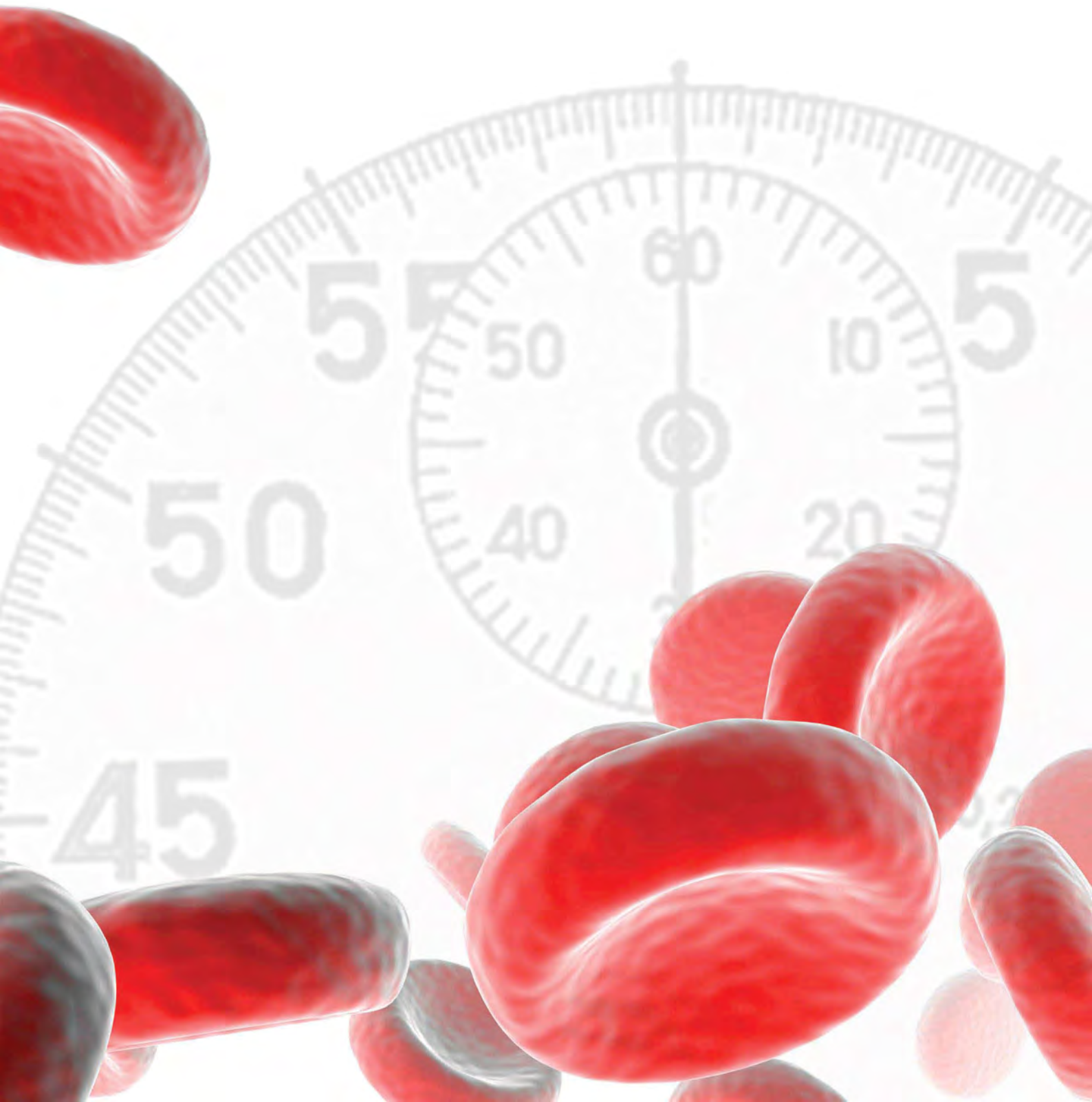
It is not permitted to download or to forward/distribute the text or part of it without the consent of the author(s) and/or copyright holder(s), other than for strictly personal, individual use, unless the work is under an open content license (like Creative Commons).

Disclaimer/Complaints regulations

If you believe that digital publication of certain material infringes any of your rights or (privacy) interests, please let the Library know, stating your reasons. In case of a legitimate complaint, the Library will make the material inaccessible and/or remove it from the website. Please Ask the Library: <https://uba.uva.nl/en/contact>, or a letter to: Library of the University of Amsterdam, Secretariat, P.O. Box 19185, 1000 GD Amsterdam, The Netherlands. You will be contacted as soon as possible.

Non-contact spectroscopic age determination of bloodstains

Rolf Bremmer



NON-CONTACT SPECTROSCOPIC AGE DETERMINATION OF BLOODSTAINS

Non-contact spectroscopic age determination of bloodstains
PhD Thesis, University of Amsterdam, The Netherlands

Publication of this thesis is kindly supported by:



Ocean Optics, Inc.



Nederlands Forensisch Instituut
Ministerie van Veiligheid en Justitie

Nederlands Forensisch Instituut

Cover design: Johan Klijn | www.klijnbedrijf.com

Author: Rolf Hendrik Bremmer

ISBN: 978-94-90371-97-5

Layout and printing: Off Page, www.offpage.nl

Copyright 2011 © Rolf Hendrik Bremmer, Amsterdam, The Netherlands. All rights reserved. No part of this publication may be reproduced, stored in a retrieval system, or transmitted in any form or by any means, electronic, mechanical, photocopying, recording or otherwise, without the prior permission of the copyright owner.

NON-CONTACT SPECTROSCOPIC AGE DETERMINATION OF BLOODSTAINS

ACADEMISCH PROEFSCHRIFT

ter verkrijging van de graad van doctor
aan de Universiteit van Amsterdam
op gezag van de Rector Magnificus
prof. dr. D.C. van den Boom
ten overstaan van een door het college voor promoties ingestelde
commissie, in het openbaar te verdedigen in de Agnietenkapel
op woensdag 29 juni 2011, te 12.00 uur

door

Rolf Hendrik Bremmer
geboren te Nijmegen

PROMOTIECOMMISSIE

Promotor: prof. dr. A.G.J.M. van Leeuwen

Co-promotor: dr. ir. M.C.G. Aalders

Overige leden: prof. dr. ir. H.J.C.M. Sterenborg

prof. dr. ir. C. Ince

prof. dr. W.J. Buma

prof. dr. R.J. Oostra

prof. dr. W. Steenbergen

Faculteit der Geneeskunde

TABLE OF CONTENTS

Introduction		7
Chapter 1	Forensic quest for age determination of bloodstains: a review	13
Chapter 2	Age estimation of bloodstains by hemoglobin derivative determination using reflectance spectroscopy	35
Chapter 3	Remote spectroscopic identification of bloodstains	49
Chapter 4	Non-contact spectroscopic determination of large blood volume fractions in turbid media	61
Chapter 5	Biphasic oxidation of oxy-hemoglobin in bloodstains	77
Chapter 6	Photon path length distribution model for reflectance spectroscopy	91
Chapter 7	Diffusion approximation beyond its assumed borders of validity	99
Conclusion		107
Bibliography		127
Publication list		135
Summary		139
Samenvatting		141
Dankwoord		145
Curriculum Vitae		147

INTRODUCTION



INTRODUCTION

Accurate determination of the time a crime was committed is one of the holy grails in forensic investigations. However, until now, using bloodstains to determine the time elapsed since the crime was committed is still not possible. From a criminalistic point of view, an accurate estimation of when the crime was committed enables to verify witnesses' statements, limits the number of suspects and assesses alibis. Despite several attempts and exploration of many technologies over the last century, no method has been materialized into forensic practice.

Techniques that have been explored for bloodstain age determination include: atomic force microscopy, electron spin resonance, oxygen electrodes, high performance liquid chromatography and RNA analysis. All these techniques will be discussed in detail in chapter 1. Two important properties of these techniques, the sensitivity to short term or long term ageing and the applicability on crime scenes are visualized in figure 1. It shows that the topic of this thesis, reflectance spectroscopy, is positioned at the left bottom corner of figure 1. Reflectance spectroscopy is most sensitive for short term ageing, i.e. up to an age of 20 days. Moreover, reflectance spectroscopy is a portable and non-invasive technique. No physical contact with the bloodstain occurs when measuring the reflectance spectrum of the bloodstain. This non-invasiveness property makes reflectance spectroscopy a very interesting technique for age determination of bloodstains.

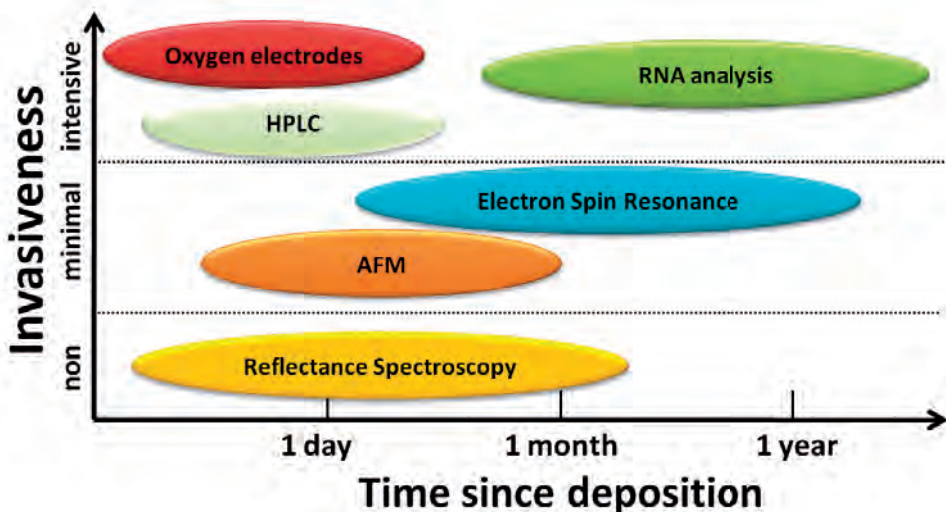


Figure 1. Overview of techniques suitable for age determination of bloodstains. Reflectance spectroscopy is a technique to measure the color. Since the color of a bloodstain changes with time from bright red to dark brown, reflectance spectroscopy seems to be the suited technique to relate the changing color to the age of the bloodstain and perhaps to understand the chemical reaction responsible for this color change.

SCOPE OF THIS THESIS

The scope of this thesis is to use spectral analysis of the reflectance spectrum of a bloodstain over a large spectral window (450 - 800 nm) and to use multi-component fitting algorithm to determine amount of hemoglobin derivatives as a function of the age of the bloodstain. Multi-component fitting analysis of reflectance spectra of tissue is routinely used in medicine to determine the oxygen saturation of blood. Yet this study is the first attempt to analyze the reflectance spectra of a bloodstain with a multi-component fit. This thesis describes the challenges and opportunities of the multi-component fitting of bloodstains.

Chapter 1 shows that reflectance spectroscopy for monitoring ageing bloodstains is not a new idea [1-5] and also not the only technique for determining the age of a bloodstain. Some techniques are based on hemoglobin, others on proteins or RNA. This chapter summarizes an extensive literature search and compares the discussed techniques on sensitivity and applicability on a crime scene.

Chapter 2 describes the first attempt to monitor ageing bloodstains, and reveal a transition of HbO_2 to met-Hb and HC. The spectral analysis is appreciated by Kubelka Munk's approximation to the transport theory of light. At the end of this chapter, a method is described to use hemoglobin derivatives for age estimation of the bloodstains.

Chapter 3 shows the possibility to use multi-component analysis of bloodstains to discriminate between blood and non-blood samples. The correlation coefficient between the reflectance spectrum and the multi-component fit is an excellent parameter to distinguish blood (high correlation) from non-blood (low correlation).

Chapter 4 shows a quantitative method for analysis of non-contact reflectance spectra. By using an empirical photon path length model the amount of hemoglobin derivatives can be determined quantitatively. The method is validated on phantom measurements.

Chapter 5 shows the use of the method of chapter 4 on bloodstains. The quantitative analysis reveals a biphasic oxidation of the oxy-hemoglobin in bloodstains. The oxidation rate is temperature depended, but humidity independent. The transition of met-Hb to HC is also biphasic, and does depend on humidity.

Chapter 6 shows that the reflectance spectrum as a function of absorption is completely determined by the photon path length distribution at zero absorption. The probe specific photon path length distribution is determined by Monte Carlo simulations.

Chapter 7 describes the phantom measurement from chapter 4 in terms of the diffusion approximation of light. Three approaches are explored for the diffusion theory, two with physical model parameters and one with empirical determined, fitted parameters.

This chapter gives an overview of an extensive search in English literature of techniques that address the quest for age determination of bloodstains. In brief, most techniques are complementary to each other, in short as well as long term age determination. Techniques are compared concerning their sensitivity for short and long term ageing of bloodstains and concerning their possible applicability to be used on a crime scene. In addition, experimental challenges like variation in substrate, interdonor variation and environmental influences are addressed. Comparison of these techniques contributes to our knowledge of the physics and biochemistry in an ageing bloodstain. Further improvement and incorporation of environmental factors are necessary to enable age determination of bloodstains to be acceptable in court.

CHAPTER 1
FORENSIC QUEST FOR AGE DETERMINATION
OF BLOODSTAINS: A REVIEW

Parts of this chapter is submitted as a review to
Forensic Science International



INTRODUCTION

Various traces found at the crime scene are candidates for determining the time a crime was committed. The technique mostly used in forensic practice is, in case of the presence of a body, measuring the rectal temperature [6-8] to relate this to the post mortem interval. Other traces potentially suited and explored for age determination are open wounds [9, 10], bruises [11, 12], latent fingerprints [13, 14], ink on questioned documents [15, 16] and bloodstains, the subject of this review. Some of these techniques are forensic routine, but all dating techniques come with large error margins.

Bloodstains are among the traces encountered most frequently at crime scenes [17]. Estimation of the age of a bloodstain can be a first indication to forensic investigators when the crime was committed, which is particularly useful when bloodstains are the only piece of evidence available. If, from other pieces of evidence, the time of committance is known, then bloodstain age determination may confirm or exclude a bloodstain as being relevant to the crime.

The aim of this chapter is to summarize potential techniques, recent developments and future challenges relevant for age determination of bloodstains. It discusses both the fundamental background as well as improvements in bio-analytical methods and developments of novel approaches. This review also evaluates the inaccuracy in age determination for various techniques, and the applicability for *on site* age determination of each method presented.

COMPOSITION OF BLOODSTAINS

Various compounds of a bloodstain can be used for age determination. Bloodstains originate from droplets of whole blood that are dried out. Whole blood contains blood cells, proteins and amino-acids; suspended in a liquid called blood plasma. There are three major types of blood cells and cell fragments: red blood cells, white blood cells and platelets. This paragraph delineates several of the compounds in bloodstains and discusses how each of these compounds can contribute to determine the age of a bloodstain.

Red blood cells

Red blood cells (RBC) are the most numerous from the three major blood cells. RBCs are donut shaped, approximately 7 μm in diameter, do not have a nucleus, and thus contain no DNA. Scanning electron microscope (SEM) and atomic force microscope (AFM) images of RBCs in bloodstains show an intact shape of the red blood cell after deposition [18, 19]. The main component of RBCs is the oxygen carrying protein hemoglobin, which makes up 97% of the blood's dry content. Hemoglobin contains iron and is responsible for oxygen transport between lungs and tissue. Hemoglobin is built up of four heme subunits; each containing one iron atom, which can bind one oxygen molecule. Hemoglobin can appear in various forms, called hemoglobin

derivatives. Conversion kinetics between various hemoglobin derivatives differ outside the human body compared to *in vivo*.

Inside a healthy human body, *in vivo*, hemoglobin molecules are mainly present in two forms: one without oxygen, de-oxyhemoglobin (Hb) and one saturated with oxygen, oxy-hemoglobin (HbO₂). When unbound to oxygen, the iron in the heme subunit is in the ferrous state. This state is bivalent (Fe²⁺) and paramagnetic. Bound to oxygen, HbO₂ is observed to be diamagnetic [20, 21] and the oxygen molecule becomes a superoxide anion [21]. The precise nature of the oxidation state of iron in HbO₂, Fe²⁺, Fe³⁺ or partial electron transfer, is topic of debate [20-23]. The iron atoms in the hemoglobin molecule, whether oxygenated or deoxygenated, exhibit no electron paramagnetic resonance (EPR) signal [24]. HbO₂ can auto-oxidize into met-Hb [25], which contains iron in the Fe³⁺ state [26] and is paramagnetic (high spin). Because met-Hb is incapable of binding oxygen, only a small part (~1%) of *in vivo* hemoglobin will be met-Hb in a healthy situation. When met-Hb is formed *in vivo* it will be reduced back to Hb by reductase protein cytochrome *b5* [27]. Met-Hb is paramagnetic and has an EPR absorption peak around $g \approx 6$ [28].

Outside the body, hemoglobin saturates completely with oxygen in the ambient environment to HbO₂. Due to a decreasing availability of cytochrome *b5*, necessary for reduction of met-Hb, the transition of HbO₂ into met-Hb will, in contrast to inside the body, no longer be reversed [27]. Once hemoglobin is auto-oxidized to met-Hb it will denature to hemichrome (HC), which is formed by an internal conformation change to the heme group [23]. HC contains a low spin [29] and has an EPR absorption peak around $g \approx 2.5$ [29]. This process of oxidation and denaturation, HbO₂ → met-Hb → HC, is accompanied by both a change in optical absorption and a change in spin configuration of the iron molecule. A summary of the properties of hemoglobin derivatives as described above is shown in table 1.

Besides a chemical change, also physical changes in the RBC can be used for age determination. The stiffness and adhesive force of a RBC are reported to increase after deposition, which can be measured by atomic force microscopy (AFM) [19, 33, 34].

Techniques that elaborate on changes in red blood cells are: EPR, HPLC, Reflectance Spectroscopy, Oxygen Electrodes and AFM.

White blood cells and platelets

White blood cells are much less numerous than red blood cells (1:700) and contribute to the immune system. Anderson *et al* and Bauer *et al* have shown the ability to use the nucleus of the white blood cell for age determination, since it contains DNA and RNA [35-37]. Whereas DNA seems to be stable in dried bloodstains [38] –as long as no bacterial overgrowth occurs; RNA is reported to be rapidly degrading. No results are reported on degradation of the cells themselves for age estimation of bloodstains.

The third group of blood cells are platelets, which are cell fragments rather than cells and responsible for clotting and coagulation of blood. When blood vessels are

Table 1. Binding, spin, optical and magnetic properties of four hemoglobin derivatives (deoxyhemoglobin (Hb), oxyhemoglobin (HbO₂), methemoglobin (met-Hb) and hemichrome (HC).

	<i>in vivo</i>			
	Hb	in bloodstains		
	Hb	HbO ₂	met-Hb	HC
Iron in Hb	Fe ²⁺ [27]	topic of debate [20-23]	Fe ³⁺ [27]	Fe ³⁺ [30]
Iron bound to	- [27]	•OO ⁻ [21]	O ₂ ⁻ [27]	Histidine group [30]
Spin complex	High [21]	Low [21]	High [21]	Low [21]
Magnetism	Paramagnetic [21]	Diamagnetic [21]	Paramagnetic [21]	Paramagnetic [21]
EPR absorption at g-value	no EPR possible [24]	no EPR possible [24]	g ≈ 6 [28, 29]	g ≈ 2.5 [29]
Wavelength of local absorption maximum	428 and 556 nm [31]	414; 542 and 576 nm [31]	406; 500 and 630 nm [31]	389 and 537 nm [32]

damaged, a plug of platelets is formed, enmeshed in a network of insoluble fibrin molecules. The coagulation process starts within a few seconds after bleeding. Because of the fast and complex mechanism of coagulation, platelets do not seem to be very applicable for bloodstain age estimation. Hence, no results are reported measuring platelets for age determination of bloodstains.

A technique that elaborates on changes in white blood cells is: RNA analysis.

Blood plasma

Blood plasma consists of serum proteins and clotting factors. The serum proteins include serum albumin, serum globulins and hormones. The serum proteins degrade after deposition and can be separated by electrophoresis. The ratio of various proteins can subsequently be used as an age indicator of the bloodstain [39, 40]. Additionally, the hormones or biomarkers, such as melatonin, can be used to determine the deposition time of a bloodstain relative to the 24h day cycle [41].

Techniques that elaborate on changes in blood plasma are: protein degradation and biomarker analysis.

TECHNIQUES FOR AGE DETERMINATION

The following paragraphs enumerate various techniques that have been explored for age determination of bloodstains. The order of discussed techniques is similar to the order of the above-mentioned bloodstain compounds. At the end, all techniques are compared on short and long term age determination and forensic applicability.

Early Pioneering

Already in the beginning of the previous century, forensic scientists have dealt with the challenge of finding methods for determining the age of a bloodstain. To our knowledge, the earliest reference in literature is by Louis Tomellini from the university of Genoa, Italy in 1907 [42]. He developed a chart with twelve figures to illustrate color changes of a bloodstain from the moment of deposition up to one year. Three years later, probably independent from Tomellini, Leers described the ageing of bloodstains from a physiological point of view as follows: “*When a bloodstain slowly dries, it shows, already after a few days, not anymore the pure HbO₂ spectrum, but the spectrum of met-Hb, or a combination of met-Hb and HbO₂*” [43]. Leers concluded this, after comparing bloodstain spectra with the hemoglobin spectra measured in 1901 by Ziemke and Franz Müller [44], see figure 1.

In the 1930s, Schwarzacher [45] attempted to correlate the age of a bloodstain with the bloodstain’s rate of solubility in water, which begins rapid and then decreases slowly as the bloodstain ages. A few years later Schwarz [46] used a guaiacum-based assay to determine catalase and peroxidase activity of hemoglobin in bloodstains. This assay showed that the intensity of the reaction’s color was inversely related to the age of

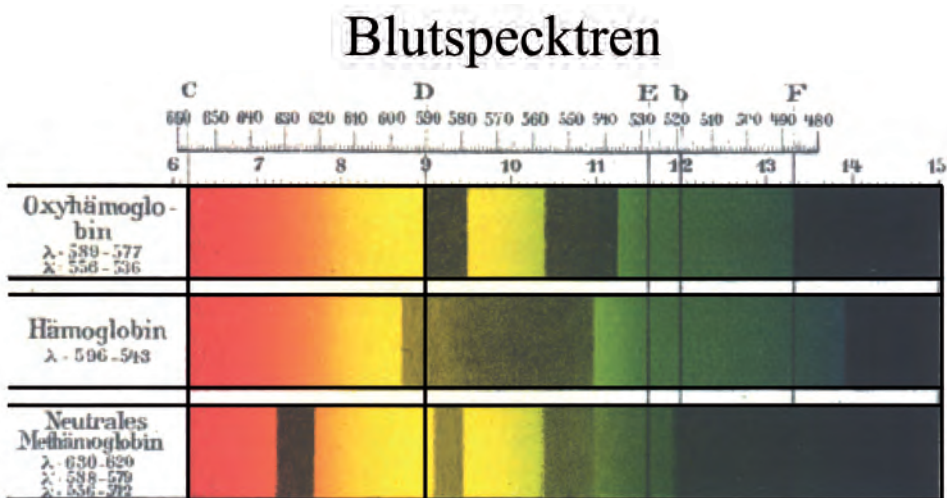


Figure 1. Qualitative absorption spectra of hemoglobin derivatives from 1901; HbO₂ (upper panel), Hb (middle panel), and met-Hb (bottom panel). The black bands depict the absorption bands, the corresponding wavelength range is presented on the left side. Image from [44].

a bloodstain. In 1960, Patterson applied photo-spectrometry. He recorded bloodstain's reflectance spectra [1] and observed that the changing color of the bloodstain depends on environmental conditions. Twelve years later, Patterson *et al* managed to quantify absorption bands in bloodstains to improve age determination [2]. Despite all these impressive results in the 20th century, most work ended after one or two publications and unfortunately did not receive follow up.

Techniques based on changes of red blood cells

High Performance Liquid Chromatography (HPLC)

High performance liquid chromatography (HPLC) is one of several separation techniques, able to identify and quantify the individual components of a mixture, including hemoglobin derivatives. Mobilized proteins are transported through a column to the detector, where they arrive at characteristic retention times typical for the various proteins. The proteins can be extracted from the bloodstain after adding de-ionized water to the bloodstain. Quantifying degradation products of heme by HPLC in bloodstains can be used as a marker for age estimation [47-50]. The detector at the end of the column measures the optical density at various wavelengths; a convenient wavelength for detection of proteins in bloodstains is 220 nm (ultraviolet). Various proteins have different retention times and the integrated peak area of a protein is a measure for the amount of proteins present. Inoue *et al* have related the ratio of the peak areas of the hemoglobin α -chain and the heme protein to the age of the bloodstain. They found a weak correlation between the age and the peak area ratio [47]. An improved age indicator was found following the discovery of the presence

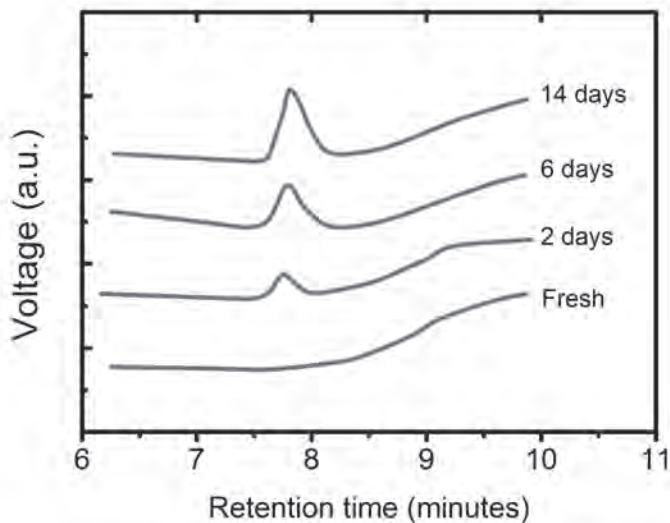


Figure 2. Appearance of the 'X' peak detected by the HPLC for bloodstains stored on cotton cloth at 37 °C during different time periods. The detection wavelength was 220 nm. Data from [49].

of an unknown protein 'X', with a retention time more than 8 times shorter than the retention time of the heme protein [48].

The peak area of protein X increases with age of the bloodstain [48, 49] and is shown in figure 2. This figure also shows that this designated 'X' protein is not present in fresh blood. The retention time in the reverse phase HPLC of 'X' is 8 times shorter than the retention time of the heme protein [48]. Inoue *et al* related the ratio of the areas underneath the peak of 'X' and the heme peak to the age of the bloodstain. This ratio is 0 for fresh blood and increases to 0.3 for bloodstains stored for 52 weeks in the dark at 37 °C. Andrasko recorded the absorption spectrum of the X-component and found only an absorption peak around 220 nm. The lack of absorption between 250-600 nm indicates that compound 'X' is not related to heme. Andrasko found the presence of additional peaks in the HPLC analysis, which were designated 'Y' and 'Z' peaks. While the origin of these peaks was not revealed, they may assist in age estimation of bloodstains by HPLC.

Reflectance Spectroscopy

The color of a bloodstain changes with time from red to brown which suggests that color quantification of bloodstains by optical spectroscopy methods can be a worthwhile approach for pursuing age determination. Various attempts have been made relating the color, based on the reflectance spectrum of the bloodstain, to its age [1-4, 51]. All these approaches operate in the visible part of the spectral range (450-700 nm), since color changes varying from red to brown refer mainly to this spectral range. This technique requires a white light source and a spectrometer. An established approach for age determination by reflectance spectroscopy is by relating the reflectance spectrum

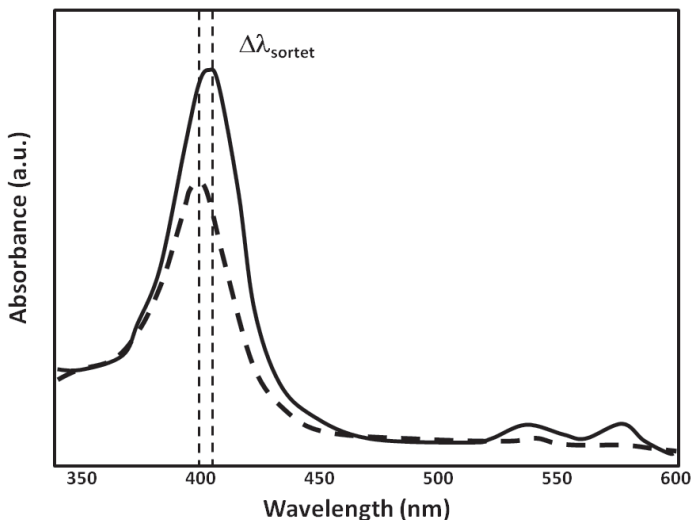


Figure 3. Spectral Shift in ageing bloodstains. Spectral profiles from bloodstains stored at room temperature for 15 minutes (solid line) and 1 year (dashed line). Analysis is in terms of difference in absorbance (parameter 1) and spectral shift of absorption maximum (parameter 2). Data from [3].

directly to the age of the bloodstain is measuring the reflectance at two wavelengths and determining the ratio.

Kind *et al* related the age of the bloodstain to the reflectance ratio at 540 and 576 nm, designated the α -ratio [2]. Another approach, suggested by Hanson and Ballantyne, is measuring the wavelength of maximal absorption around 414 nm, the so-called Soret absorption band and relating the spectral blue shift of the Soret band relative to 414 nm to the age of the bloodstain [3], see figure 3.

Apart from the visible part of the optical spectrum, functional information on the ageing stage of the bloodstain can also be obtained in the near infrared (NIR) region [52, 53]. This approach has recently been explored to discriminate between bloodstain and non-bloodstains by infrared hyper-spectral imaging [54-56]. Analysis of NIR spectra is more complicated than analysis of reflectance spectra in the visible part of the optical spectrum, because the characteristic spectral features do not only originate from hemoglobin derivatives, but also from water, lipids, and various proteins. The loss of water plays a significant role in establishing the initial change in the spectra. The H₂O absorption band between 1350-1500 nm is not overlapped by any other chromophore absorption and the area underneath this absorption band vanishes almost completely during the first hour of ageing, see figure 4. After evaporation of water, a consistent series of absorption bands due to proteins appears between 1900 and 2500 nm, but does not reveal much alteration during ageing [52]. The appearance of a spectral band between 1450-1900 nm is attributed to the formation of met-Hb with subsequent binding of water during the ageing of bloodstains. While results appear elicited, Botonjic

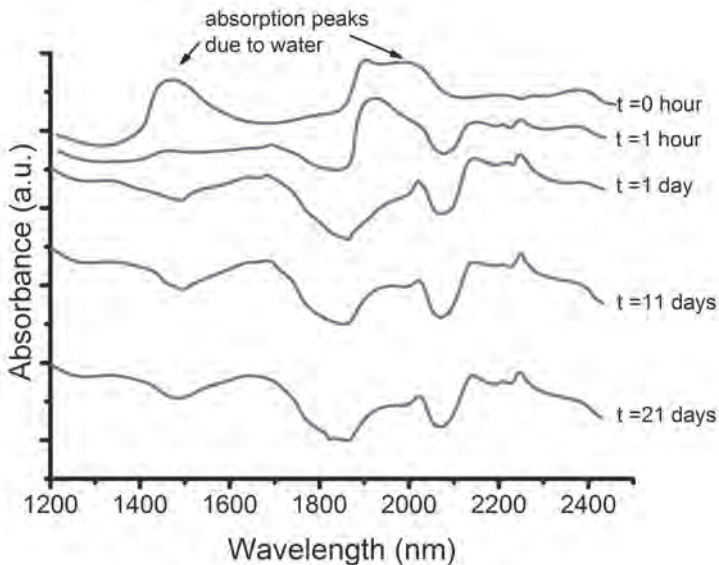


Figure 4. Representative NIR spectra of a bloodstain on gauze aged over a period of 22 days. Note that the area underneath the H₂O curve vanishes almost completely after one hour. Data from [52].

et al ignore HC in their analysis of the ageing bloodstain spectra [52], which may have caused an overestimation of the amount of met-hemoglobin.

Oxygen Electrodes

The amount of HbO_2 in bloodstains can be established by using oxygen electrodes [57], dissolving the bloodstains in a saline solution and using a polarographic oxygen analyzer. The oxygen is measured from an electron current by a negative electrode in a hydroxide bath. Matsuoka *et al* have monitored ageing bloodstains for ten days [57]. Figure 5 shows the decay of fractional HbO_2 measured at several temperatures. At room temperature, the decay of HbO_2 is at first rapid, but decreases after a few hours. At $T = 5^\circ\text{C}$ no oxidation was measured at all. Bloodstains stored at higher temperatures reveal a faster decay of HbO_2 [57], while after 24 hours, no further decay is measured.

Electron Paramagnetic Resonance (EPR)

The denaturation of hemoglobin in dried bloodstains is governed by a spin state change of the iron ion in the hemoglobin molecule, which can be measured by EPR (Electron Paramagnetic Resonance) [29, 58, 59]. Bloodstains give four striking EPR signals in the $g = 6.2$ (g6); 4.3 (g4); 2.27 (H); and 2.005 (R) regions of the paramagnetic center's electronic structure. These four signals represent ferric high-spin (g6), ferric non-heme (g4), ferric low-spin (H) and free radical species (R), respectively. As far as hemoglobin derivatives concern, g6 has been related to met-Hb and H to HC [29]. Yet it remains unclear to which compounds g4 and R should be related to [29]. HbO_2 is diamagnetic and consequently has no EPR spectrum [21, 24]. The EPR signal intensity as a function of age of the bloodstain is shown in figure 6. Fujita *et al* found that the age of a bloodstain could be related to the ratio of the H/g4 signal. For all four signals,

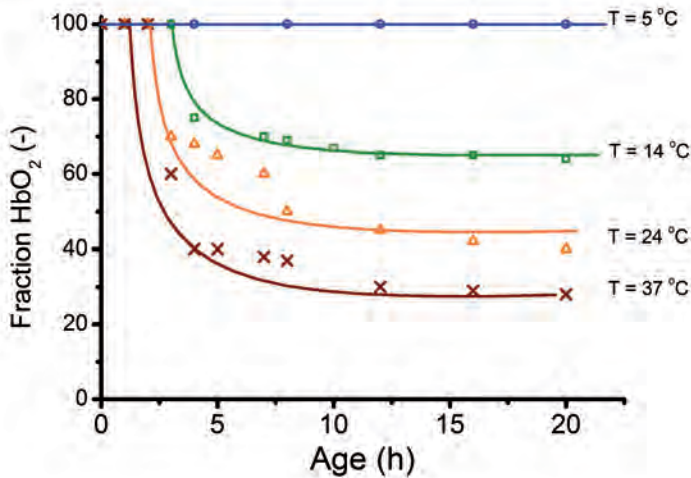


Figure 5. Changes in fractional HbO_2 in bloodstains recorded by oxygen electrodes stored at various temperatures. $T = 5^\circ\text{C}$ (open dots); 14°C (open squares); 24°C (open triangles); 37°C (crosses). Data from [57].

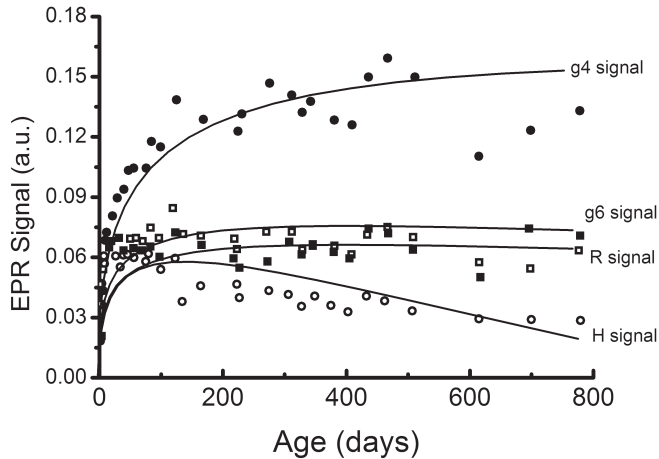


Figure 6. EPR signal intensity at four g-values as a function of age of the bloodstain and at 25 °C. Data points represent g6 (high-spin iron (III) species, methemoglobin, closed squares), g4 (non-heme iron(III), closed circles), H (low-spin heme (III), hemichrome, open circles) and R (free radicals, open squares). Solid lines are empirical fit calculations. Data from [58].

during the first 30 days an increase in EPR signal was found. After 30 days, the g6, (met-Hb) stays at a constant level, while the H signal (HC) decreases after 30 days. The increment of all four EPR signals during the first 30 days suggests that the sum of the chemical components responsible for the EPR signals is not conserved. This hampers relating the EPR signals to the oxidation and denaturation chain of hemoglobin in a bloodstain.

Atomic Force Microscopy (AFM)

Atomic Force Microscopy (AFM) is a high resolution type of scanning probe microscopy that scans a surface with the tip of a cantilever with nanometer resolution. By externally oscillating the cantilever, AFM can determine the elasticity of a surface by assessing the cantilever's resonance frequency. Subsequently, AFM can determine the elasticity of extracorporeal RBCs. The tensile elasticity, or Young's modulus of a normal red blood cell is 40 kPa [33]. This relatively low value of elasticity corresponds with a high flexibility, necessary for RBCs to penetrate in the smallest capillaries in the microcirculation. Strasser *et al* have investigated the elasticity of red blood cells in bloodstains by AFM as a function of bloodstain age [19]. The elasticity of the red blood cells increases when becoming *extracorporeal*. They found that the elasticity of a red blood cell increases almost 8-fold to 300 kPa when measured 1.5 hours after bleeding. Within 30 hours, the elasticity becomes 600 kPa; and after 30 days it reaches 2.5 GPa. Figure 7 shows the elasticity as a function of the age of the bloodstain. While the elasticity increased, the shape of the red blood cell remained intact. Neither the erythrocytes nor the cracks in the bloodstain showed any morphological alterations during the observation period of 31 days [19].

Measuring Young's modulus of red blood cells in bloodstains can be worthwhile in age estimation. This method is minimally invasive and one sample can be measured multiple times. However, the large standard deviation of these measurements, in the order of 60% of the measured elasticity, precludes inaccurate age estimation. Wu *et al* have used AFM measurements to determine RBC cell volume and adhesive forces. They found that the cell volume remains constant after deposition, while the adhesive force shows a sudden increase after seven days [34].

Techniques based on white blood cells

RNA, which can be extracted from the nucleus of a white blood cell, is not as stable as DNA; hence RNA degradation measurements seem a suitable candidate for age determination of bloodstains. RNA degradation in bloodstains has been used for age determination by Bauer *et al* [35] and Anderson *et al* [36, 37]. RNA expression can be measured in Ct (cycle threshold) values, which is the value of the n^{th} cycle at which the fluorescence generated within a reaction exceeds a certain fluorescence threshold. Various RNA species are highly abundant in blood. The instability of RNA implies that small changes induce polymorph RNA species. Polymorphism which occurs between RNA species can be exploited to provide species specific tests. Two types of RNA examinations have been explored: 1) semi-quantitative duplex Polymerase Chain Reaction (PCR) [35] for reversely transcribing RNA into cDNA, which is then amplified by PCR and 2) quantitative PCR, used to measure the quantity of a PCR product, commonly in real-time [37]. A relation between the age of the bloodstain and RNA degradation was found when the ratio of 18 S rRNA to β -actin mRNA was investigated. Both 18 S and β -actin are considered "housekeeping genes" which are

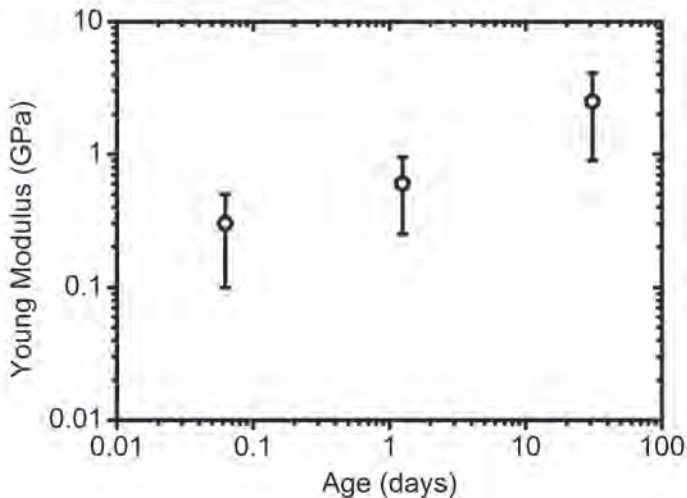


Figure 7. Elasticity of red blood cells versus the age of the bloodstain. The whisker displays the standard deviation of the force curves. Data from [19].

expressed in all cell types at relatively high levels, thus the RNA products from cells are likely to be recovered at crime scenes. The Ct value of 18 S did not change over the course of 150 days, but the Ct values for β -actin became significantly reduced as a function of time, thus the relative ratio of 18 S rRNA to β -actin mRNA increased over time [36] as is shown in figure 8. The age estimation of Anderson *et al* was limited to half a year of ageing, while Bauer *et al* showed that quantification of degraded RNA is possible for bloodstains stored up to 15 years [35]. Improvement in age estimation was found when a multivariate analysis of the RNA species was implemented [37]. Finally, it was shown that the forensic function of mRNA markers in bloodstains are not limited to age estimation, but can also be used for discrimination between blood and menstrual blood [60].

Techniques based on blood plasma

Proteins present in blood, especially those in the serum, will deteriorate gradually when bloodstains are formed. Rajamannar studied the decomposition of various α , β and γ -globulins, as well as albumin in bloodstains ranging in age from fresh up to a year old [39]. In this study, the presence of the proteins was determined by immunoelectrophoresis, which is an invasive technique and requires cotton fibers soaked with blood for analysis. It was observed that all globulins and albumin were present in fresh bloodstains. After 15 days, the α -globulins and the albumin were decomposed. Thereafter, the β and γ -globulins gradually decomposed, until after a year no globulins were found in the bloodstain. Hence, the presence and concentration of globulins could be an indicator for the age of the bloodstain.

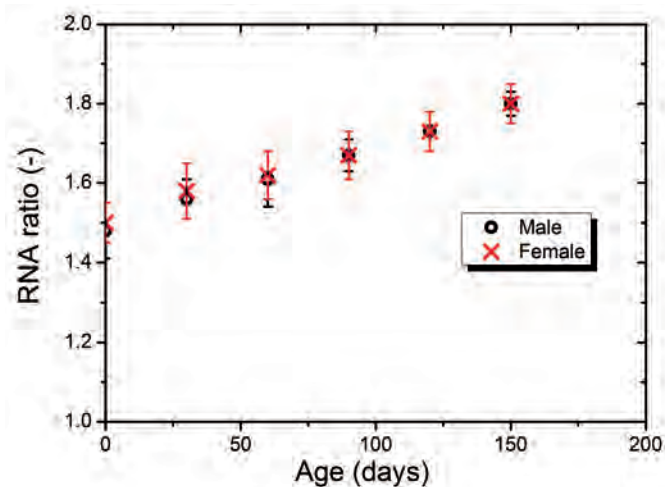


Figure 8. RNA ratio in bloodstains as a function of age. Data represent the ratio of 18 S rRNA to β -actin mRNA as determined by real-time reverse transcriptase PCR. Each data point represents average \pm SD for N=72. Data from [36].

UV absorbance photometry is another method to detect the presence of enzyme activity. Tsutsumi *et al* used this method to quantify the activity of lactate dehydrogenase (LDH), glutamic oxaloacetic transaminase (GOT) and glutamic pyruvic transaminase (GPT) [40]. They found a higher activity of these enzymes in bloodstains than in serum and a comparable activity in completely hemolyzed blood. Age estimation up to 12 weeks after formation of the bloodstain was established by a combination of LDH/GOT and GOT/GPT ratios. This method requires removal of the bloodstain, extraction with saline, labeling of the enzymes and detection at a wavelength of 340 nm. Tsutsumi *et al* found that the GOT/GPT ratio remains stable over the first weeks, while the LDH/GOT ratio is at first high (>10), and decreases to a ratio of 5 after eight weeks.

A more recent approach, by Ackermann *et al* is to estimate trace deposition with circadian biomarkers [41]. By using commercial enzyme-linked immunosorbent assays they show that the characteristic 24-h profile of two circadian hormones, melatonin (concentration peak at late night) and cortisol (peak in the morning) can be reproduced from small samples of bloodstains. This approach differs from all other age determination methods described in this review, because it cannot determine the age of the bloodstain, but only the trace deposition time within the 24-h cycle. It was observed that melatonin is quite stable up to 28 days after storage, whereas decay with storage time was observed for cortisol. The technique requires a 30-80 μ l sample of dried bloodstain for *in vitro* analysis at -80 °C. Figure 9 shows that the melatonin concentration remains <10 pg/ml during office hours. But it reaches a maximum of 60 ± 20 pg/ml around 3 am at night. This approach opens a new field of circadian biomarkers for forensic applications.

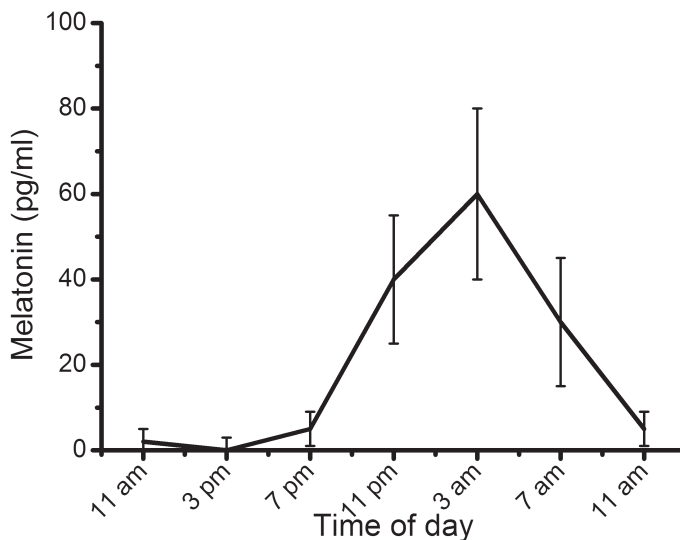


Figure 9. Twenty-four-hour profiles of melatonin concentrations in blood samples from six subjects and the mean (\pm SD) values. Data from [41].

Comparison of techniques

The various techniques discussed can be compared on many levels. First and one of the most important aspects of a technique is the inaccuracy. We quantified the inaccuracy in age estimation of three techniques, based on the reported results for AFM from Strasser *et al* as shown in figure 7 [19], RNA from Anderson *et al* as shown in figure 8 (male data points only) [36], and EPR from Fujita *et al* as shown in figure 6 [58]. We calculated the trend line in ageing for these four techniques and converted the reported standard deviation into an inaccuracy. The conversion was based on the calculated trend. Figure 10 shows the inaccuracy for these three techniques. This figure is based on single measurements, for bloodstains stored under laboratory circumstances. For instance, the tabulated data of RNA ratio of 18S rRNA to β -actin mRNA is reported to be 1.56 ± 0.05 after 30 days (see figure 8) For this specific technique, a standard deviation of 0.05 corresponds to an inaccuracy of 25 days in age estimation, based on the trend line. This means that a bloodstain that is measured to be 30 days may in fact be 5-55 days old.

For all techniques, the inaccuracy ranges from 1 day for AFM to 15 days for RNA for bloodstains of 0.1 days of age. The inaccuracy for RNA remains approximately constant around 20 days, which makes RNA especially suitable for long term age determination. The inaccuracy of AFM only contains three data points, i.e. one day at $t=0.1$ days, an inaccuracy of 4 days at $t=1.25$ days and an inaccuracy of 23 days at 31 days. The inaccuracy for EPR increases with age, and has been measured up to 750 days. Final note on the inaccuracy, figure 10 is based on single measurements in laboratory circumstances. Performing age determination based on multiple measurements may improve the accuracy, while going to unknown environmental storage conditions will make age estimation less accurate.

The second important aspect in age determination is whether a technique is sensitive for short term or long term changes. Alterations in hemoglobin derivatives occur already within a few hours, and changes are minimal after two months, suggesting suitability for short term age determination. In contrast, the sensitivity of RNA does not depend much on the age of the bloodstains, and is therefore more suitable for long term age determination.

A third feature for which the techniques differ from each other is the level of invasiveness or destructiveness. Ideally, traces are examined and interpreted in the original context, at the crime scene [61]. For preservation of the crime scene and for securing DNA evidence, non-destructive tests are very much appreciated [62]. Figure 11 compares the degree of invasiveness for several techniques discussed in this review for short term or long term age determination. Non-invasive indicates no sample preparation and a technique applicable on the crime scene. Minimally invasive indicates no sample preparation, but it does require transportation to the laboratory. Intensively invasive techniques require transportation to the laboratory and sample preparation. Often, preparation incorporates dissolving the bloodstain in water, a procedure that can only be performed once and hampers a possible second opinion measurement.

The least invasive technique is reflectance spectroscopy. This technique uses a light source, a fiber probe and a spectrometer, all portable and relatively cheap. This

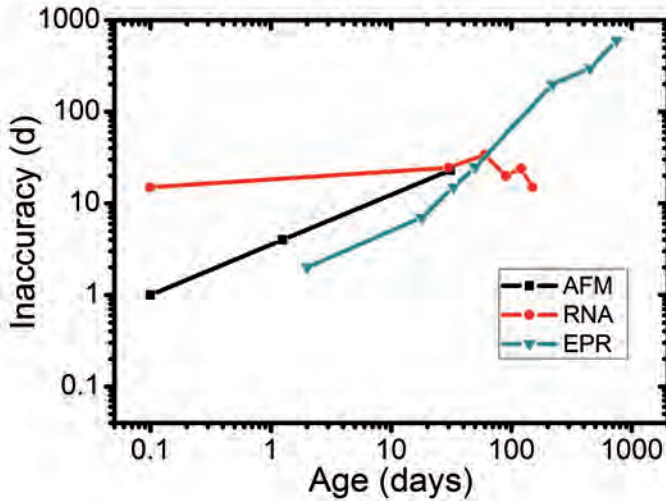


Figure 10. Inaccuracy of age determination as a function of the actual age, determined for four techniques: AFM, black squares, data from [19]; RNA, red circles, data from [36]; and EPR, green triangles, data from [58].

technique requires no sample preparation, and is non-destructive, because there is no physical contact and the light doses are low. Successful age determination by reflectance spectroscopy however, is yet limited to bloodstains found on a white background. Samples deposited on a non-white substrate require a more sophisticated optical sampling and analysis method. A possible suggestion to overcome the drawback of background color is the use of a hyper-spectral imaging system [63]. Spectral imaging allows imaging of the crime scene and optics-based chemical analysis of the imaged object. So far, most reflectance spectroscopy techniques focus on ages not longer than 60 days [3, 52].

Bloodstain age estimation by AFM does not require sample preparation and can be measured under ambient conditions in the laboratory. However, the background surface has to be non water absorbing. Therefore, bloodstain age determination by AFM is yet limited to bloodstains on tiles, glass and plastic. Strasser *et al* observed that the AFM measurements showed a high standard deviation (figure 2), which they explained by the non-homogeneous composition of the blood clot [19]. The AFM measurements are performed up to 31 days; the long term ageing effects on the stiffness of red blood cells remain currently unclear.

EPR measurements have to be performed in the laboratory as well. The technique requires no sample preparation, but the bloodstain and substrate have to be cooled down to -196 °C. This does not hamper performing multiple measurements on the same bloodstain, but not all substrates are suitable to resist cryogenic conditions. Fujita *et al* performed their EPR measurements on bloodstains ranging in age from 2 days up to 2.5 year and found changing EPR ratios over the entire time span [58]. Therefore, EPR seems suitable for both short and long term bloodstain age determination.

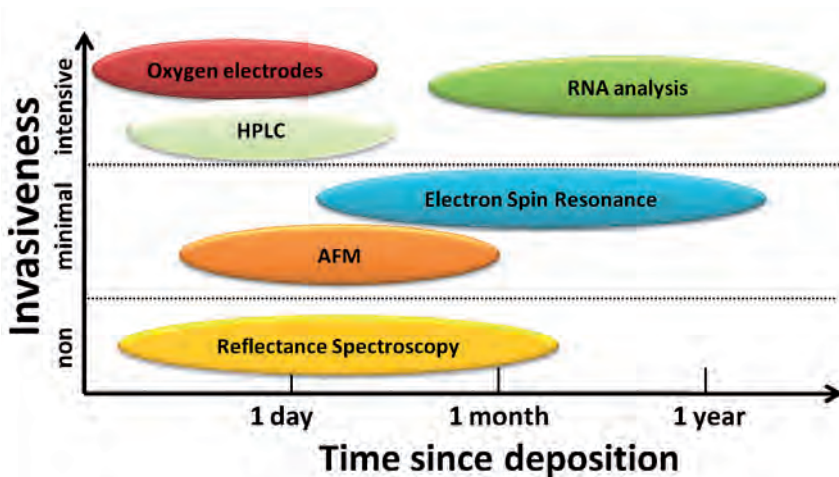


Figure 11. Overview of techniques suitable for age determination of bloodstains. The horizontal axis shows the time scale for which each technique is most suited, ranging from less than one day to more than one year. The vertical axis depicts the level of invasiveness of the technique.

HPLC and oxygen electrode are sensitive to short term variations in the concentration of hemoglobin derivatives. Both techniques require dissolving the bloodstain, HPLC in distilled water and oxygen electrodes in a saline solution. Sample preparation for age estimation by RNA [64] or biomarkers [41] requires swabbing of the bloodstain by TRI Reagent B; which is a standard procedure for use in the simultaneous isolation of RNA and DNA from whole blood. RNA measurements are tested over a time span up to 150 days and come with large standard deviations. Biomarkers have the potential to reveal the hormonal level of the donor of the bloodstain, which can be related to the time of the day the bloodstain was deposited. Therefore, biomarker measurements can be worthwhile in combination with other techniques.

Experimental Challenges

Performing a measurement on ageing bloodstains may seem straightforward. But, regardless of the technique, the experimental materials and methods have to be chosen thoughtfully. This section addresses the challenges for experiments on ageing bloodstain that apply regardless of selected technique.

Use of Anticoagulants

To simulate blood at crime scenes as realistic as possible, it is recommended to use untreated whole blood for preparation of bloodstains. Most experiments discussed in this review have used anti-coagulants to prevent early clotting. Without adding anti-coagulant blood will clot within 30 seconds [65]. Many anti-coagulants exist for preventing *in vitro* blood coagulation, including heparin, citrate, and EDTA. Among these three, EDTA is found to be favorite for preservation of DNA extraction from blood [66]. However, no evidence is reported in the literature of anti-coagulants influencing the

processes associated with ageing of bloodstains. Bauer *et al* found that the use of EDTA in conventional concentrations does not significantly influence RNA degradation [35].

Interdonor Variation

Few reports address the interdonor variation amongst bloodstains. The interdonor variation has been tested for RNA and reflectance spectroscopy. A larger spread in RNA ratios was expected for bloodstains from females due to altered hormonal levels encountered during the monthly estrus cycle. We have performed a one-way ANOVA test on the tabulated RNA ratio of 18 S rRNA to β -actin RNA from [36] between males and females and found no significant difference at the $p < 0.05$ level. The insignificant differences between sexes are confirmed by a larger population study [64]. Chapter 3 will show that for reflectance spectroscopy, no significant interdonor variations were found ($p < 0.05$) among forty bloodstains from eight donors. The amount of interdonor variations will most probably depend on the measurement technique.

Bloodstain Substrate

The substrate of the bloodstain is an important parameter in bloodstain pattern analysis [17, 67], yet few reports have addressed the influence of substrate on bloodstain ageing, despite its importance. Most studies described in this review have created the bloodstains on white cotton fabric or filter paper. These substrates adsorb the blood and are diffuse reflectors as well. The first property is useful for extraction to *in vitro* analysis, while the latter property is advantageous for reflectance spectroscopy. For the AFM study (section 3.1), bloodstains on glass were used, to fulfill the requirement of having a nearly flat surface. Only one study, with HPLC, has compared the effect of ageing bloodstains on two substrates: cloth and paper and in this case no significant difference was found in the age estimation [49]. A candidate for future research is the possible difference in ageing for bloodstains on adsorbing versus non-adsorbing substrates or the difference between hydrophobic and hydrophilic surfaces.

Environment

Already in the 1960s Patterson reported that the changing color of the bloodstain depends on environmental conditions, including temperature, humidity and exposure to (sun)-light [1]. Identifying and accounting for the influence of the ambient environment is among the greatest challenges in the quest for age determination of bloodstains. Not only is the influence of the environment complex, it also affects the oxidation of hemoglobin, although probably in a different manner than the decomposition of enzymes or the degeneration of RNA. These differences hamper unification of accounting for the environmental factors among the various age determination techniques. Nevertheless, an overview of the efforts of all studies regarding the influence of environment is summarized in table 2. It shows the measured parameter specific for that technique for a fresh bloodstain and after eight weeks of storage at two temperatures, i.e. at 4 °C and 22 °C. These temperatures are conveniently selected in many studies for storage in the refrigerator and at room temperature. However, not all studies have measured up to eight weeks or at these two temperatures, and if measured otherwise this is mentioned

Table 2. Influence of temperature, humidity and exposure to light for various techniques. The fourth column shows the quantity of the measured parameter for fresh bloodstains. This value is compared with the measured quantity in the fifth and sixth column at two temperatures. The measured quantity in the 4th, 5th and 6th column is shown in bold face.

Study	Technique	Measured parameter	Data Fresh Bloodstain	Data first Temp	Data second Temp	remark
Andrasko [49]	HPLC	X-peak / heme peak ratio	0	5 after 56 days at 0 °C	20 after 56 days at 22 °C	
Inoue [48]	HPLC	α-globin	6500	4300 after 56 days at 4 °C	3800 after 56 days at 22 °C	dark
Inoue [48]	HPLC	α-globin	6500	5900 after 56 days at 4 °C	5000 after 56 days at 22 °C	fluorescent light
Hanson [3]	Spectro-scropy	Abs max (nm)	414	411 after 7 days at 4 °C	409 after 7 days at 22 °C	Humidity =50%
Hanson [3]	Spectro-scropy	Abs max (nm)	414		413 after 7 days at 22 °C	Humidity =90%
Fujita [58]	EPR	Log (H/g4)	1	0.45 after 56 days at 20 °C	-0.8 after 56 days at 40 °C	dark
Fujita [58]	EPR	Log (H/g4)	1	-0.7 after 56 days at 20 °C		sunlight
Matsuoka [57]	Oxygen electrodes	Fractional HbO ₂ (%)	100	50 after 10 days at 5 °C	30 after 10 days at 24 °C	
Tsutsumi [40]	Enzyme	GOT (IU/I)	500	500 after 56 days at 4 °C	500 after 56 days at 37 °C	
Tsutsumi [40]	Enzyme	LDH/ GOT	7000	7000 after 56 days at 4 °C	500 after 56 days at 37 °C	

in table 2. Also, comparison between bloodstains stored in the dark and bloodstains exposed to light; as well as comparison between bloodstains stored at medium and high humidity has been inserted into table 2.

The influence of temperature in the results is unanimous: decomposition, oxidation and denaturation of bloodstains are faster at higher temperatures [3, 40, 48, 49, 57, 58]. However, defining a general relation between ageing and temperature is hampered by the small number of only five temperatures included in the studies. Future work is required to indicate whether the relation is linear, contains a threshold temperature or can be derived from first order kinetics.

The influence of exposure to light is even more complicated, with three different and contradicting influences reported from negative to neutral and positive effects on ageing. No study specifies the intensity and the wavelength of the light to which the bloodstain was exposed, yet these are essential parameters to identify the influence of light exposure on ageing bloodstains. Inoue *et al* found a slower rate of ageing for bloodstains exposed to a fluorescent lamp, compared to those stored in the dark. However, wavelength and intensity were not mentioned [48]. Bauer *et al* found no difference in RNA degradation between bloodstains exposed to sunlight and those stored under sunlight protection [35]. On the other hand, Fujita *et al* observed with EPR that bloodstains exposed to sunlight showed signs consistent with an increased rate of ageing. Bloodstains exposed to sunlight at $T = 20\text{ }^{\circ}\text{C}$ behaved similar to bloodstains stored at $40\text{ }^{\circ}\text{C}$ in the dark [58]. Thus the effect of sunlight on the ageing of bloodstains seems to be method-specific. Finally, the effect of humidity has only been studied by Hanson and Ballantyne with reflectance spectroscopy [3]. By exploring the range of 50-90%, they observed that the spectral blue shift in ageing bloodstains is highest at 50% and lowest at 90% humidity.

Experimental protocol

Without pretending to provide the rules for the ideal experiment, the authors would recommend standardized experimental guidelines for future experiments. Our suggestions are shown in table 3.

Table 3. Suggested guidelines for future bloodstain ageing experiments.

Method	Recommendation
Anti-coagulant	EDTA
Amount of stains per measurement	3
Interdonor variation	No
Substrate	Cotton
Measurement time	technique dependent*
Frequency of measuring	technique dependent†
Temperature	22 °C
Humidity	~ 40%
Light	No, i.e. in the dark

*The recommended measurement time for hemoglobin-based techniques is 10 days, and one year for other techniques.

†The recommended frequency for hemoglobin-based techniques is twice a day, and for other techniques once every month.

DISCUSSION AND CONCLUSION

Numerous techniques have been explored during the last century to address age determination of bloodstains. All techniques are still in the experimental phase and come along with large standard deviations and inaccurate age estimation. Reducing the standard deviation is very important for implementation into forensic practice and eventually in court.

An additional challenge in the age determination is the relative age of one bloodstain compared to another bloodstain, possibly formed at different points in time. However, little research has been reported addressing the challenge of relative age determination. The order of formation of bloodstains can confirm or exclude specific scenarios, especially in cases of questioned self-defense. The resolution of a technique to discriminate the deposition time of two bloodstains depends very much on the ages of the bloodstains. Yet the environmental factors are less complicating than for absolute age determination and the forensic demand is omnipresent. The side conditions for successful relative age determination are very much case-dependent, since figure 10 shows that the inaccuracy for most techniques increases with age of the bloodstain. We look forward to seeing the first case reports of this new future development, whenever a technique is used for relative age determination in a criminal case.

Bloodstains can be crucial in reconstructing crime events. However, no reliable methods are currently available to establish the age of a bloodstain on the crime scene. We show that determining the fractions of three hemoglobin derivatives in a bloodstain at various ages enables relating these time varying fractions to the age of the bloodstain. Application of light transport theory allows addressing the spectroscopic changes in ageing bloodstains to changes in chemical composition, i.e. the transition of oxy-hemoglobin into met-hemoglobin and hemichrome. We have found in twenty bloodstains that the chemical composition of the bloodstain with age, called hemoglobin reaction kinetics, under controlled circumstances, shows a distinct time-dependent behavior, with a unique combination of the three hemoglobin derivatives at all moments in time. Finally, we employed the hemoglobin reaction kinetics inversely to assess the age of twenty other bloodstains studied, again over a time period of 0-60 days. We estimated an age of e.g. 55 days correct within an uncertainty margin of 14 days. In conclusion, we propose that the results obtained under controlled conditions demand further evaluation of their possible value for age determination of bloodstains on crime scenes.

CHAPTER 2

AGE ESTIMATION OF BLOODSTAINS BY HEMOGLOBIN DERIVATIVE DETERMINATION USING REFLECTANCE SPECTROSCOPY

Forensic Science International February 206 166-171 (2011)



1. INTRODUCTION

1.1 Age determination of bloodstains

Bloodstains at crime scenes have enormous forensic value, ranging from DNA-profiling for verifying the suspect's identity to pattern analysis for reconstructing the crime. However, until now, the potential of using bloodstains to determine the time when a crime was committed has not yet been materialized, despite several attempts. Already in the 1930s Schwarzbacher attempted to correlate the age of a bloodstain with the bloodstain's rate of inhibition of solubility in water, which begins rapid and then decreases slowly as the bloodstain ages [45]. Over the last two decades, many more techniques have been explored for the forensic quest, including oxygen electrodes [57], RNA degradation [35], atomic force microscopy [19], and electron spin resonance spectroscopy [58]. Although all of these approaches confirm that the physical and chemical properties of bloodstains change over time, no technique has yet shown the precision and reproducibility that is needed for age determination in forensic practice.

The color of a bloodstain changes with time from red to brown which suggests that color quantification of bloodstains by optical methods can be a worthwhile approach for pursuing age determination. Patterson was the first to recognize this approach in 1960. He recorded bloodstain's reflectance spectra [1], and observed that the changing color of the bloodstain depends on environmental conditions. Twelve years later, Patterson *et al* managed to quantify absorption bands and suggested to use these spectra for age determination [2]. A similar approach, but only using a small spectral window has been suggested by Blazek and Lins [51].

We propose Diffuse Reflectance Spectroscopy (DRS) for determining the age of a bloodstain. DRS is based on non-specular reflection of light to determine a material's optical properties. This technique has proven its value in various disciplines ranging from materials science [68] to tissue diagnostics and is routinely used in medicine to determine the oxygen saturation of blood [69]. Our approach of DRS elaborates on recent progress in biomedical optics which allows quantifying the fractions of relevant bloodstain chromophores by multi-component spectral fits. Subsequently, these fractions which change with time are then related to the age of the bloodstain.

1.2 Hemoglobin reaction kinetics

Hemoglobin is the iron containing protein responsible for oxygen transport between lungs and tissue. It is the main chromophore in blood, since hemoglobin makes up 97% of the blood's dry content. Hemoglobin can appear in various forms, called hemoglobin derivatives. Conversion between various hemoglobin derivatives is different outside the human body, than inside. Inside a healthy human body, hemoglobin molecules are mainly present in two forms: one without oxygen: de-oxyhemoglobin (Hb) and one saturated with oxygen: oxy-hemoglobin (HbO₂). The average saturation level of arterial blood is >90% and of venous blood >70%. Only a small part (~1%) of HbO₂ is auto-oxidized into a third form, met-hemoglobin (met-Hb) [25], which is reduced back

to Hb by reductase protein cytochrome *b5* [27]. Outside the body, blood will totally saturate to HbO₂ as soon as it comes in contact with the oxygen in the atmosphere. However, due to a decreasing availability of cytochrome *b5*, necessary for reduction of met-Hb, the transition of HbO₂ into met-Hb will no longer be reversed. Once hemoglobin is auto-oxidized to met-Hb it will denature to hemichrome (HC). HC is formed through changes of protein conformation so that atoms endogenous to the protein become bound to the iron at the sixth ligand [23].

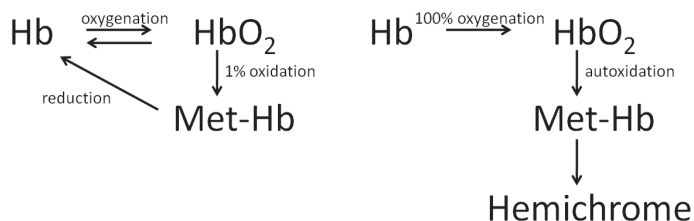


Figure 1. Simplified hemoglobin reaction kinetics inside the body (left hand) and reaction in bloodstains (right hand).

Figure 1 shows a schematic overview of the hemoglobin reaction kinetics, of both *in-vivo* and of extracorporeal blood. Since the absorption spectra of HbO₂, met-Hb, and HC differ from each other (see figure 2) this transition is accompanied by a color change from deep red to dark brown.

We will use DRS to monitor this chemical process in bloodstains and our research question is whether the fractions of the various hemoglobin derivatives allow estimation of the age of bloodstains under controlled environmental conditions.

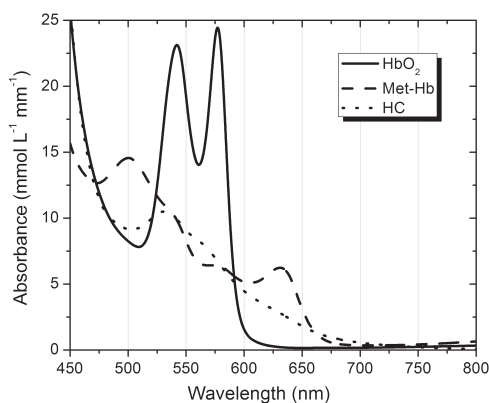


Figure 2. Absorption Spectra of the three hemoglobin derivatives used for the analysis of the bloodstain reflectance spectra. Data of the absorption spectrum of HbO₂ and met-Hb is from [70] and HC data from [32]. Isosbestic points of HbO₂ and HC at 525 nm and 585 nm are used to match the HC spectrum with the HbO₂ and met-Hb spectrum.

2. METHODS

2.1 Sample preparation

We created 40 bloodstains, five stains from each of eight healthy male volunteers. Two tubes (5 ml) of blood were drawn from the donors. One tube, with anti-coagulant, was sent to the hematology department for hematocrit determination and found to be 0.44 ± 0.02 . The second tube, without anti-coagulant, was used to create the bloodstains on white cotton, five stains per donor with a stain diameter of 21 ± 4 mm (see figure 3). The time between the donation of the blood and the creation of the bloodstain was less than 15 seconds. The temperature in the laboratory, monitored with an I-button (Maxim-DS1920) was stable at 22.3 ± 0.5 °C.

2.2 Non-contact Diffuse Reflectance Spectroscopy

The non-contact diffuse reflectance measurements were performed with a combination of a tungsten-halogen light source (Ocean Optics, DH-2000) and a reflection probe in fixed position containing six 400 μ m core diameter delivery fibers, circularly placed around a similar central collecting fiber. The probe was positioned perpendicular to and centered 1 cm above the surface. The illumination spot diameter was 5 mm. The collected light was back scattered into the central collection fiber and sent to a compact CCD spectrometer (Ocean Optics, USB 4000). First, a spectral measurement of a clean spot of the white cotton was taken for reference, R_0 . Thereafter, we measured the reflectance of the bloodstain, R . The ratio R/R_0 is the reflectance signal used for data analysis. In one measurement series we recorded the reflectance signal of all forty bloodstains. In the first ten days, we performed at least one measurement series per day. Thereafter, we measured every two days and after week four, every week. A total of 1412 reflectance spectra were measured in 60 days.

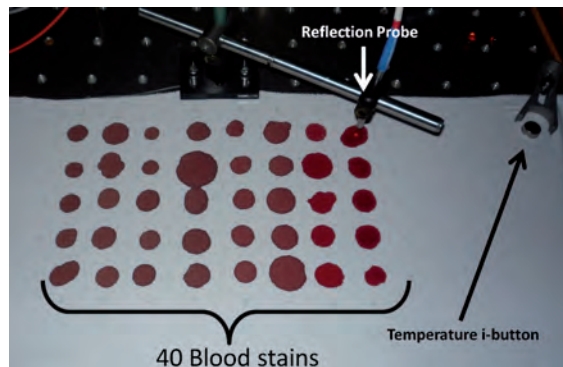


Figure 3. Experimental setup for measuring the bloodstains' reflectance spectra. The forty bloodstains are measured with the reflectance probe. Simultaneously the temperature was monitored with an i-button.

The reflectance spectra were recorded by 4096 pixels in the wavelength range 350–1050 nm; however the optical resolution of the spectrograph was 5 nm. Oversampling of the data was used by averaging data into bins of 10 pixels, which allows calculation of a standard deviation that represents noise within the signal.

2.3 Data Analysis

The two-flux solution of the general radiation transport theory was used to describe the diffuse reflectance signal. This theory is used to relate Kubelka Munk absorption and scattering coefficients with their transport theory equivalents [71-73]. It assumes that the sample possesses (i) inhomogeneities which are small compared to the sample thickness; (ii) that the light field is diffuse; and (iii) that reflections occurring at boundaries can be neglected. For bloodstain reflectance, all three conditions are met, since (i) inhomogeneities are caused by hemoglobin packaged in red blood cells which are much smaller than the bloodstain thickness; (ii) and (iii) are fulfilled when the bloodstain is created on a highly diffuse reflecting background, like cotton. The formulas that were used for the data analysis are given in appendix A.

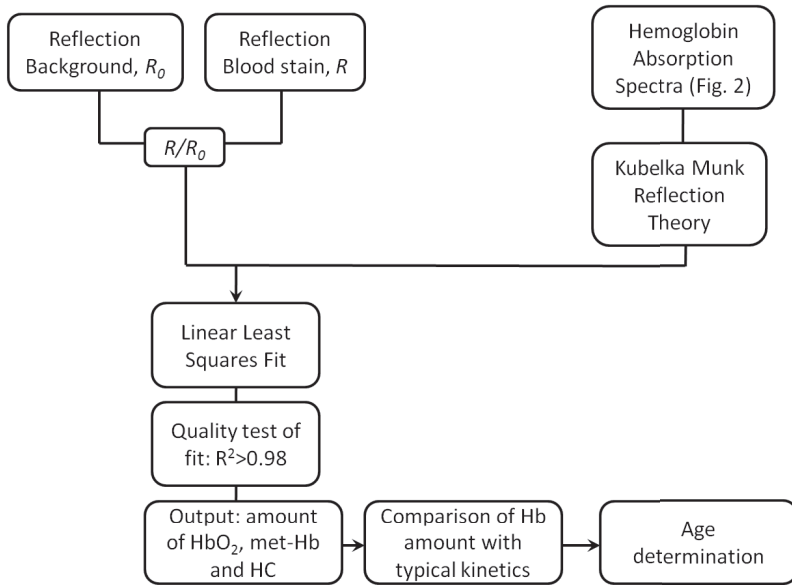


Figure 4. Flow chart of the various steps in data analysis: from bloodstain reflectance measurement to age determination.

The fractions of HbO₂, met-Hb and HC within the bloodstain were determined by performing a linear least squares (LLS) fitting algorithm between the Kubelka Munk theory, with the known absorption spectra [70], [32] of the three hemoglobin

derivatives (shown in figure 2) as input, and the bloodstain reflectance signal between 450-800 nm. Consequently, we had to account for scattering and spectral flattening. The latter was achieved by assuming chromophore packaging in the erythrocytes, with an erythrocyte radius of 3 μm [74]. To account for scattering by the erythrocytes, a Lorentz-Mie behavior was employed, see Appendix A.

The LLS fitting algorithm varies the amplitudes of the three absorption spectra in order to find the combination of the three with a minimum of difference between the spectrum of the three amplitude fractions and the diffuse reflectance spectrum. The LLS-fitting procedure yields the estimated fractions of HbO_2 , met-Hb and HC. Correct data analysis requires a high correlation between the reflectance signal and the LLS-fit. If the correlation is poor, overcompensation by one of the derivatives may occur, and the outcome of the fitting procedure becomes unreliable [75]. To prevent this, a quality test between data and fit is utilized and we only accepted LLS-fits with correlation coefficient $r^2 > 0.98$; which holds true for 91% of the measurements in this study. The 127 measurements with correlation lower than 0.98 were homogeneously distributed over the range of ages. Finally, all steps described above were scripted into Labview code (vers. 8.6 National Instruments). The data analysis is schematically drawn in a flow chart in figure 4.

2.4 Age determination

The bloodstain samples were divided into two equal subsets, according to the standard approach called one round cross-validation[76]. Accordingly we divided the total set of bloodstains into two groups: twenty bloodstains from four donors in the *training set* and twenty bloodstains from four other donors in the *age estimation set*. First, we determined the fractions of Hb, met-Hb and for all time points in the training set. These fractions averaged over the four donors constituted the lines of laboratory bloodstain calibration kinetics. Secondly, from the age estimation set of twenty bloodstains we also determined the fractions of hemoglobin, met-Hb and HC for all time points. These fractions of Hb, met-Hb and HC, determined at a certain time point, were matched to the laboratory calibration kinetics. The age at which the relative difference between the sum of the three measured fractions and the laboratory calibration kinetics was minimal is the estimated age of the bloodstain. Every measured bloodstain from the age estimation set provides a single estimated age. The range of estimated ages of all bloodstains measured at a single time point indicates the error margin of the age estimation.

3. RESULTS

3.1 Reflectance spectra of bloodstains

Figure 5 plots four typical reflectance spectra with corresponding blood component fit. Figure 5a shows a bloodstain one hour after deposition. The spectrum has two distinct dips, one at 540 nm and one at 576 nm, corresponding to the HbO_2 absorption spectrum (figure 2). This spectrum also has a very steep slope between 600 and 650 nm corresponding to the absence of met-Hb and HC. Figure 2b, at an age of one day, also shows dips in the reflectance spectrum at 540 and 576 nm, according to a large amount of HbO_2 , but the slope between 600 and 650 nm is not as steep as in the spectrum at $t=1\text{h}$. After one day, already a reasonable amount of HC has been formed. As the time increases, the dips in the reflectance spectra at 540 and 576 nm become smaller, and the slope between 600 and 650 nm becomes less steep, as is shown in figure 5c and 5d at ages of $t=7\text{d}$ and $t=63\text{d}$ respectively.

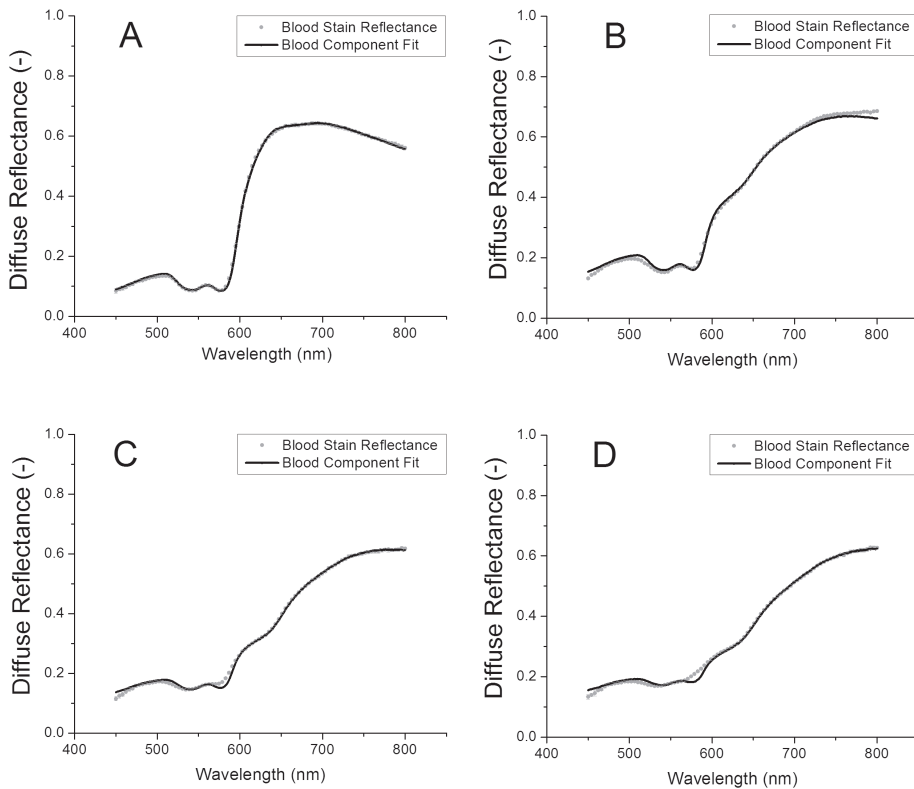


Figure 5. Four typical bloodstain reflectance measurements. A) age = 1h; B) age = 1d; C) age = 7d; D) age = 63d. The gray dots are the recorded reflectance spectrum, the solid black line is the blood component fit.

3.2 Hemoglobin reaction kinetics

Figure 6 plots the hemoglobin fractions of HbO_2 , met-Hb and HC as a function of time. The data points \pm SD are the average of twenty bloodstains from the training set, measured at that time point. The fractions of hemoglobin derivatives in bloodstains show a distinct temporal behavior. At $t=0$, all hemoglobin appears to be HbO_2 . After deposition of the bloodstains, the amount of HbO_2 decreases, and both met-Hb and HC are formed. The transition rate of HbO_2 into met-Hb and HC is at first rapid, but decreases as the bloodstain ages. HbO_2 shows a biphasic autoxidation curve. For $t < 10\text{d}$ the decay constant is larger than for $t > 10\text{d}$. This biphasic effect is also observed for autoxidation of HbO_2 in aqueous form [77].

The amount of met-Hb is zero at $t=0$, and increases slowly. However, the amount of met-Hb appears to be always smaller than the amount of HC. Met-Hb reaches a maximum fraction of 0.2 at an age of approximately 15 days and thereafter the amount decreases. We found that the sum of the three hemoglobin fractions remained approximately constant over the total time period and close to 1 (not shown). Hence, suggesting all HbO_2 is transformed into met-Hb and HC and no other derivatives are formed. At all moments, we found that a unique combination of these three hemoglobin derivatives exists, which can be utilized for age determination.

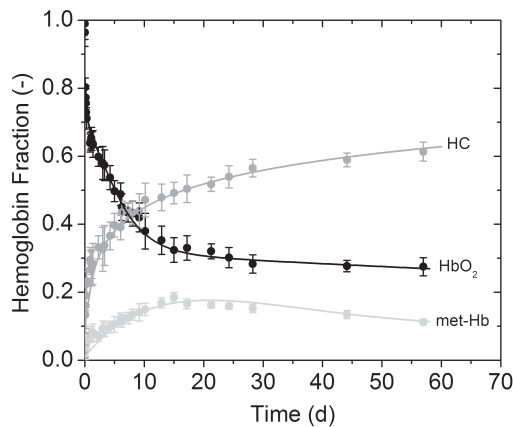


Figure 6. Average fractions of HbO_2 , met-Hb and HC for twenty bloodstains from training set. Error bars represent the standard deviation. Solid lines are smoothed average hemoglobin fractions.

3.3 Age determination

The average hemoglobin fractions, as a function of time are determined on the bloodstains from the training set and are shown as solid lines in figure 6. Subsequently figure 7 shows the comparison between the average hemoglobin fractions from the training set and all measured hemoglobin fractions for twenty bloodstains from the

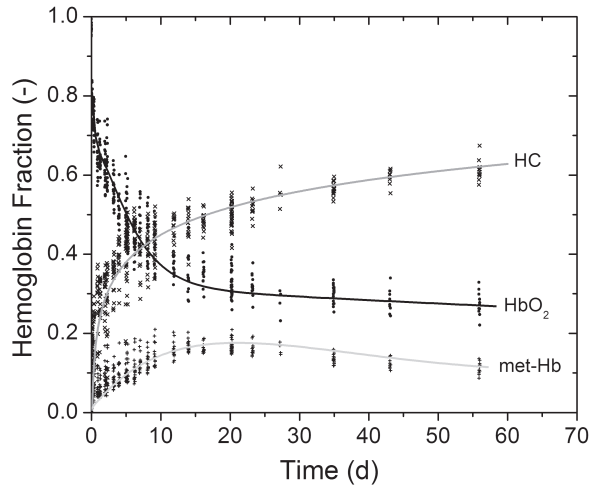


Figure 7. Combination of smoothed average hemoglobin fractions from training set (solid lines) and fractions of HbO₂ (dots), met-Hb (plusses) and HC (crosses) for twenty bloodstains from the validation set. The determined hemoglobin fractions from every bloodstain from validation set is plotted as a single data point.

validation set. The variation among bloodstains from the validation set is observed as the data scatters around the line representing the average hemoglobin fraction.

The estimated age of bloodstains from the validation set follow by comparing the measured hemoglobin derivative fractions with the lines of average fractions from the training set. Figure 8 plots the actual age of the bloodstain against the estimated age, based on the above described procedure. The age estimation satisfies over a wide range of ages (range: 0-60 days). However, the combination of biological variation and small

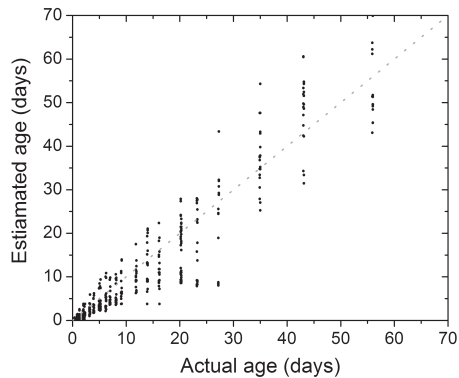


Figure 8. Age estimation of bloodstains of the validation set plotted versus actual age. Data points measured at the same time are scattered to various estimated ages, indicating the error margin of age estimation.

uncertainties in the measurement procedure cause uncertainty in age estimation, this effect is observable in the plot as the data scatters around the line of unity. Discrimination in age between bloodstains of different ages is possible, when the scattering range of the estimated ages do not overlap. To illustrate this, at an age of 3 days, the estimated ages vary between 1.5 and 6 days; at an age of 12 days, the estimated ages vary between 6 and 16 days; and at an age of 35 days, the estimated ages vary between 25 and 55 days. Hence discrimination of age among these three examples is possible

4. DISCUSSION AND CONCLUSION

We showed that age determination of bloodstains is feasible under controlled environmental conditions. The excellent short- and long-term fits (figure 5) of the DRS measurements in oxy-Hb, met-Hb and HC strongly suggests that the oxidation cascade of extracorporeal blood as well as the absorption spectra utilized for these derivatives at a large spectral range are essentially correct. Thus, the combination of oxidation cascade and optical DRS requires further consideration in pursuing age determination of bloodstains found under non-laboratory conditions and perhaps even on crime scenes.

The division of the bloodstains samples into two groups allowed for independent determination of average hemoglobin reaction kinetics and age estimation, according to one round cross-validation[76]. Determination of the average kinetics based on the total sample size of 40 bloodstains, instead of only 20 does not change the average hemoglobin fractions very much, e.g. the average HbO₂ fraction after 1 day for 20 bloodstains is 0.65 ± 0.02 and for 40 bloodstains 0.66 ± 0.02 ; and the HbO₂ fraction after 17 days for 20 bloodstains is 0.33 ± 0.04 and for 40 bloodstains 0.33 ± 0.03 . Alternative method for age determination would be the leave-one-out (n-fold cross-validation) approach, but this approach requires much more calculation and will not improve the age estimation, considering the small differences between average hemoglobin fractions based on 20 or 40 bloodstains.

Our simultaneous measurements of 40 stains required displacement of the probe. For all measurements we kept the probe in same configuration at 10 ± 1 mm height and perpendicular to the surface. In additional serial experiments on one stain with the probe in fixed position over the total measured time period (not shown), we found similar hemoglobin kinetics, but with much lower spreading of data. Thus, in a forensic situation, multiple consecutive measurements can be performed, which allow determination of the hemoglobin fractions and the *in situ* hemoglobin kinetics. Hence evolving age estimation, based on multiple measurements can be more precise than shown in this study.

Owing to the capillary flow [78], the edge of a bloodstain appears slightly darker and thus contains more chromophores. Although this effect is very limited in bloodstains on cotton; we measured the reflectance at the center of the bloodstain. Inhomogeneities within a bloodstain or small bloodstains can still be accounted for when a spectral imaging setup is used. This technique has also been suggested for age determination

of bruises [79] and would be a suited technique for age determination of bloodstains as well.

The diffuse reflectance spectroscopy setup is portable, cheap and non-invasive and non-destructive, all favorable properties when measuring in a forensic setting [62]. However, prior to forensic implementation, we believe that knowledge of the reaction rates of HbO₂ to met-Hb and HC as a function of temperature, humidity and e.g. exposure to sun light needs to be attained and incorporated in the optics analysis. In addition, also the influence of the surface background of the bloodstain on DRS requires further study.

In conclusion, our results suggest that determination of hemoglobin derivatives by means of diffuse reflectance spectroscopy demands further consideration in pursuing for age determination of bloodstains under non-laboratory, forensic conditions. Successful age determination at crime scenes requires more knowledge of the kinetics of the Hb cascade under environmental conditions and their incorporation in the optics analysis method.

APPENDIX A

The Kubelka Munk theory was employed to analyze the recorded diffuse reflectance spectra described in the data analysis section. We used the following formulae:

$$\frac{R(\lambda)}{R_0(\lambda)} = 1 - \frac{K}{S} \left(\sqrt{1 + \frac{2S}{K}} - 1 \right) \quad (1)$$

Here $R(\lambda)$ denotes the bloodstain's reflectance, and $R_0(\lambda)$ is the reflectance of the white substrate surface, both depend on wavelength λ . K and S represent the absorption and scattering of the bloodstain. Here $K = \mu_a / \eta$, with μ_a the absorption coefficient per unit length which depends on wavelength and η being a dimensionless function depending on albedo. Because the chromophores are packed in red blood cells, the absorption spectra as shown in figure 2 are flattened. We corrected for this flattening effect, as described by Finlay and Foster[74], with an erythrocyte radius of 3 μm .

This relation is described in detail elsewhere [71], [73]. For scattering S we assumed Lorentz-Mie scattering:

$$S = S_0 \cdot \left(\frac{\lambda}{\lambda_0} \right)^{-0.4} \quad (2)$$

The scattering S depends on the wavelength λ in nm, λ_0 is 450 nm and the scattering coefficient at 450 nm, S_0 is 13.5 mm^{-1} . We set the scattering to be constant over the total measured time period.

Blood detection and identification at crime scenes are crucial for harvesting forensic evidence. Unfortunately, most tests for identification of blood are destructive and time consuming. We present a fast and non-destructive identification test for blood, using non-contact reflectance spectroscopy. We fitted reflectance spectra of 40 bloodstains and 35 non-bloodstains deposited on white cotton with spectroscopic features of the main compounds of blood. Each bloodstain was measured 30 times to account for ageing effects. The outcome of the blood measurements was compared with the reflectance of blood mimicking stains and various body fluids. We found that discrimination between blood and non-blood deposited on white cotton is possible with a specificity of 100% and a sensitivity of 98%. In conclusion, a goodness of fit between the sample's reflectance and the blood component fit may allow identification of blood at crime scenes by remote spectroscopy.

CHAPTER 3

REMOTE SPECTROSCOPIC IDENTIFICATION OF BLOODSTAINS

Journal of Forensic Science 2011, in print



INTRODUCTION

Identification of bloodstains at a crime scene is of critical importance in criminal investigations. Ideally, traces are judged and interpreted in the original context, at the crime scene [62]. Thus, there is a need for techniques that allow for remote, non-contact identification of evidence. Many screening tests, routinely used in forensic practice, use chemical methods for identification of blood to discriminate it from other body fluids or red substances. Most chemical tests, including tetra-base [80] and Kastle-Meyer [81] employ peroxidase activity of hemoglobin molecules. The peroxidase either causes a color change or induces chemiluminescence. A common example of the latter is the luminol test. By spraying luminol onto the suspected area, the reactant will glow in the presence of blood [82]. This test is especially appropriate for indicating bloodstains after cleaning attempts. Most of these tests are presumptive in nature, not confirmative, since several other substances are reported to catalyze this peroxidase reaction [83]. More reliable, confirmatory tests are based on hemoglobin derivative crystals [84, 85] or RNA markers in blood [86]. However, these tests require advanced sample preparation and microscopic observation, and are therefore not applicable for interpreting traces in its original context, at the crime scene.

Recently, however, optical techniques have been suggested for bloodstain identification. Hemoglobin has specific absorption bands at 420, 540 and 576 nm [31]; it fluoresces at 465 nm, when excited at 321 nm [87]; and heme provides Raman-bands at 1.222 and 1.542 cm^{-1} [88]. All these corresponding techniques have the potential to allow *on field* identification of blood based on the specific spectroscopic features of hemoglobin [88, 89]. Despite promising results, these techniques have not been reported to be implemented in forensic practice. Accordingly, all these techniques have their own drawback. Measuring Raman signals is highly complicated by interference with the fluorescence signal of the trace and its background. A fluorescence signal on its turn is difficult to measure, because of the high absorption properties of hemoglobin in the UV/VIS spectral range. Blood identification based on the absorption properties has been investigated by Kotowski *et al* in a microspectrophotometry setup [90]; De Weal *et al* recently confirmed these findings [89]. Their approach however, requires advanced sample preparation and a laboratory environment for accurate measurements.

We propose a non-destructive and non-contact reflectance spectroscopy technique for the identification of bloodstains, which can be used at the crime scene. Reflectance spectroscopy is a widely used technique to determine the optical properties of turbid materials. Based on spectroscopic analysis of the reflected light, tissue chromophore concentrations can be estimated. In bloodstains, mainly three compounds are present, oxy-hemoglobin, methemoglobin and hemichrome [23]. In chapter 2 we showed that fitting the absorption spectra of the hemoglobin compounds to the measured reflectance spectrum allows determination of the compound fraction estimation of the age of a bloodstain. The goodness of fit between the absorption spectra reported in literature and the measured bloodstain can be expressed in a Pearson correlation coefficient.

In this experiment we have investigated whether blood can be discriminated from other body fluids and substances visually mimicking blood, based on the correlation coefficient between the reflectance spectrum and a blood-component fit. To test the sensitivity and specificity of this method two sets of samples are analyzed: a set of blood samples and a set of red/brown colored substances and various body fluids. Finally, an example is given of a recent forensic case, in which our technique was applied.

MATERIALS AND METHOD

Sample preparation

Forty blood samples were obtained from eight healthy male donors. These samples were prepared by depositing a small drop on a piece of white cotton, creating a stain with a diameter of 21 ± 4 mm. We performed 1200 measurements on the forty blood samples; thirty measurements per sample in the time span from a few seconds after deposition until a year after deposition. When not being measured, the bloodstains were stored in a dark laboratory at 22.3 ± 0.5 °C, up to a year.

The second set contained 35 non-blood samples. Among the samples are 31 samples visually mimicking blood, including ketchup, red wine and fake blood; and four body fluids commonly found at crime scenes: saliva, semen, urine and perspiration. These samples were created similarly to the bloodstains on a piece of white cotton.

Non-contact reflectance spectroscopy

Reflectance measurements were performed with a combination of a spectrograph (USB 4000; Ocean Optics; Duiven, the Netherlands), a tungsten-halogen light source (H-2000; Ocean Optics; Duiven, the Netherlands) and a non-contact probe (QR400-7-UV/BX; Ocean Optics; Duiven, the Netherlands). This probe contains six 400 μ m core diameter delivery fibers, circularly placed around an identical central collecting fiber. Figure 1 shows the schematic of the setup. The probe is positioned 1 cm above the specimen. During measurements, photons emitted by the delivery fibers scatter through

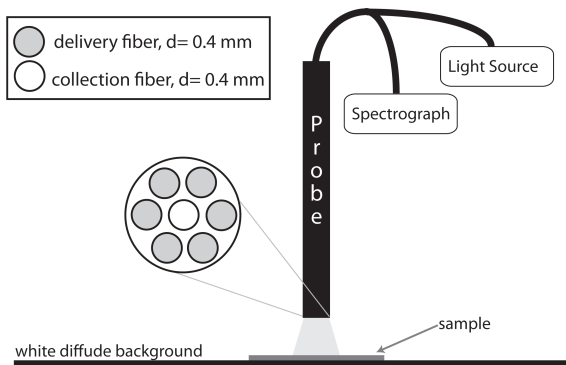


Figure 1. Schematic of the measurement setup. The reflection probe tip shows six delivery fibers, circled around a central collection fiber. The delivery fiber is connected to the light source and the collection fibers are connected to the spectrograph.

the sample, and are collected with the central fiber. The light intensity measured with the collection fiber is the reflectance $R(\lambda)$, which is wavelength (λ) dependent. For each measurement a reflectance spectrum of the sample, $R(\lambda)$ and a reflectance spectrum of the background material (cotton), $R_0(\lambda)$ was obtained.

Analysis of reflectance spectrum

The reflectance ratio of the sample and its background $R(\lambda)/R_0(\lambda)$ were analyzed with a multi-component linear least squares fit. The absorption spectra of the three compounds present in blood: oxy-hemoglobin, met-hemoglobin and hemichrome[23] were used as input. A light transport model was employed to translate the absorption spectra into a reflectance spectrum, which is described in the appendix. The fitting algorithm varies the amplitudes of the three absorption spectra, in order to find the combination of the three with a minimum of difference between the theory and the diffuse reflectance spectrum.

Coefficient of determination

The Pearson correlation coefficient gives information about the goodness of fit between the measured reflectance spectrum and the multi-component blood-fit [91]. The coefficient of determination, r^2 , is the square of Pearson's correlation coefficient. When blood is present and the light transport model is correct, the coefficient of determination between the blood-fit and the specimen will be high and approach one. The r^2 value of all reflectance measurements has been calculated and tested for discrimination between blood and non-blood samples.

ANOVA-test

One way ANOVA tests are performed on the blood samples to test on differences within the total bloodstain population. Three individual, one way ANOVA tests are taken on samples ($n=40$), donors ($n=8$) and ageing. For ageing testing, we grouped the bloodstains in four categories: age < 1 day; 1 day < age < 1 week, 1 week < age < 1 month and age > 1 month. Significance is defined if $p < 0.05$.

RESULTS

Blood samples

The upper part of figure 2 shows two typical diffuse reflectance spectra of blood samples: of one day old (figure 2a) and a year old (figure 2b). The spectrum in figure 2a shows two distinct dips, one at 540 nm and one at 576 nm, corresponding to the oxy-hemoglobin absorption spectrum [31]. The calculated coefficient of determination between the blood reflectance spectrum and the blood component-fit is very high: $r^2=0.996$. The spectrum of figure 2b has fewer features than figure 2a, because of the nature of the absorption spectrum of hemichrome, the main component of old blood.

The reflectance spectrum of all blood samples was obtained and all corresponding coefficients of determination were calculated. For the total of 1200 measurements we found $r^2=0.986\pm 0.012$.

Three one-way ANOVA tests were performed to test on differences in sample, donor and ageing. The outcome of the tests show that at a 0.05 level, no significant difference is found among sample variation (F-value = 0.8014, prob >F = 0.8040) and donor variation (F-value = 0.8215, prob >F = 0.569). However, for ageing, a significant difference is found (F-value = 64.4, prob >F = 0). For both ages smaller than one day and ages between a day and a week $r^2=0.99\pm 0.01$; for ages between a week and a month and older than one month $r^2=0.98\pm 0.01$. This difference in r^2 -value between stains measured within a week and after a week of deposition is found significant at a 0.05 level.

Non-blood samples

The lower parts of figure 2 show two typical reflectance spectra of blood mimicking samples: ketchup (figure 2c) and lip-gloss (figure 2d). The agreement between the reflectance spectrum of ketchup (Albron; The Netherlands) and the blood-fit is poor, especially for $\lambda < 600$ nm, resulting in a relatively low coefficient of determination:

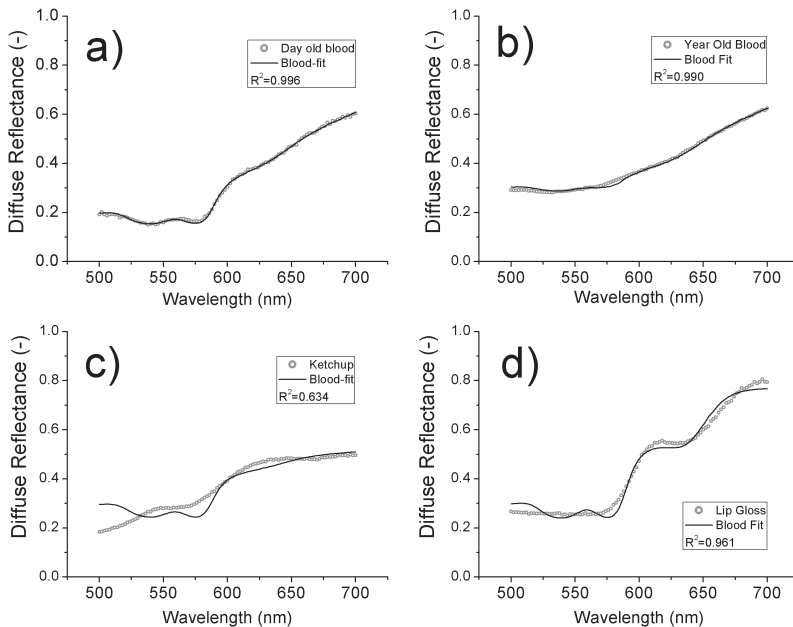


Figure 2. Diffuse reflectance signal (gray dots) with corresponding blood-fit $R(\lambda)/R_0(\lambda)$ (black line). Four typical measurements are shown: a) a blood sample of one day old with $r^2=0.996$; b) a blood sample of one year old with $r^2=0.990$; c) a non-blood sample with relative low correlation: ketchup, $r^2=0.634$; d) a non-blood sample with relative high correlation: lip gloss, $r^2=0.961$.

$r^2=0.634$. The agreement of the reflectance spectrum of lip-gloss (Brown Lipgloss, Etos; The Netherlands) and the blood-fit is relatively high: $r^2=0.961$. This high r^2 -value is because of a shouldered feature in the reflectance spectrum of Lip-gloss around $\lambda=630$ nm. This feature is also found in the absorption spectrum of met-hemoglobin, one of the main compounds present in bloodstains. However, for $\lambda < 600$ nm the reflectance spectrum of lip-gloss differs distinctively from the blood-fit since the characteristic dips of oxy-hemoglobin around 540 nm and 576 nm are absent in the Lip-gloss reflectance. Nevertheless, this particular Lip-gloss scored the highest r^2 -value of all non-blood samples. For the total population of 35 non-blood samples $r^2=0.67\pm 0.21$ was found.

Coefficients of determination

Figure 3 shows the coefficients of determination of four typical bloodstains samples and all measured non-blood samples. The blood samples, colored in black in figure 3, have the following coefficients of determination: immediately after deposition, $r^2=0.997$; after one day: $r^2=0.996$; after one month: $r^2=0.982$ and after one year: $r^2=0.984$. The non-blood samples are colored in gray. The non-blood samples with highest r^2 are colored lip gloss: $r^2=0.961$ and red wine: $r^2=0.954$. Non-red body fluids, shown on the right side of figure 3, score low correlations, saliva: $r^2= 0.199$, semen: $r^2=0.476$ perspiration: $r^2=0.669$ and urine: $r^2= 0.381$. The patterned column on the far right resembles the measured r^2 of the case study, which will be discussed below in paragraph 4.

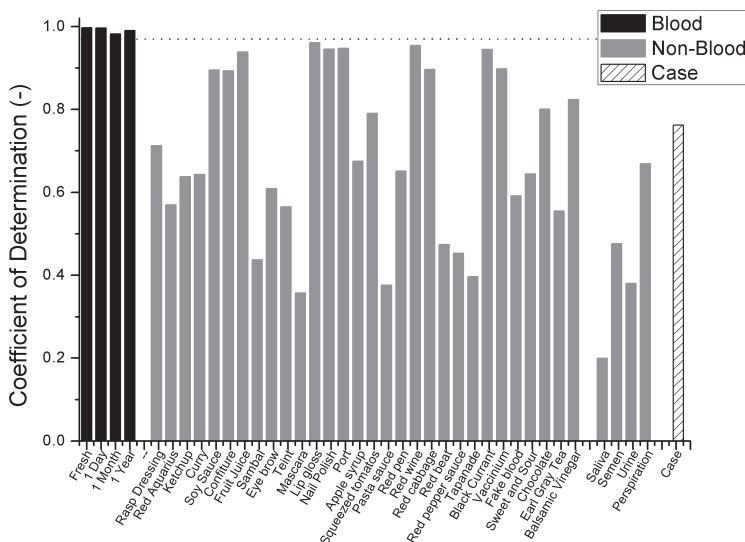


Figure 3. Column plot of coefficients of determination of four typical blood samples (black), all non-blood samples (gray) and case study (patterned).

Figure 4 plots the distribution of the obtained r^2 -values for all samples. The box plot shows the distribution of 25%, 50% and 75% of the samples, the whiskers show 1% and 99% of samples. The vertical axis of figures 4 plots 1- coefficient of determination on a logarithmic scale to enable visualization of the distribution in both blood and non-blood samples.

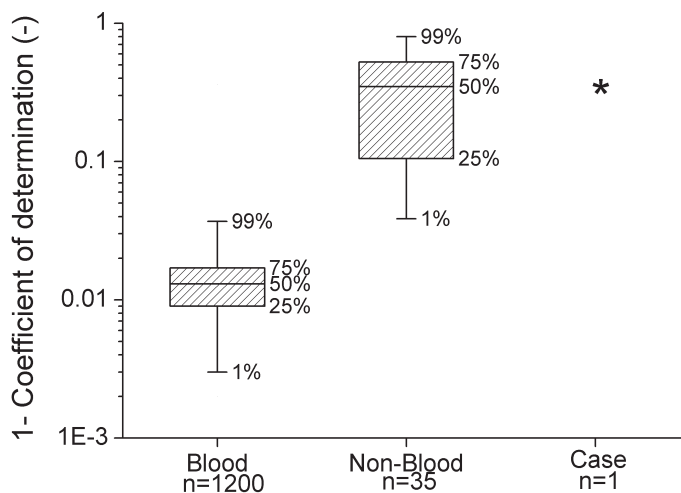


Figure 4. Box plot of the distribution of observed coefficients of determination of all blood measurements ($n=1200$) and all non-blood samples ($n=35$). On the right the outcome of the case example.

Case Example

The method presented in this paper was applied for investigational purposes in a case where someone was suspected of multiple burglary cases. The paint can found at one of the crime scenes contained latent traces of a fingerprint, possibly printed in blood. Confirmation or exoneration was crucial for the processing of this particular crime. Figure 5 shows a photograph of the object found at the crime scene. We obtained a diffuse reflectance spectrum of the object and found an r^2 -value of 0.672, indicative of a non-blood material.

To verify the optical identification for this case example, an additional tetrabase test [80] was performed on the same spot. Tetrabase tests are routinely used in forensic practice. According to the instructions, filter paper was swept onto the paint can. Thereafter the filter paper was treated with the tetrabase chemicals. The filter paper did not color up after deposition of the tetrabase, indicating no presence of blood on the paint can. The tetrabase test was performed twice, once with dry filter paper, and once with wet filter paper. The results of these tests are in agreement with the outcome of the spectroscopic identification.

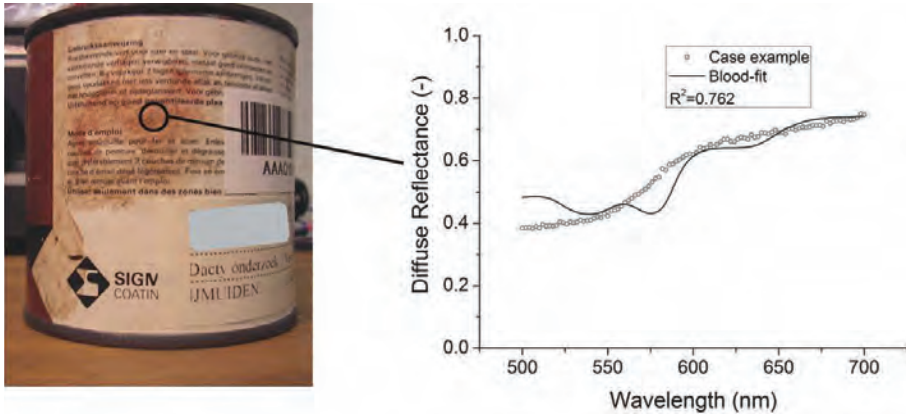


Figure 5, Left: Photograph of paint can of interest for blood test. The black line with open circle shows the spot where the reflectance spectrum is recorded. Right: Diffuse reflectance signal with corresponding linear least squares fit.

DISCUSSION AND CONCLUSION

We report on a remote blood identification test which is fast, non-destructive and applicable on crime scenes. We showed that discrimination between blood and non-blood samples is possible, based on the coefficient of determination between the sample's reflectance spectrum and a multi-component blood-fit. For blood samples $r^2=0.986\pm 0.012$ and for non-blood samples $r^2=0.67\pm 0.21$. Discrimination between blood and non-blood is possible by setting the threshold at $r^2=0.97$. No non-blood samples were reported with $r^2>0.97$ and only 1.9% of the blood samples were found to have $r^2<0.97$. Equally important, an ANOVA-test showed no significant differences between bloodstains from various samples or from various donors. A small significant difference was found among bloodstains, when tested on age of the bloodstains. Yet, these differences did not hamper discrimination between blood and non-blood samples.

For every sample the reflectance ratio of the sample and its background $R(\lambda)/R_0(\lambda)$ was analyzed, with typical examples shown in figure 2. To this, a reflectance spectrum of the background material, $R_0(\lambda)$ was obtained. All measurements in this study were performed on samples deposited on white cotton. Samples deposited on a non-white substrate require a more sophisticated optical sampling and analysis method. For application in forensic practice the influence of background color has to be evaluated. A possible suggestion to overcome the drawback of background color is the use of a hyper-spectral imaging system [63]. Spectral imaging allows imaging of the crime scene and chemical analysis of the imaged object. Although this approach is beyond the scope of this study, it is an interesting topic for future research.

Figure 3 shows the wide variation of non-blood samples investigated. The outcome of coefficients of determination of some samples is remarkable: for instance, visually well

mimicking samples like fake-blood (Vampire in a box, Running Press) scores a relatively low $r^2=0.59$, while lip gloss (Brown Lipgloss, Etos; The Netherlands) scores exceptionally high: $r^2=0.96$. The high correlation of Lip-gloss suggests room for improvement in the fitting procedure for future work. Figure 4 plots the distribution of all samples and enables differentiation between blood and non-blood samples. By setting the threshold at $r^2=0.97$, a specificity of 100% of the investigated samples is realized, combined with a sensitivity of 98%. A higher sensitivity can be obtained by lowering the threshold; however lowering the threshold will decrease the specificity as well.

In conclusion, we showed that discrimination between blood and non-blood sample on white cotton is possible with non-contact spectroscopy. The high sensitivity and specificity indicate that this optical test is close to confirmative. Our blood identification test was successfully applied in a forensic case example. However, before further forensic implementation, future research on colored substrates with various structures can be recommended.

APPENDIX

For analysis of the sample's reflectance, we used Kubelka Munk's theory of reflectance:

$$\frac{R(\lambda)}{R_0(\lambda)} = 1 - \frac{K}{S} \left(\sqrt{1 + \frac{2S}{K}} - 1 \right) \quad (1)$$

Here $R(\lambda)$ denotes the sample's reflectance, and $R_0(\lambda)$ is the reflectance of the white substrate. K and S represent the absorption and scattering coefficients. For a blood component fit we take K being the sum of the absorption spectra of oxy-hemoglobin, met-hemoglobin and hemichrome. Because these chromophores are packed in red blood cells, the absorption spectra are flattened. We corrected for this flattening effect, as described by Finlay and Foster[74], with an erythrocyte radius of 3 μm . For scattering S we assumed Lorentz-Mie behavior as function of wavelength λ : with scattering power of -0.4 : $S=(\lambda/\lambda_0)^{-0.4}$, with $\lambda_0=450$ nm.

We report on a non-contact method to quantitatively determine blood volume fractions in turbid media by reflectance spectroscopy in the VIS/NIR spectral wavelength range. This method will be used for spectral analysis of tissue with large absorption coefficients and assist in age determination of bruises and bloodstains. First, a phantom set was constructed to determine the effective photon path length as a function of μ_a and μ_s on phantoms with an albedo range: 0.02-0.99. Based on these measurements, an empirical model of the path length was established for phantoms with an albedo > 0.1 . Next, this model was validated on whole blood mimicking phantoms, to determine the blood volume fractions $\rho=0.12-0.84$ within the phantoms ($r=0.993$; error $< 10\%$). Finally, the model was proved applicable on cotton fabric phantoms.

CHAPTER 4
**NON-CONTACT SPECTROSCOPIC DETERMINATION OF LARGE BLOOD
VOLUME FRACTIONS IN TURBID MEDIA**

Biomedical Optics Express, Vol. 2, Issue 2, pp. 396-407 (2011)



INTRODUCTION

Optical measurements of biological media (e.g. whole blood or tissue) can be used to estimate physiological or morphological parameters of the sampled medium. Therefore, reflectance spectroscopy is a widely used technique to determine the optical properties of turbid media. Classical reflectance probe geometries involve contact between the probe and tissue. However, some applications in the forensic and clinical fields favor, or even require, no contact with the sample during measurement.

In forensic science, age determination of bloodstains can be crucial in reconstructing crime events. Upon blood exiting the body, hemoglobin saturates with oxygen in the ambient environment. Over time, the oxyhemoglobin auto-oxidizes into methemoglobin, and finally methemoglobin denaturates into hemichrome [23]. This oxidation cascade is typical for extracorporeal blood and the state of oxidation indicates the age of the bloodstain. Discrimination between these hemoglobin derivatives requires sampling in the wavelength range where these chromophores can be distinguished on the absorption properties, which is in the spectral range 450–650 nm. Despite several attempts [19, 35, 58], currently no reliable methods are available for determining the age of a bloodstain. In chapter 2, we showed that reflectance spectroscopy is a suitable candidate for age estimation, by determining the composition of various hemoglobin compounds in a bloodstain. Reflectance spectroscopy has the potential to detect the unique absorption bands of each of the heme-containing compounds, and potentially provide age-information about the bloodstains. In order to avoid contamination and cross-contamination and preserve the original crime scene [62], the measurement ideally must be made without contacting the sample.

Recent studies have shown the potential of non-contact reflectance spectroscopy for PDT monitoring [92, 93], monitoring apoptosis [94] and lung cancer detection [95]. These applications of spectroscopy do not require quantitative analysis of the reflectance spectra. Yu *et al* [96] and Saager *et al* [97] have shown a quantitative non-contact system, but their approaches require lenses, complicated scanning and only have small working distance, moreover not very applicable on crime scenes. In addition, those systems can only measure absorption coefficients up to 0.3 mm^{-1} , not high enough to measure the absorption coefficient of whole blood in the VIS/NIR spectral range. An alternative approach to non-contact spectroscopy is hyper-spectral imaging, but most spectral imaging systems are also only suitable in the low absorption regime [98].

Quantitative analysis of reflectance spectra is complicated because the path travelled by collected photons depends on the optical properties of the sampled medium. Yet by establishing a relation between the absorption and scattering properties of the sample and the photon path length, the chromophores and photon path length can be determined simultaneously. For measurements of extracorporeal blood, bruises [99] or other tissue containing large blood volume fractions, a reflectance spectrum in the visible, near-infrared wavelength region can cover an extreme range of absorption coefficients, $\mu_a = 0.1\text{-}30 \text{ mm}^{-1}$ [31]. Reflectance analysis techniques that are based on the diffusion

approximation [100] are not *a priori* applicable to these measurements as diffusion theory requires $\mu_s' \gg \mu_a$. Many more (semi-) empirical models have been reported in literature for quantitative analysis of reflectance spectroscopy measurements in contact mode [101-104]. Although these studies describe reflectance analysis methods, none has proven applicable on large absorption coefficients. However, recent studies have shown that quantitative analysis of reflectance spectra is achievable if the relationship between the photon path length and optical properties are well-defined [105-107].

This study presents a method for a quantitative determination of μ_a by analysis of non-contact reflectance measurements containing high absorption values. The difficulty and novelty of this work is combining non-contact, high absorption and quantitiveness. A quantitative method is required for measuring perfusion or blood volume fraction in a bruise, non-contact is required for avoiding contamination in case of a bloodstain; and high absorption is required considering the high absorption coefficients of whole blood in the visible part of the spectrum. This work investigates the sensitivity of the detected attenuation in the reflectance signal to the probe position and orientation to the measured sample. By mixing Intralipid 20%, a saline solution and Evans Blue, phantoms with a wide range of optical properties were constructed. Following the approach of Kanick *et al* [105, 106], we measured optical phantoms to construct an empirical model of the non-contact reflectance photon path length dependence on the absorption coefficient and reduced scattering coefficient of the optically sampled medium. The model of path length is utilized on whole blood mimicking phantoms for a spectral analysis algorithm to quantitatively determine chromophores concentrations. Finally the model is tested feasible for reflectance measurements on cotton fabric.

METHODS

Non-contact reflectance spectroscopy

The reflectance measurements were performed with a device composed of a spectrograph (USB 4000; Ocean Optics; Duiven, the Netherlands), a tungsten-halogen light source (HL-2000; Ocean Optics; Duiven, the Netherlands) and a non-contact probe (QR400-7-UV/BX; Ocean Optics; Duiven, the Netherlands). This probe contains six 400 μm core diameter delivery fibers, circularly placed around an identical central collection fiber. The core-to-core fiber distance is 450 μm , and the fiber has an NA of 0.22. The illumination spot size diameter is 6 mm, which realizes an overlap between illumination field and detection field. Figure 1 shows the schematic of the setup. The probe is positioned above the phantom, such that the probe angle α , and probe height h can be controlled. Only photons that have travelled through the phantom are considered useful, therefore specular reflection should be avoided. During measurements, photons emitted by the delivery fibers scatter through the phantom, and are collected with the central fiber. The light intensity measured with the collection fiber is the reflectance $R(\lambda)$, which is wavelength (λ) dependent. Attenuation

of R by the presence of chromophores can be described using an application of the Beer Lambert law, as follows:

$$R(\lambda) = R_0(\lambda) \exp[-\mu_a^i(\lambda) \cdot c_i \cdot \tau(\mu_s', \mu_a)] \quad (1)$$

In Eq. (1) R_0 is the reflectance of the phantom without the presence of absorbers. The specific absorption coefficient $\mu_a^i(\lambda)$ ($\text{l}\cdot\text{g}^{-1}\cdot\text{mm}^{-1}$) depends on wavelength, whereas c_i is the concentration of chromophore i ($\text{g}\cdot\text{l}^{-1}$). Finally, $\tau(\mu_s', \mu_a)$ is the effective path length (mm) of collected photons, which depends on μ_s' and μ_a of the phantom, and in turn, is wavelength-dependent.

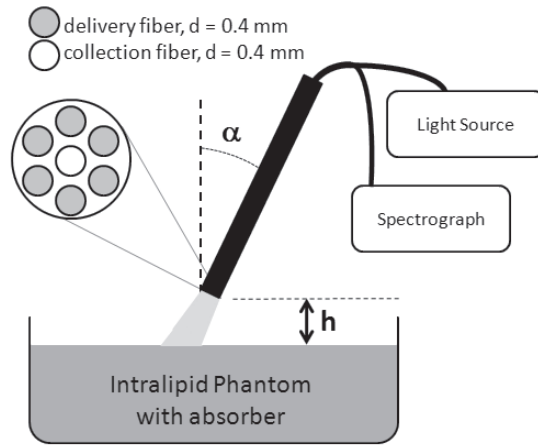


Figure. 1. Schematic of the non-contact reflection spectroscopy probe. The probe tip shows six delivery fibers, circulated around a central collection fiber. The delivery fiber is connected to the light source and the collection fibers are connected to the spectrograph.

Phantom preparation

This study involved three series of optical phantom experiments: 1) phantoms containing Evans Blue as an absorber; 2) phantoms containing hemoglobin for experimental validation of the analysis algorithm and 3) Evans Blue on cotton fabric.

For the first phantom series μ_a was controlled by varying the concentration of Evans Blue, which has a specific absorption maximum of $18 \text{ l}\cdot\text{g}^{-1}\cdot\text{mm}^{-1}$ at 611 nm. The μ_s' of each phantom was selected by varying the amount of Intralipid 20% (Fresenius Kabi AG, Bad Homburg, Germany), which has in undiluted form a reduced scattering coefficient, μ_s' of 18 mm^{-1} and an anisotropy of $g=0.75$ at 611 nm [108]. Estimations of reduced scattering coefficient for high Intralipid concentrations ($>8\%$) were corrected for dependent scattering effects[109]. Optical phantoms containing Evans Blue were constructed with absorption coefficients of $\mu_a = [0.1, 0.2, 0.4, 1, 2, 3, 5, 10, 20] \text{ mm}^{-1}$, at both $\mu_s' = 1 \text{ mm}^{-1}$ and at 11.5 mm^{-1} . Also a set was constructed with varying reduced scattering coefficients of $\mu_s' = [0.2, 0.5, 1, 2, 3.8, 5.5, 8.9, 11.5, 12.8, 13.6, 15.3] \text{ mm}^{-1}$,

at both $\mu_a=1 \text{ mm}^{-1}$ and at $\mu_a=10\text{mm}^{-1}$. The phantoms cover a range of albedo values, $A = \mu_s' / (\mu_s' + \mu_a) = [0.02-0.99]$. Additional phantoms were prepared at each selected μ_s' with no Evans Blue added, which were utilized to obtain baseline measurements of R_0 that represented $\mu_a=0 \text{ mm}^{-1}$ at 611 nm. For high reduced scattering, $\mu_s' > 2 \text{ mm}^{-1}$, each phantom was 40 mL and hold in cylindrical container with radius of 44 mm and height 7 mm. For low reduced scattering, $\mu_s' < 2 \text{ mm}^{-1}$, each phantom consisted of a 6-L sample hold within a 20-cm-edge cubed container. The large set of optical properties represents the wide range of absorption coefficients of bloodstains in the VIS/NIR wavelength region.

The second phantom series contained hemoglobin as the absorber. Aqueous hemoglobin was prepared by drawing human blood from a healthy, nonsmoking volunteer. The whole blood was washed by centrifuging the suspension at 2000 rpm, after which the supernatant was decanted. The remaining red blood cells (RBC) were resuspended with an amount of PBS equal to the decanted volume. This process was repeated twice. After the third time, when the supernatant was clear, the resuspension was performed with demineralized water for hemolysing the RBCs. The aqueous hemoglobin was removed from the suspension by centrifuging the suspension at 8000 rpm and decantation. In order to keep the amount of hemoglobin equivalent to the original blood volume fraction, the amount of resuspended liquid was kept equal to the amount of decanted liquid. The undiluted solution was assumed to have an amount of hemoglobin equivalent to a blood volume fraction, ρ , of 1; which corresponds to a hemoglobin concentration of 150 mg/ml and a molar concentration of 9.3 [mM] [110]. The phantoms were constructed with a range of absorption coefficients, equivalent to a blood volume fraction of $\rho = [0.84, 0.60, 0.47]$ for $\mu_s' = 3.5 \text{ mm}^{-1}$, $\rho = [0.75, 0.54, 0.42]$ for $\mu_s' = 6 \text{ mm}^{-1}$, $\rho = [0.50, 0.36, 0.28]$ for $\mu_s' = 10 \text{ mm}^{-1}$, and $\rho = [0.25, 0.18, 0.14]$ for $\mu_s' = 12 \text{ mm}^{-1}$. Additional phantoms were also prepared at each selected μ_s' with no hemoglobin added, to obtain baseline measurements of R_0 . The optical properties of the hemoglobin phantoms are chosen such that they fall with the range of optical properties of the Evans Blue phantoms. All Hb phantoms consisted of 40 mL and hold in cylindrical container with radius 44 mm and height 7 mm.

A third phantom series was made by pipetting aqueous Evans Blue onto white cotton fabric, creating stains with a diameter of 2.5 cm. After vaporization of the water, the reflectance of the white cotton fabric R_0 and the reflectance of the Evans Blue stain R were measured. We observed that the Evans Blue was distributed over a smaller area than the solvent. The absorption coefficient in the stain was estimated to be equal to absorption coefficient of aqueous Evans Blue, as measured by transmission spectroscopy, multiplied by the ratio of the areas of the stain without and with Evans Blue (see inset of figure 7 for a photograph of an Evans Blue stain on cotton). These areas were calculated by using a line gauge for measuring the radii of the stain without r_1 , and with Evans Blue r_2 . This introduces a potential error in estimation of the absorption coefficient; which will be addressed in the discussion section.

2.3 Analysis of photon path length

Eq (1) was used to describe the attenuation between spectra measured in phantoms with and without absorber present. The difference between the reflectance R , with absorber, and R_0 , without absorber, was attributed to the difference in absorption coefficient between the two samples. The reflectance was recorded at a resolution of 0.17 nm per pixel over a wavelength range of 450-900 nm. The data were smoothed by averaging data into bins of 10 pixels, which allowed the calculation of a standard deviation that represents noise within the signal. The effective photon path length for the Evans Blue phantom series was determined at 611 nm as shown in Eq. (2):

$$\tau_{611} = \frac{-\ln[R(611)/R_0(611)]}{\mu_a^i(611) \cdot c_i} \quad (2)$$

2.4 Empirical model of the photon path length

Based on observations of the effect of μ_a and μ_s' on the effective path length of the detected photons, and based on the photon path behavior for a single fiber geometry [105], the following empirical model for the effective path length was selected:

$$\tau_{\text{mod}}(\mu_s', \mu_a) = \frac{p_1(d \cdot \mu_s')^{p_2}}{p_3 + (d \cdot \mu_a)^{p_4}} \quad (3)$$

The empirical model Eq (3) has four fit parameters, two for the dependence on reduced scattering and two for the dependence on absorption. Here, the parameter set $[p_1, p_2, p_3, p_4]$ is fitted by minimizing the residual error between measured photon path length τ , and the predicted photon path length τ_{mod} . p_1 has units of mm, whereas p_2 - p_4 are dimensionless, finally d is a constant of unit length, set to be $d=1$ mm. The estimation of model parameters was achieved using a Levenberg-Marquardt fitting algorithm. The fit was weighted by the measured path length value at that point. The error margin on parameter estimation is represented by the 95% confidence intervals.

2.5 Spectral fit and determination of chromophore concentrations

Our observations on Evans Blue as absorber are employed for the phantoms with hemoglobin, which is more realistic for forensic applications. The attenuation of the reflectance signal with respect to the reflectance without absorber is the product of the absorption coefficient and the modeled photon path length. The total absorption is the sum of the three hemoglobin derivatives possible present in the phantom:

$$\mu_a = x_1 \cdot \mu_a^{\text{Hb}} + x_2 \cdot \mu_a^{\text{HbO}_2} + x_3 \cdot \mu_a^{\text{met-Hb}} \quad (4)$$

Knowledge of the absorption coefficients of deoxygenated, oxygenated, and met-hemoglobin for a large spectral range [31] enables a spectral fit. The spectral fit processes three fitted parameters. $[x_1, x_2, x_3]$ were obtained by reducing the weighted sum squared error between measured and model estimated reflectance. x_1 is the concentration of deoxygenated hemoglobin, x_2 is the concentration of oxygenated

hemoglobin, and x_3 is the concentration of met-hemoglobin. The total absorption μ_a is implemented in the empirical path length model, while the modeled effective path length τ is adjusted simultaneously as a function of the total absorption, according to Eq. (3). The total blood volume fraction is given as the sum of x_1 , x_2 and x_3 ; finally the oxygen saturation is given as: $x_2/(x_1 + x_2)$. The empirical model has an additional fit factor x_4 to correct mismatches in reflectance amplitude; typically these mismatches were less than 5%. Summarizing, the spectral fit for reflectance ratio of the empirical model is a combination of Eq. (3) and Eq. (4):

$$\frac{R(\lambda)}{R_0(\lambda)} = x_4 \exp\{-\mu_a \cdot \tau_{\text{mod}}\} \quad (5)$$

Eq. (5) has four fit parameters: $[x_1, x_2, x_3, x_4]$. Parameter estimation was achieved using a Levenberg-Marquardt algorithm that was scripted into LabView code (National Instruments); which allows for real-time fit parameter estimation. This model accounts for wavelength dependent scattering as an input into τ . In this study, μ_s' estimation was performed by relating it to the concentration of Intralipid as by Van Staveren [108].

RESULTS

3.1 Reflectance data

Figure 2 shows the reflectance ratio of an optical phantom of Intralipid with Evans Blue, R ($\mu_a=2.5 \text{ mm}^{-1}$ and $\mu_s' = 11.5 \text{ mm}^{-1}$) and a phantom of Intralipid without Evans blue R_0 ($\mu_a=0 \text{ mm}^{-1}$ and $\mu_s' = 11.5 \text{ mm}^{-1}$). At $\lambda=611 \text{ nm}$, Evans Blue has its absorption maximum, which is shown by the minimum in the reflectance ratio. At longer wavelengths, $\lambda>750 \text{ nm}$, Evans Blue does not absorb, so the reflectance ratio approaches 1. The effective photon path, τ of the collected photons with $\lambda=611 \text{ nm}$ from the measurement of Intralipid and Evans Blue can be calculated with Eq 2; here $\tau = 0.61 \text{ mm}$.

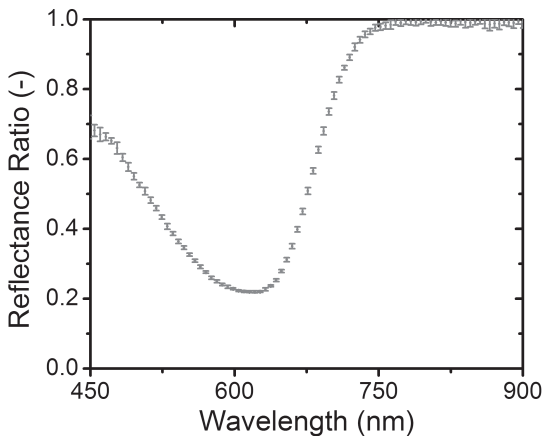


Figure 2. Reflectance ratio of phantom containing Evans Blue + IL and Intralipid without absorber. Only the reflectance ratio at $\lambda=611 \text{ nm}$ is used of the path length analysis. Here at $\lambda=611 \text{ nm}$, $\mu_a=2.5 \text{ mm}^{-1}$ and $\mu_s' = 11.5 \text{ mm}^{-1}$. The error margin represents SD.

By adjusting the height and the angle of the probe, the dependency of the effective photon path on the probe position could be determined. We found that for probe heights $h > 15$ mm, the variations in effective photon path length are below 3%. Also for $\alpha > 10^\circ$ the effective photon path length becomes insensitive for changes of probe angle, variations in effective photon path length on probe angle are below 2% for $\alpha > 10^\circ$. Based on these observations we use a probe geometry with a height $h = 17$ mm and an angle $\alpha = 13^\circ$ for the rest of the experiments.

3.2 Path length dependence on μ_a and μ_s'

Figure 3 shows the effective photon path length versus μ_a at high reduced scattering, $\mu_s' = 11.5 \text{ mm}^{-1}$, and at low reduced scattering, $\mu_s' = 1 \text{ mm}^{-1}$. The figure shows that the effective photon path length decreases for increasing absorption coefficient, both for high and low reduced scattering coefficient; an expected result as photons with longer path lengths are more likely to be absorbed, and therefore, less likely to be detected, resulting in the reduction of the path length. Figure 4 shows the effective photon path length versus μ_s' at high absorption, $\mu_a = 10 \text{ mm}^{-1}$, and at low absorption, $\mu_a = 1 \text{ mm}^{-1}$. At low absorption, the effective photon path length decreases for increasing reduced scattering. The effective photon path length is almost insensitive for changes in reduced scattering at high absorption. In both figure 3 and 4 the empirical path length model at our region of interest is plotted as a solid line.

The smallest residual error between measured data and model predictions resulted in the following estimated parameter values: $p_1 = 2.73 \pm 0.33$ mm, $p_2 = -0.32 \pm 0.03$, $p_3 = 0.22 \pm 0.11$, $p_4 = 0.68 \pm 0.06$. The empirical model shows good agreement with the measured data, as showed by the Pearson correlation coefficient: $r^2 = 0.997$. The empirical model holds over a wide range of optical properties and photon path lengths (range: 0.15 – 6.4 mm). However, attempts to construct a model for the total set were not successful. Therefore we had to excluding data points with albedo < 0.1 . The excluded regions of the model are plotted with a dashed line in figures 3 and 4.

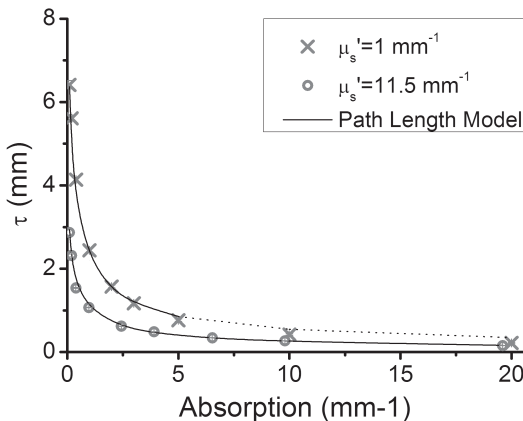


Figure 3. Effective photon path length vs absorption, the absorption coefficients was varied from $\mu_a = 0.1$ - 20 mm^{-1} ; measured at a reduced scattering coefficient of $\mu_s' = 1 \text{ mm}^{-1}$ (crosses) and $\mu_s' = 11.5 \text{ mm}^{-1}$ (open circles). The black line shows the path length model; dotted black line show model predictions for excluded data points.

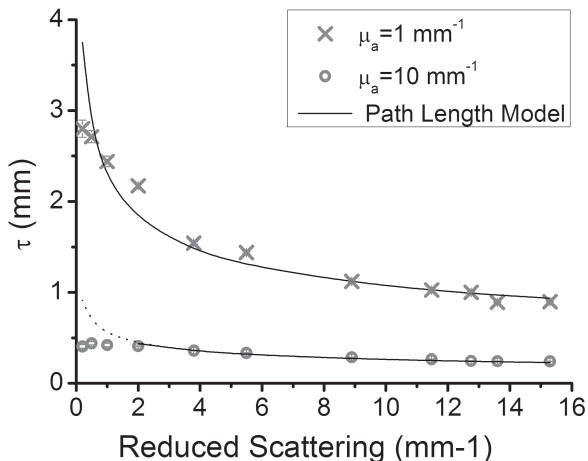


Figure 4. Effective photon path length vs reduced scattering. The reduced scattering coefficient varies from $\mu'_s = 0.2$ - 15.3 mm^{-1} . Measured at an absorption coefficient of $\mu_a = 1 \text{ mm}^{-1}$ (crosses) and $\mu_a = 10 \text{ mm}^{-1}$ (open circles). The solid line shows the path length model; dotted black line shows model predictions for excluded data points.

3.3 Hemoglobin Phantoms

Figure 5 shows the reflectance ratio of an optical phantom of Intralipid 10% with and without hemoglobin, for the spectral range of 450-900 nm. The gray dots represent the measured reflectance ratio, and the solid line is a spectral fit to model the reflectance measurement. The attenuation of the reflectance signal with respect to the reflectance without absorber is the product of the absorption coefficient and the modeled photon path, (Eq 3) with the parameter values as presented in section 3.2. The squared Pearson product correlation coefficient for the spectral fit is: $r^2=0.999$. The determined effective photon path through the phantom is shown on the right vertical axis. At $\lambda=576 \text{ nm}$, at the absorption maximum of HbO_2 , the effective photon path is 0.5 mm , whereas at $\lambda=675 \text{ nm}$, at which HbO_2 has an absorption minimum, light penetrates the optical phantom much deeper, accordingly $\tau = 4 \text{ mm}$.

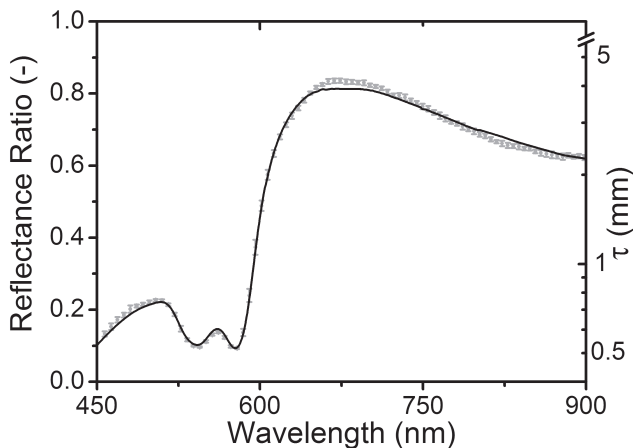


Figure 5. Typical reflectance measurements of an optical phantom containing of $\mu'_s = 10 \text{ mm}^{-1}$ at $\lambda=611 \text{ nm}$. The measured ratio is the ratio of the reflectance of an optical phantom with and without hemoglobin as absorber. Solid line is the spectral fit of the reflectance with HbO_2 ; $\rho=0.28$. The right hand axis shows the corresponding effective photon path through the phantom.

Figure 6 plots the measured blood volume fraction versus the experimental blood volume fraction. Model predictions were significantly correlated with measured values, as evidenced by a squared Pearson product correlation coefficient of $r^2 = 0.993$; this effect is observable in the plot as the data are scattered about the line of unity. The model holds for a wide range of blood volume fractions (range: 0.12-0.84) and absorption coefficients (range: 0.01-24 mm^{-1}), all with an albedo > 0.1 . The difference between input BVF and estimated BVF was less than 10% for all measurements. Model estimates of oxygen saturation, $x_2/(x_2+x_1)$ in Eq. (5), were determined to be close to fully oxygenated for all measurements: $99.6 \pm 0.9\%$ and no formation of methemoglobin was observed.

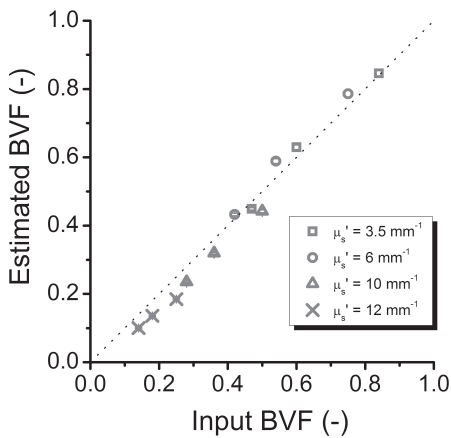


Figure 6. Optically estimated BVF, based on the spectral fits plotted against input BVF based on the phantom preparation for all twelve Hb phantoms at various reduced scattering coefficients.

3.4 Evans Blue on cotton

The effective photon path length as a function of absorption coefficient exhibits the same trend on cotton as in Intralipid: for increasing absorption, the photon path length decreases, which is shown in figure 7. The inset of figure 7 shows the radii of the stain, without and with Evans Blue, which is discussed at the end of the methods section. Determination of these radii and estimation of the absorption coefficient in the center of the stain introduces a potential error, which is depicted by the (horizontal) error bars in absorption coefficients. The effective photon path length is fitted by performing a non-linear least squares fit on Eq. (3) with only the reduced scattering coefficient of the cotton as fit parameter; other model parameters are based on the Intralipid measurements as presented in section 3.2. The fit is weighted by the inverse of the measurement error. We found: $\mu_s' = 53 \pm 31 \text{ mm}^{-1}$; here the error margins represent the 95% confidence interval of the fit. The origin of the large error margin will be addressed in the discussion.

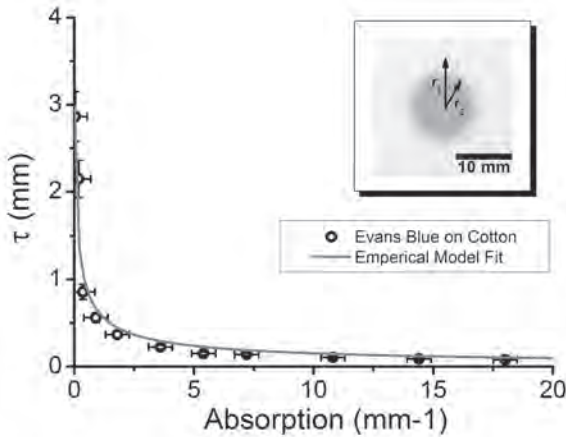


Figure 7. Effective photon path length vs absorption in white cotton fabric. The dots show the measured effective photon path length through Evans Blue and cotton. The blue line is the fit of the empirical path length. The inset is a photograph of the Evans blue on cotton showing the inner and outer radius of the stain, with and without Evans Blue.

DISCUSSION AND CONCLUSION

This study presents an analysis method that provides quantitative determination of μ_a for a non-contact reflectance spectroscopy device. Varying probe height and angle led to selection of probe setup that enables repeatable measurements, insensitive to small changes in height and angle. Observations of the dependency of the effective photon path length on the optical parameters of the tissue allowed implementation of an empirical model. The model gives a relation between μ_a and μ_s' of the phantom and the measured effective photon path length. Furthermore, the empirical model allows multi-component fit analysis of the reflectance spectra which enables quantitative chromophore determination. Conformation was found for the hemoglobin phantoms with a blood volume fraction of $\rho = [0.14-0.84]$. To the best of the authors' knowledge, this is the first time a non-contact device could quantitatively measure blood volumes over this wide range of optical properties and with μ_a up to 25 mm^{-1} .

Baseline measurements in this study were recorded using phantoms without the presence of absorbers. The baseline measurements account for the spectrum of the lamp, fiber through put, and need to be performed in similar probe configuration (height and angle) as the actual reflectance measurement. For application of measuring the reflectance of a bloodstain, baseline reflectance can be obtained by measuring the non-absorbing host matrix, such as cloth or paper. Similarly, reflectance measurements on bruises [99] can be performed in a kindred way when baseline measurements are taken on healthy skin, where absorption is more than ten times lower than in a bruise.

The effective photon path length for variations in absorption and reduced scattering coefficient had to be determined. A distinct trend was observed: τ decreases for increasing μ_a , however for μ_s' the observed trend is less definite (figure 4). At low absorption ($\mu_a = 1 \text{ mm}^{-1}$), τ decreases for increasing μ_s' , but at high absorption ($\mu_a = 10 \text{ mm}^{-1}$), τ is less sensitive to changes in μ_s' and does not follow a clear pattern especially in the low μ_s' region. This complicates the description of effective photon path length dependence on μ_a and μ_s' for low albedo values. Therefore, phantoms with albedo values

smaller than 0.1 were excluded and this model was selected based on the remaining data points. For most clinical and forensic application, the combination of high absorption and low scattering is not very relevant. Since *in vivo* the blood volume fraction does not exceed $\rho=0.2$, accordingly the absorption will be less than 6 mm^{-1} . However for bloodstains, higher absorption coefficients are present. Therefore, this approach is limited to bloodstains on host materials with high scattering coefficients, like paper or cotton. When the bloodstain has dried, the scattering of the bloodstain on cotton will be similar to the scattering of the cotton. In figure 4, the empirical model predictions deviate from the measurements for albedo < 0.1 , shown by dashed lines. Therefore, this model cannot be used in for on samples with an albedo < 0.1 . The developed relation for the effective photon path length is based on a single anisotropy value of $g=0.75$. Whole blood is known to have much higher anisotropy, $g>0.99$ [111]. Studies of other reflectance devices have shown that varying the anisotropy to higher g -values, while keeping μ_s' constant, did not influence the effective photon path length [105].

A typical reflectance measurement with corresponding spectral fit of a hemoglobin phantom is shown in figure 5. This spectral fit enables determination of the hemoglobin compounds, resulting in estimation of oxygen saturation and blood volume fraction. The spectral fit has a very high correlation with the measured reflectance and a nearly flat residue. The latter is required to ensure that the model is correct [75]. Because of the high affinity of hemoglobin for oxygen and the presence of oxygen in the atmosphere the hemoglobin will saturate totally as soon as it comes in contact with air. Hence the oxygen saturation in the hemoglobin phantoms was found nearly to be 100% for all measurements. No presence of met-hemoglobin was measured in the phantom, since all measurements were performed within an hour after phantom construction, which is too short for occurrence of autoxidation to methemoglobin. Figure 6 shows the determined BVF for the range of $\rho=0.14-0.84$. The spectrally determined BVF differs less than 10% from the true BVF for all measurements. The good agreement in combination with the expected high oxygen saturation indicates that all fitted parameters are correct and that quantitative determination of hemoglobin chromophores is possible.

The measurements with Evans Blue on cotton show that the cotton has a high reduced scattering coefficient at 611 nm: $\mu_s' > 20 \text{ mm}^{-1}$. We assumed that the scattering of the dried Evans Blue stain is similar to the reduced scattering of the cotton fabric without Evans Blue. The large error margin of the determined reduced scattering coefficient of cotton fabric is because the effective photon path is almost insensitive for changes in μ_s' for high values of μ_s' . This insensitiveness of μ_s' is also shown in figure 4, where it shows that the trend of effective photon path as a function of reduced scattering coefficient becomes almost flat for $\mu_s' > 10 \text{ mm}^{-1}$. We have assumed homogenous stains on cotton. This method will be applicable on bloodstains if the scattering of a bloodstain on cotton is similar as the scattering of clean cotton. Implementation on multi-layered structures, as bruises, which have a low absorbing layer (skin) on top of high absorbing layer (blood pool) will require validation on multi-layered phantoms [112].

In forensic science, these spectroscopic measurements will assist in detection and identification of traces at the crime scene [62]. The result of this study enables

analysis of bloodstain towards reconstruction of the time of crime, since determination of hemoglobin compounds in bloodstains or bruises allows estimation of the age of a bloodstain or bruise [99]. Especially for *on-site* bloodstain analysis, non-contact measurements are required to avoid trace contamination. To keep consistent optical coupling for bloodstain and baseline measurements a fixed probe is preferred. Bloodstains deposited on a non-white substrate would require a more sophisticated optical sampling and analysis method. For application in forensic practice the influence of background color has to be evaluated in a future study. Equally important are benefits for medical applications: non-contact measurements avoid pressure between skin and probe and therefore allow more reliable oxygen saturation measurements [113].

To conclude, the results presented in this study show that a simple non-contact spectroscopy device with a light source, fiber probe and spectrograph enables quantitative chromophore determination in the VIS/NIR wavelength range in homogeneous media. Furthermore we showed that these measurements can be used for forensic application as bloodstains on cotton fabric. This result expands the oxygen saturation measurements to fields with application specific requirements: no pressure and without blocking treatment light. Even more important, it allows implementation of reflectance spectroscopy in a forensic setting: on a crime scene.

Background: In forensic science, age determination of bloodstains can be crucial in reconstructing crimes. Upon exiting the body, bloodstains transit from bright red to dark brown, which is attributed to oxidation of oxy-hemoglobin (HbO_2) to met-hemoglobin (met-Hb) and hemichrome (HC). The fractions of HbO_2 , met-Hb and HC in a bloodstain can be used for age determination of bloodstains. In this study, we further analyze the conversion of HbO_2 to met-Hb and HC, and determine the effect of temperature and humidity on the conversion rates.

Methodology: The fractions of HbO_2 , met-Hb and HC in a bloodstain, as determined by quantitative analysis of optical reflectance spectra (450-800 nm), were measured as function of age, temperature and humidity. Additionally, Optical Coherence Tomography around 1300 nm was used to confirm quantitative spectral analysis approach.

Conclusions: The oxidation rate of HbO_2 in bloodstains is biphasic. At first, the oxidation of HbO_2 is rapid, but slows down after a few hours. These oxidation rates are strongly temperature dependent. However, the oxidation of HbO_2 seems to be independent of humidity, whereas the transition of met-Hb into HC strongly depends on humidity. Knowledge of these decay rates is indispensable for translating laboratory results into forensic practice, and to enable bloodstain age determination on the crime scene.

CHAPTER 5
BIPHASIC OXIDATION OF OXY-HEMOGLOBIN IN BLOODSTAINS

Submitted to PLoS One



INTRODUCTION

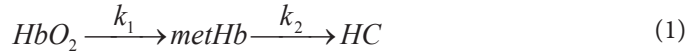
Bloodstains at crime scenes have prominent forensic value. The blood spatter pattern can assist in reconstructing crime events and DNA-profiling may lead to the suspect's identity. Despite the fact that determination of the age of a bloodstain has been a forensic quest in the last decades, the potential of age determination has not been exploited up till now. Techniques ranging from Atomic Force Microscopy [19], Electron Paramagnetic Resonance [58], and RNA degradation [64] have been explored to fulfill this omission. All these approaches confirm that the physical and chemical properties of bloodstains change over time. However, no technique has yet shown the precision and reproducibility needed for age determination in forensic practice. In chapter 2, we have demonstrated that non-contact reflectance spectroscopy is a suitable candidate for bloodstain age estimation.

Reflectance spectroscopy is a widely used technique to determine the optical properties of biological samples. Quantitative analysis of reflectance spectra requires knowledge of two parameters: (i) the absorption coefficients of the expected chromophores, and (ii) the path length the photons have travelled through the sample prior to detection. When both are known, Beer's law can be applied for determination of the concentration of the chromophores. Multiple chromophores can be determined when the reflectance is measured and analyzed over a large spectral range, in our case 450-800 nm. The spectral absorption coefficients of the three main chromophores in bloodstains, $\mu_a(\lambda)$, with λ denoting the wavelength, are very well known [31], and cover a range from 0.1 to 30 mm^{-1} . The second parameter, the path length of the detected photons, however, does not only depend on the geometry of the illumination and detection setup, but also on the chromophores present. The latter dependency complicates the analysis of the reflectance spectra. Yet, by defining a relation between the absorption and scattering properties of the sample and the photon path length, the chromophores and photon path length can be measured simultaneously [105].

Quantitative analysis of the reflectance spectra by photon path length modeling so far included the assumption that the scattering properties of the reference material and the bloodstain are equal [105]. Therefore, additional experiments to determine whether scattering of the bloodstain on cotton is similar to clean cotton fabric are needed, e.g. by optical coherence tomography (OCT) [114]. OCT is a high-resolution, cross-sectional imaging technique widely used for medical applications [115, 116]. Quantitative analysis of the OCT signal in depth allows the determination of the scattering properties of the tissue under study [117].

Hemoglobin is the oxygen transporting molecule and consists of four heme subunits: two α chains and two β chains. Hemoglobin is the main chromophore in blood, since hemoglobin makes up 97% of the blood's dry content. Inside a healthy human body hemoglobin is mainly present in two forms: one without oxygen, deoxyhemoglobin (deoxy-Hb), and one saturated with oxygen, oxy-hemoglobin (HbO_2). Only a small part ($\sim 1\%$) of HbO_2 is auto-oxidized into met-hemoglobin (met-Hb) [25], which is reduced back to Hb by the reductase protein cytochrome *b5* [27]. Upon blood

exiting the body, hemoglobin saturates with oxygen in the ambient environment. Due to a decreasing availability of cytochrome *b5*, the transition of HbO₂ into met-Hb will no longer be reversed. Once hemoglobin is auto-oxidized to met-Hb, it will denature to hemichrome (HC) [23, 118], as is shown in Eq (1):



The transition rate of HbO₂ to met-Hb is represented by k_1 , and the transition rate of met-Hb to HC is represented by k_2 . Tsuruga *et al.* have shown that the autoxidation rate of aqueous HbO₂, rate k_1 , can be described by first-order reaction kinetics [77]. The two oxidation rates of HbO₂ rate have been attributed to fast oxidation of the α chains of hemoglobin and slow oxidation of the β chains. These oxidation rates have only been reported in aqueous solutions and not *in vivo* or in bloodstains. Because of the biphasic nature of the transition of HbO₂ into met-Hb, k_1 can be described as the sum of a fast rate and a slow rate, $k_1 = k_f + k_s$. According to Tsuruga *et al.* [77] the oxidation of HbO₂ is given by:

$$\frac{[HbO_2]_t}{[HbO_2]_0} = P \cdot \exp(-k_f t) + (1 - P) \cdot \exp(-k_s t) \quad (2)$$

In Eq (2). $[HbO_2]_t$ is the relative fraction of HbO₂ in the bloodstain at time t , $[HbO_2]_0$ the relative fraction at $t=0$, k_f the fast rate constant, k_s the slow rate constant, and P the fraction of the rapidly oxidizing hemoglobin.

The present study shows, to our best knowledge for the first time, oxidation decay rates of the subsequent steps in bloodstains and the dependency of these reaction rates on temperature and humidity. Until now, the ageing of bloodstains has been interpreted by empirical models [3, 57, 58], which hamper understanding of the oxidation decay rates and its dependency on temperature and humidity. We present reflectance spectroscopy measurements of bloodstains on cotton to determine the amount of hemoglobin derivatives in ageing bloodstains. Cross-sectional measurements of the bloodstain were recorded by optical coherence tomography to confirm the assumptions made for the quantitative reflectance approach. Validation of the method for chromophore concentration estimation was achieved by diluting whole blood with phosphate buffered saline and correlating the input dilution to the sum of the determined chromophores. Finally, bloodstains, stored under various environmental conditions were monitored for ten days. From the relative oxy-hemoglobin concentration biphasic oxidation rates were determined and measured as function of temperature and humidity.

METHODS

Ethics Statement

All research involving human subjects has been conducted on anonymized tissue. Informed written consent was obtained from each donor. The Internal Review Board of the Academic Medical Center Amsterdam was informed about design and purpose of

this study. The IRB waived the need for approval, because of the non-clinical purpose of this study.

Bloodstains

Blood was drawn from a healthy nonsmoking volunteer. Three sets of samples were created. The first set was created by diluting whole blood with phosphate buffered saline to create eight stains on white cotton. All stains contained 50 μl of dilutions with varying blood volume fractions (BVF) ranging from 0 (no blood) to 1 (whole blood), with the following BVF: [0, 0.1, 0.2, 0.4, 0.6, 0.8, 1]. The bloodstains were measured three hours after deposition to allow the water in the bloodstain to evaporate.

The second set contained five times three bloodstains of 50 μl created on white cotton which were stored in a dark box at a temperature $T = [-20\text{ }^\circ\text{C}, 4\text{ }^\circ\text{C}, 22\text{ }^\circ\text{C}, 29\text{ }^\circ\text{C}, 37\text{ }^\circ\text{C}]$ and at a humidity of $45 \pm 5\%$. During the first day the reflectance of bloodstains was measured every hour, thereafter daily for 10 days.

The third set contained three times three bloodstains of 50 μl created on white cotton which were stored in a dark box at $T = 37 \pm 1\text{ }^\circ\text{C}$ at varying humidity of [20%, 50%, 70%]. During the first day the reflectance of bloodstains was measured every hour, thereafter daily for 8 days.

Optical Coherence Tomography

The OCT measurements were taken around 1300 nm where the absorption of the hemoglobin derivatives is minimal. By fitting the attenuated OCT signal to Beer's law, the attenuation coefficient can be determined. The cotton, with and without bloodstains, was probed and visualized with a commercially available 50 kHz swept source OCT system (Santec HSL 2000, 1300 nm center wavelength, 10 μm axial resolution, 11 μm lateral resolution). No additional image enhancement was performed on the presented image.

Using Beer's law, the detector current i_d of the system is described as $i_d \propto [\exp(-2\mu_t z)]^{1/2}$ where μ_t is the attenuation coefficient and z is the depth of the light in the sample. The square root accounts for the fact that the detector current is proportional to the field rather than the intensity. The attenuation coefficient is then extracted from the OCT data by fitting Beer's law to the averaged A-scans from a selected region of interest in the OCT image (~1000 A-scans of 4096 points, covering 1.5 mm scan length) [112]. To account for surface roughness of the cotton, all A-scans are aligned to straighten the transition between air and cotton. The fit model features three parameters; an amplitude for scaling signal intensity, the attenuation coefficient μ_t , and a measure for the scattering of the cotton. The offset is fixed at the mean noise level.

Non-contact reflectance spectroscopy

Quantitative determination of the chromophore fraction requires two reflectance measurements: one of the bloodstain and one of the host material. The latter reference measurement is needed to correct for the scattering of the host material, lamp spectral calibration and system throughput. The calibration procedure and analysis of the

reflectance spectra have been described in detail elsewhere in chapter 4. The attenuation of the reflected light from the bloodstain, \mathbf{R} with respect to the cotton, \mathbf{R}_0 is the product of the total absorption and the photon path length, τ , as shown in Eq. (3):

$$\mathbf{R} = \mathbf{R}_0 \exp\left\{-\tau\left(x_1 \cdot \mu_a^{HbO_2} + x_2 \cdot \mu_a^{met-Hb} + x_3 \cdot \mu_a^{HC}\right)\right\} \quad (3)$$

All symbols in bold face are considered wavelength dependent. Knowledge of the absorption coefficients of HbO₂, met-Hb and HC for a large spectral range [31] enables a spectral fit. In blood, hemoglobin is packed in red blood cells of 7 μm diameter, which was accounted for as described in [119]. The spectral fit yields three fit parameters [x₁, x₂, x₃]. These were obtained by minimizing the weighted sum squared error between measured and model estimated reflectance. Since the absorption coefficient is converted for the absorption of whole blood, the fit parameters [x₁, x₂, x₃] represent the fraction of the various hemoglobin derivatives: x₁ is the fraction of HbO₂, x₂ is the fraction of met-Hb, and x₃ is the fraction of HC. During the fit procedure, the effective mean photon path length τ (see Eq (3)) is adjusted simultaneously as a function of the total absorption, while the reduced scattering of the cotton and bloodstain is set to $\mu_s' = 40 \text{ mm}^{-1}$ for the entire spectral range. The total blood volume fraction is defined as the sum of x₁, x₂ and x₃. The relative amounts of the various hemoglobin fractions are determined by x_i/(x₁+x₂+x₃). All steps described above were scripted into Labview code (version 8.6, National Instruments).

Biphasic autoxidation of HbO₂ in bloodstains

Following the results of Tsuruga *et al.* [77] the autoxidation process of HbO₂ is interpreted by initial fast rate and final slow rate as shown in Eq. (2). The fast and slow decay rates are determined at various temperatures from least-squares fits of all measured [HbO₂] data points to Eq (2).

RESULTS

OCT measurement of bloodstains on cotton

Figure 1A shows a false color cross-sectional image of cotton fabric. The left side of figure 1A (red box) shows the cotton with a dried bloodstain of 24 hours old; the right hand side the clean cotton (black box). The attenuation of the OCT signal is depicted as the top part of the cotton is colored in white/yellow; the signal attenuates as the light penetrates deeper into the cotton. No differences in structure were observed between the bloodstain and the clean cotton fabric. The two regions of interest for performing attenuations fits are shown in figure 1B. We determined a value of μ_t of $16 \pm 1 \text{ mm}^{-1}$ for the bloodstain and $17 \pm 1 \text{ mm}^{-1}$ for the clean cotton fabric at 1300 nm.

Bloodstain dilutions

Figure 2 shows the diffuse reflectance ratio \mathbf{R}/\mathbf{R}_0 of an undiluted bloodstain in the spectral range of 450-800 nm. The solid line depicts the multi-component fit based

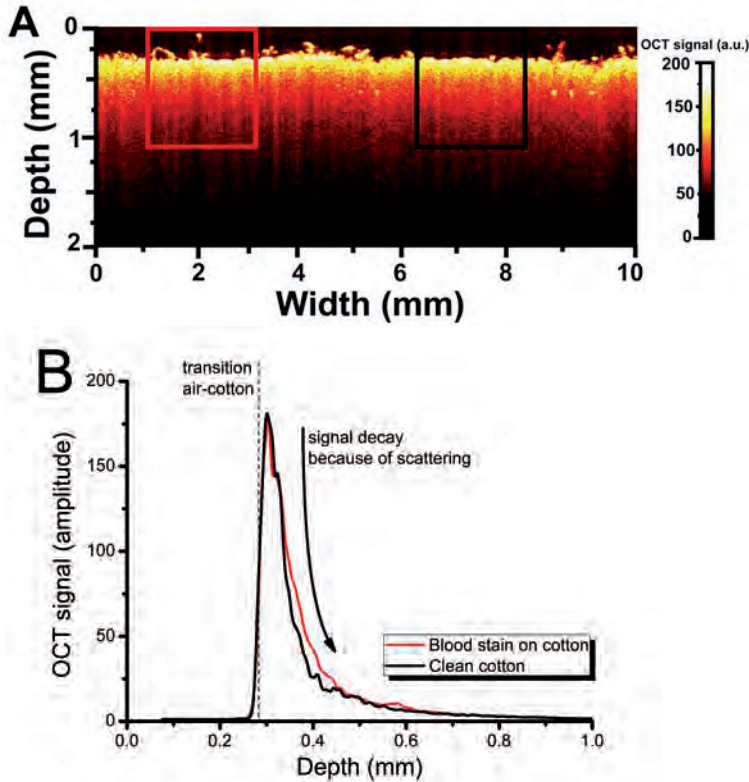


Figure 1. A) Cross-sectional OCT image of cotton fabric with a bloodstain. The left region of interest (red box) shows the position of the bloodstains. The right region of interest (black box) shows a clean spot of cotton fabric. B) Attenuation fits of the OCT signal of bloodstain (red line) and clean cotton (black line).

on the three hemoglobin derivatives and the modeled photon path, as written in Eq. (3). The outcome of the fit parameters $[x_1, x_2, x_3]$ represent the fraction of the three hemoglobin derivatives, HbO_2 , met-Hb, and HC, respectively: $x_1 = 0.85 \pm 0.04$, $x_2 = 0.02 \pm 0.01$ and $x_3 = 0.19 \pm 0.02$. The error represents the 95% confidence interval of the fit. The estimated blood volume fraction (BVF) is the sum of the three chromophores, $\text{BVF} = 1.06 \pm 0.05$. The estimated blood volume fraction was correctly estimated within 15% for all measurements as evidenced by figure 3. In this figure, the slope of the optically estimated BVF is 0.99 ± 0.05 . The correlation between the bloodstain's reflectance and the multi-component fit as shown in figure 2, $r^2 = 0.998$.

Autoxidation of HbO_2 in bloodstains

The outcome of the fit parameters $[x_1, x_2, x_3]$ was used to monitor the ageing bloodstains. To minimize noise on the hemoglobin fraction, we set the sum of the hemoglobin fractions to one for every measurement. Figure 4 plots the relative fractions of the three

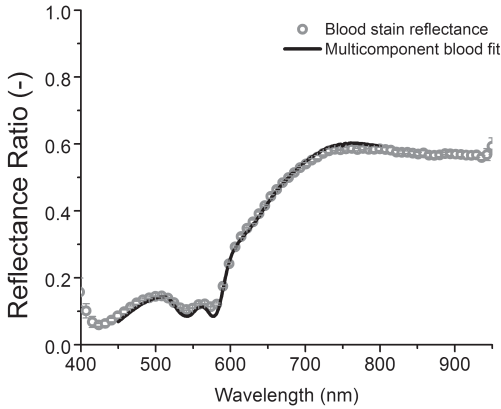


Figure 2. The measured reflectance ratio R/R_0 of an undiluted bloodstain (BVF=1) on cotton fabric measured in the spectral range from 450-800 nm. The gray dots depict the bloodstain reflectance and the solid black line represents the multi-component fit.

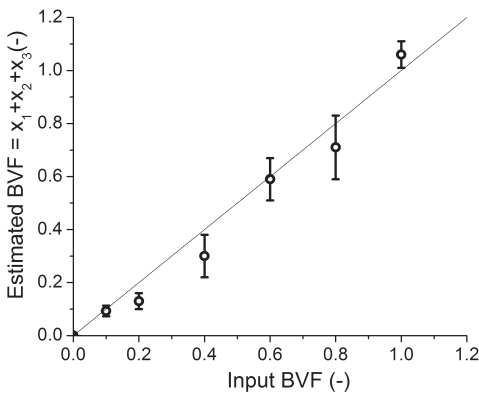


Figure 3. Optically estimated BVF, based on the spectral fits plotted against input BVF based on the mixing whole blood with PBS for eight various dilutions. The solid line represents the line of unity.

hemoglobin derivatives, as the average (\pm the standard deviation) of three bloodstains in the time span of 0-10 days for $T = 22^\circ\text{C}$ and humidity is $45\pm 5\%$. The transition of the HbO_2 into met-Hb and HC is rapid at first and after ten hours the transition rate changes into a lower rate. The blue line in figure 4 shows the relative oxy-hemoglobin amount fitted by the biphasic oxidation decay Eq. (2). $[\text{HbO}_2]_0$ is 1 for a fresh bloodstain since no met-Hb and HC is formed at $t=0$. The correlation coefficient between the measured $[\text{HbO}_2]$ and the biphasic autoxidation curve is $r^2 = 0.983$.

Temperature

Figure 5 shows the biphasic rates k_f and k_s (\pm standard deviation) as a function of temperature. The fast rate, k_f , increases from 6.3 d^{-1} for $T = -20^\circ\text{C}$ to 37.5 d^{-1} for 37°C , the slow rate, k_s , increases from 0.02 d^{-1} for $T = -20^\circ\text{C}$ to 0.36 d^{-1} for 37°C . Also the fraction of the rapid oxidizing hemoglobin, P in Eq (2), increases from 0.22 for $T = -20^\circ\text{C}$ to 0.39 for 37°C .

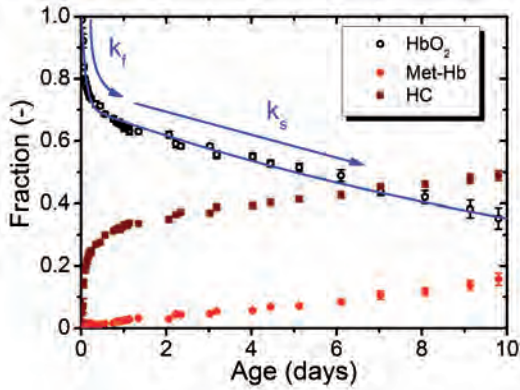


Figure 4. Fractions of HbO₂, met-Hb and HC in bloodstains (n=3) monitored for ten days. The amount of HbO₂ decrease while met-Hb and HC increases after deposition of the bloodstain. Error bars represent the standard deviation. The blue line shows the biphasic oxidation of [HbO₂].

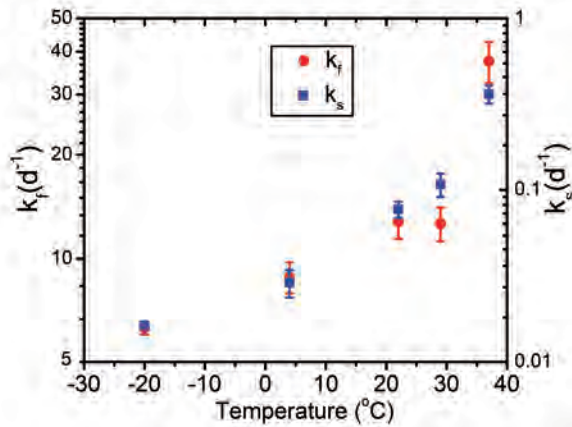


Figure 5. Parameters k_f and k_s as function of temperature. The fast oxidation (k_f) is plotted on the left axis, and slow oxidation (k_s) is plotted on the right axis.

Humidity

Figures 6A and 6B show the influence of humidity on k_1 and k_2 . Figure 6A shows the fraction of HbO₂ as a function of age for three values of humidity at T = 37 °C. No significant difference is observed in the fraction of HbO₂ for these three values of humidity.

Figure 6B shows the fraction of met-Hb as a function of age for three values of humidity at T = 37 °C. The temporal fraction of met-Hb does depend on humidity; more met-Hb is formed at higher humidity. While the fraction of met-Hb increases as function of humidity and the fraction of HbO₂ remains constant, the fraction of HC decreases, since the sum of the three hemoglobin derivatives accumulates to 1.

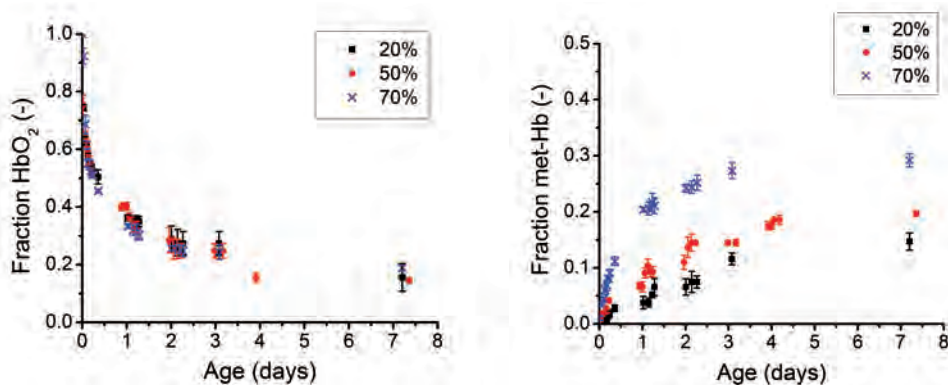


Figure 6. A) HbO₂ fraction as function of age of the bloodstain for humidity 20%, 50% and 70%. B) met-Hb fractions as function of age of the bloodstain for humidity 20%, 50% and 70%.

DISCUSSION AND CONCLUSION

This study shows spectroscopic monitoring of bloodstains to reveal the biphasic oxidation of oxy-hemoglobin in bloodstains. Analysis of the reflectance spectra was used in order to determine the amount of oxy-hemoglobin, met-hemoglobin and hemichrome in a bloodstain. Observations on diluted bloodstains showed that the absolute amounts of hemoglobin derivatives could be determined within 15%. The relative amounts of HbO₂, met-Hb and HC in bloodstains were followed for ten days at room temperature and could be described by first-order kinetics. We found that the oxidation of HbO₂ is rapid at first, but decreases after a few hours. These oxidation rates are strongly temperature dependent. The oxidation of HbO₂ does not depend on humidity, in contrast to the transition of met-Hb into HC which does depend on humidity.

First, the scattering of the substrate with and without the presence of a bloodstain was measured in order to understand the contribution of scattering to the measured signal. We found no significant difference in scattering for clean cotton ($17 \pm 1 \text{ mm}^{-1}$) vs. a bloodstain on cotton ($16 \pm 1 \text{ mm}^{-1}$). This indicates that the scattering of cotton fabric is not influenced by the presence of dried blood, which enables quantitative spectroscopic analysis, an observation which was confirmed by validating bloodstain dilutions and shown by a slope of 0.99 in figure 3.

Secondly, the absolute amounts of hemoglobin derivatives were verified. Ideally, amounts of HbO₂, met-Hb and HC are confirmed individually. However, currently no suitable techniques exist for individual chromophore validation, since most physical properties of HbO₂, met-Hb, and HC, including molar weight and magnetic properties, are nearly identical. A potential candidate for *in situ* confirmation of the decay of chromophores might be Raman spectroscopy [120], but Raman spectroscopy is hindered by the fluorescing properties of the heme groups [87]. In the present study validation was achieved by diluting whole blood with phosphate-buffered saline

and correlating the input dilution to the sum of the determined chromophores. All measurements in this study were performed on samples deposited on white cotton. Samples deposited on non-white substrates require a more sophisticated optical sampling and analysis, with both colored and non-colored background as reference. An alternative to overcome the drawback of background color is the use of a hyper-spectral imaging system similar to what has been used for age determination of bruises [79]. Spectral imaging allows imaging of the bloodstain and its host material and allows both spectral and spatial analysis of the bloodstain. Although this approach is beyond the scope of the present study, it is an interesting topic for future research.

The biphasic oxidation model has a high correlation with the measured $[\text{HbO}_2]$ fraction, $r^2 = 0.983$. Yet, around the transition between the fast and slow decay, after 10h in figure 4, the biphasic model shows small, but consistent deviations from the measured $[\text{HbO}_2]$ fraction. Fitting $[\text{HbO}_2]_t$ with a triphasic model results in a smaller residue, but also requires five instead of three fit parameters. F-test comparison between the bi- and triphasic model over the total time range indicates that the decrease in residue for the triphasic model is smaller than the decrease in degrees of freedom [121]; hence, the biphasic model is preferred. Tsugaru *et al.* and Sugawara *et al.* found that the autoxidation rate of oxy-hemoglobin in aqueous solutions is very much pH dependent [77, 118]. By increasing the level of acidity from pH = 8 to pH = 5, k_s increases 10-fold and k_f increases 100-fold. In healthy circumstances, blood has pH = 7.4 [122]. Unfortunately, the influence of water evaporation on pH in a bloodstain is not clear. Dehydration also increases the salt concentration, which may influence the autoxidation rate as well [123]. The pH and salt concentration dependence of decay rates may also explain the fact that in our studies we find $P=0.30$, while Tsugaru *et al.* found $P=0.50$, the latter value agreeing well with a priori expectations based on the equal amounts of α - and β -chains in the hemoglobin molecule. Exploration of the pH and temperature dependence on fit parameters P , k_s and k_f in bloodstains is therefore an important venue for future research. Finally, we observed that the conversion of met-Hb to HC is marked by the inverse biphasic decay of HbO_2 , while the amount of met-Hb increases only slowly. Therefore, the conversion rates of all three hemoglobin derivatives appear more complicated than first-order reaction kinetics and are also topic of future research.

The transition rate of HbO_2 to met-Hb and HC are very much temperature dependent. We found that the fast oxidation rate of HbO_2 , k_p increases 6-fold over the temperature range of -20 to 37 °C; the slow oxidation, k_s , increases 18-fold over the same temperature range. Similar temperature dependencies were found for the transition of met-Hb to HC. The influence of humidity on the transition rate is more complex. We observed that the humidity has no influence on the oxidation of HbO_2 , rate k_1 . However, it does have significant influence on the transition of met-Hb to Hc, rate k_2 . The amount of met-Hb increases as humidity increases. Consequently, the fraction of HC decreases, since the fraction of HbO_2 is humidity independent and the sum of the three hemoglobin components is set to one. It seems that for the limit humidity

→ 100%, no HC is formed at all, a suggestion which is supported by the observations of Tsuruga *et al.* When measuring HbO₂ oxidation in an aqueous solution (100% humidity) no HC formation is observed at all [77]. This observation was confirmed in our laboratory (data not shown). For humidity → 100%, the rate of met-Hb to HC, $k_2 \rightarrow 0$. When exploring the opposite limit: humidity → 0% it seems that the amount of met-Hb decreases. Possibly for humidity → 0%, the transition rate of met-Hb to HC will become larger than the transition of HbO₂ to met-Hb ($k_2 > k_1$) and consequently no met-Hb will be formed.

In conclusion, we have shown that the oxidation of oxy-hemoglobin in bloodstains follows a biphasic decay and that the rates can be described by first-order reaction kinetics. In addition, it was shown that all reaction rates show a positive correlation with temperature and that the transition of met-Hb to HC also depends on humidity. This relationship of the oxidation of bloodstains as a function of temperature and humidity enables the implementation of age determination of bloodstains at a forensic setting, where a wide variety of environmental factors can be encountered.

The precise determination of chromophore concentration in scattering media is hampered by the influence of the setup geometry and the absorption on the path length distribution, $P(\ell)$, of the detected photons. We show that $P(\ell)$, as determined by Monte Carlo (MC) simulations for a non absorbing sample, can be used to describe the reflectance spectroscopy measurements as function of absorption by simply applying Beer's law. For low scattering ($\mu'_s=1 \text{ mm}^{-1}$) and high scattering ($\mu'_s=11.5 \text{ mm}^{-1}$), the simulated reflectance highly correlated with non-contact reflectance spectroscopy measurements without the use of fitting parameters. In hemoglobin containing samples we show that the simulated relation between reflectance and absorption can be used to determine the absorption spectrum of the medium without using additional light transport models. In conclusion, the reflectance spectroscopy signal as a function of absorption is completely determined by the photon path length distribution at zero absorption. The simulated reflectance ratios allow for rapid determination of absorption coefficients based on reflectance spectroscopy measurements of highly scattering samples.

CHAPTER 6
PHOTON PATH LENGTH DISTRIBUTION MODEL
FOR REFLECTANCE SPECTROSCOPY

Submitted to Optics Letters



INTRODUCTION

Conventional reflectance measurements are routinely used in medicine e.g. to determine the oxygen saturation of blood [69]. Applications of reflectance spectroscopy are not limited to determining oxygen saturation, but may also assist in determination of the age of bloodstains (Chapter 2) or bruises [99]. These measurements require translating reflectance spectroscopy values into absorption coefficients to determine the presence of clinically, or forensically relevant chromophores as (oxy)-hemoglobin, met-hemoglobin, bilirubin or hemichrome [97, 105, 125, 126] in highly scattering tissues. To enable differentiation between these chromophores, measurements over a large spectral range are required. The influence of the optical properties and probe geometry on the path length of the light travelling through the tissue under study results in a non-linear relation between reflectance and absorption. This relation can be determined by the diffusion approximation model, empirical model [105], or a lookup table [97]. An alternative approach, albeit time consuming, is performing MC simulations to determine the relationship between reflectance and absorption [125, 126]. In principle, reflectance spectra of absorbing tissues can be calculated by combining Beer's law of absorption with the path length distribution of the detected photons, $P(\ell)$, in non-absorbing tissues. $P(\ell)$ can be measured in a Mach-Zehnder setup [127] or by time resolved experiments [128]. The influence of absorption on these photon path length distributions can be measured [129] or simulated [130]. However these techniques are cumbersome and currently limited to a too small spectral wavelength range for chromophore identification. In this study, we show that by using $P(\ell)$ as determined by MC simulations, the effect of absorption on reflectance measurements can be precisely described. Vice versa, using $P(\ell)$, absorption spectra of scattering samples can be assessed over a sufficiently large spectral range for chromophore determination in tissues.

METHODS

Our setup geometry specific $P(\ell)$ was determined from a single MC simulation at zero absorption (so called white MC) with the proper fiber probe arrangement and optical properties (scattering, refractive index). The simulated ratios between the reflectance with and without the presence of absorption were compared with reflectance ratios measured on phantoms with low ($\mu'_s=1 \text{ mm}^{-1}$) and high ($\mu'_s=11.5 \text{ mm}^{-1}$) reduced scattering properties.

The reflectance spectra were recorded with a non-contact reflectance spectroscopy setup, containing a USB4000 spectrograph, DH-2000 light source and QR400-7-UV/BX probe, all from Ocean Optics. The probe, consisting of 6 illumination fibers surrounding the center detection fiber, was tilted 13° off-normal and positioned at a height of 17 mm above the phantom. This configuration makes the reflectance measurements insensitive to direct reflections and to changes in the probe position (Chapter 4). The reflectance spectra were recorded over the wavelength range of 400-900 nm, and averaged into bins of 10 pixels, which allowed calculation of a standard deviation.

Phantoms consisted of a mixture of Intralipid 20% (Fresenius, Kabi AG), phosphate buffered saline, and varying concentration of Evans Blue (Sigma Aldrich) to control the amount of absorption. Additional phantoms were prepared at the two selected μ_s' -values with no Evans Blue added, which were utilized to obtain baseline measurements, $R(\mu_s', \mu_a=0) = R_0$. Figure 1 shows typical reflectance spectra of two phantoms, without and with absorber added ($\mu_a = 0.2 \text{ mm}^{-1}$). First, we analyzed the data for a single wavelength, $\lambda=611 \text{ nm}$, for the Evans Blue phantoms at the maximum reflectance difference between the non-absorbing and absorbing phantoms. For instance, at $\lambda=611 \text{ nm}$, the reflectance of the phantom without absorber and $\mu_s'=1 \text{ mm}^{-1}$ is 0.071 and with absorber ($\mu_a = 0.2 \text{ mm}^{-1}$) 0.024, so the ratio R/R_0 is 0.34.

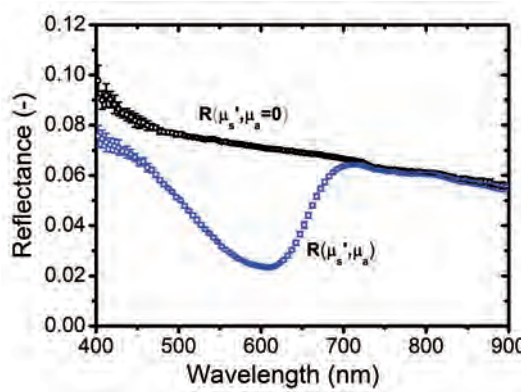


Figure 1. Reflectance spectra normalized to the reflectance of a Spectralon™ standard from an Intralipid solution ($\mu_s'=1 \text{ mm}^{-1}$ at 611 nm) without (black) and with Evans Blue added (blue, $\mu_a=0.2 \text{ mm}^{-1}$ at 611 nm).

Monte Carlo simulations with the experimental probe geometry, refractive index of 1.35 and a Henyey-Greenstein scattering phase function $g=0.75$ as input parameters were performed using the code of De Mul *et al* [132]. The reflectance signal in the absence of absorption R_0 , is the sum of the photon path length distribution over all path lengths:

$$R_0 = \sum_{\ell=0}^{\infty} P(\ell) \quad (1)$$

The simulation was terminated when 100,000 photons were collected ($R_0=100,000$). Knowledge of the path length distribution allows determination of the reflected signal in the presence of an absorber, by applying Beers law to all individual path lengths.

$$R = \sum_{\ell=0}^{\infty} P(\ell) \cdot \exp(-\mu_a \ell) \quad (2)$$

RESULTS

The reflectance ratio R/R_0 at a specific absorption is then calculated from Eq (2) and (1). Figure 2 shows the path length distributions $P(\ell)$ for the two scattering conditions $\mu'_s = 1$ and 11.5 mm^{-1} , and Figure 2 shows the path length distributions $P(\ell)$ for the two scattering conditions $\mu'_s = 1$ and 11.5 mm^{-1} , and for $\mu_a = 0$ and 1 mm^{-1} . The distribution of photon path lengths is very broad. For high scattering, $\mu'_s = 11.5 \text{ mm}^{-1}$, the most common path length is 0.54 mm , while the average photon length is 5 mm . Because of this wide range, the reflectance signal is sensitive to both very low and very high absorption. Please note that the number of photons detected remains finite for small photon path lengths, which can be attributed to our probe geometry in which the field of view of collection and delivery fiber overlap. Since diffusion theory requires a minimum of scattering events: $N \geq 4/(1-g)$ [133], and accordingly a minimal path length: $\ell \geq 4/\mu'_s$, this requirement excludes application of diffusion theory, neither as time resolved [134] nor as steady state [100].

The sum of all counts over all photon path lengths accumulates to the total number of photons detected. Figure 3 compares the measured reflectance ratios at $\lambda = 611 \text{ nm}$ with the simulated ratio (Eq (2) over Eq. (1)) for absorption coefficients varying between $\mu_a = 0.1$ and 20 mm^{-1} for both the low and high scattering conditions. Please note the excellent agreement between experiment as shown in figure 1 and simulation. Good correspondence between measurements and simulations is found for large range of absorption coefficients without the use of fitting parameters (Pearson correlation coefficient, r^2 , of 0.997 for $\mu'_s = 1 \text{ mm}^{-1}$ and 0.998 for $\mu'_s = 11.5 \text{ mm}^{-1}$). Still, at large absorption values and low scattering the agreement between measurements and simulations deviates, which is merely attributed to the low signal to noise level of the reflected light, and can be minimized by measuring dark references, as described in [105].

Next we performed the reverse procedure, recovering absorption spectra from an analysis of the data over the full spectral range. To validate our method on a blood

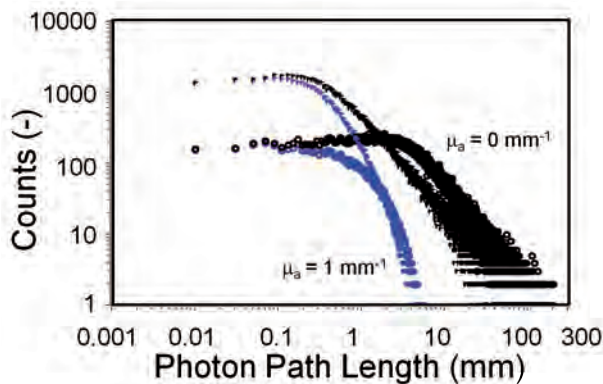


Figure 2. MC simulated photon path length distributions for non-contact reflectance spectroscopy for $\mu'_s = 11.5 \text{ mm}^{-1}$ (+) and for $\mu'_s = 1 \text{ mm}^{-1}$ (o) without (black) and with absorption (blue, $\mu_a = 1 \text{ mm}^{-1}$).

resembling phantom, we performed additional spectral measurements on a phantom containing Intralipid ($\mu'_s=11.5 \text{ mm}^{-1}$ at 611 nm) and 27 mg/ml oxy-hemoglobin (HbO_2).

Figure 4 (top panel) shows the normalized reflectance spectra of Intralipid without and with HbO_2 added. Based on the measured reflectance ratio of figure 4A and the simulated relation between the reflectance ratio and absorption for $\mu'_s = 11.5 \text{ mm}^{-1}$ depicted in figure 3, the absorption spectrum of HbO_2 can be recovered for the entire wavelength range of 400-900 nm (figure 4B) panel). Again, good agreement is observed between assessed and literature HbO_2 absorption [31] for a large range of absorption coefficients ($r^2 = 0.974$). Yet, μ'_s decreases with increasing wavelength, which is not

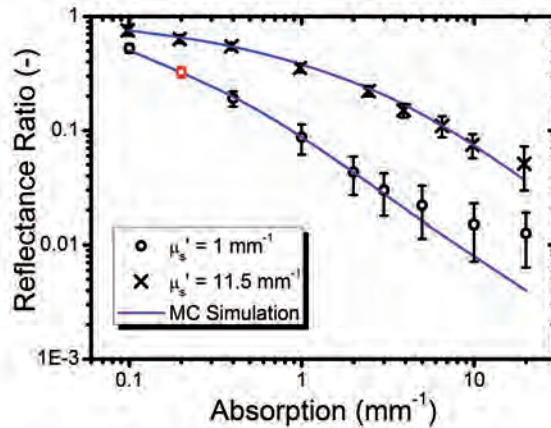


Figure 3. Reflectance ratio R/R_0 at various absorption values for high scattering (x, $\mu'_s=11.5 \text{ mm}^{-1}$) and low scattering (o, $\mu'_s=1 \text{ mm}^{-1}$) as measured at $\mu=611 \text{ nm}$ and as determined by MC simulations (blue lines). Red dot resembles measurement from figure 1.

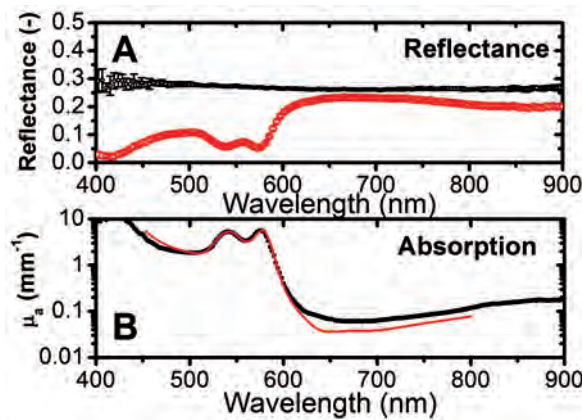


Figure 4. A) Normalized reflectance spectra from Intralipid solutions ($\mu'_s=11.5 \text{ mm}^{-1}$ at 611 nm) without (black) and with HbO_2 added (red) B) Absorption of HbO_2 as assessed from reflectance measurements (black dots), and from literature (red line) [31].

accounted for in figure 4B. This induces the absorption to be underestimated at shorter wavelengths, and slightly overestimated at longer wavelengths.

DISCUSSION AND CONCLUSION

Comparison between white MC simulations and reflectance measurements requires measuring a reference reflectance at zero absorption. In virtually all clinical reflectance measurements another e.g. contra lateral location exists where the optical properties (refractive index and tissue scattering) can be considered virtually identical to those of the target tissue. Examples are forensic bloodstain studies on a cotton background [124], bruises from physical abuse on the body [99], and facial port wine stains [135]. Here, the reflectance spectrum of the other, virtually identical location may then serve as the R_0 . However, a small correction of the endogenous absorption, in skin the natural amount of blood (volume fraction of ~ 0.01) and melanin, over the spectral range may then be needed. From the ratio R/R_0 the absorption coefficient can be determined, which can then be used to identify the concentrations of chromophores present in the tissue under study. Measuring the local reference reflectance may eliminate the use of Spectralon™ reference, since this measurement value would be divided out when calculating the ratio.

We have shown the influence of absorption on the photon path length distribution. Next, the influence of scattering on $P(\ell)$ has to be determined. The relation between photon path length distribution and reduced scattering might be complicated and is topic of future study. Eventually, the μ_s' of the tissue under study also has to be estimated or measured. For high μ_s' the reflectance becomes insensitive for changes in μ_s' (Chapter 4), and estimation would be sufficient. Yet for low scattering coefficients, μ_s' and g could be measured by a different techniques, as low coherence spectroscopy [136] or optical coherence tomography [137] and subsequently simulated by a white MC. Another option might be to build a database of $P(\ell)$ for a range of μ_s' value or to measure $P(\ell)$ experimentally [129].

In conclusion, the reflectance spectroscopy signal as a function of absorption is completely determined by the photon path length distribution at zero absorption. The simulated reflectance ratios allow for rapid determination of absorption coefficients based on reflectance spectroscopy measurements of highly scattering samples.

Diffuse reflectance spectroscopy is a common technique for determining the optical properties of biological samples. Proper data analysis is often based on the diffusion approximation to the radiative transfer equation. This theory is assumed to be only valid for regimes where scattering is dominant over absorption, $\mu_s' > 10 \cdot \mu_a$. However, we observe excellent agreement between reflectance measurements of phantoms and an equation derived by Zonios et al. [100] from diffusion theory. However, two parameters were fitted to all experiments, including strongly absorbing samples, implying that the reflectance equation cannot be considered as being diffusion theory any more. This approach predicts the diffuse reflectance very well ($r^2=0.994$) for a large range of optical properties and is potentially valid in a larger optical regime than previously assumed.

CHAPTER 7
DIFFUSION APPROXIMATION BEYOND ITS
ASSUMED BORDERS OF VALIDITY

In preparation



INTRODUCTION

Interpretation of reflectance spectroscopy measurements requires translating reflectance values into absorption coefficients. In a previous study, we showed that an empirical model connecting path lengths with absorption and reduced scattering coefficients can assist in relating reflectances to absorption, as shown in chapter 4. Defining an empirical path length model for a specific experimental geometry is a recognized method [105-107] for analysis of reflectances and many more (semi-) empirical models have been reported in literature [101-104]. During our search of finding an appropriate empirical path length model we also explored the applicability of an equation proposed by Zonios *et al.* [100], because it allows effortlessly matching theory with our experimental setup. This equation is derived from diffusion theory and hence is not *a priori* applicable to reflectance measurements when tissue absorption dominates over scattering. In the VIS/NIR wavelength range the reduced scattering coefficients, μ_s' , of tissues vary between 0.5-10 mm⁻¹, whereas the absorption coefficient, μ_a , of whole blood in this wavelength range can be 0.1-30 mm⁻¹. The use of diffusion theory, requiring $\mu_s' \gg \mu_a$, is therefore assumed to be limited to tissue types with small (<1%) blood volume fractions, and excludes studying well perfused organs, bruises [11], let alone whole blood itself.

In this chapter we use phantom measurements to explore the model by Zonios *et al.* [100] including the possible validity of diffusion theory at high absorption coefficients.

METHODS

Diffuse reflectance spectroscopy (DRS)

The DRS measurements presented in this study use the same phantoms and the same measurement setup as presented in chapter 4 and chapter 6, i.e. utilizing the reflectance ratio, $R(\mu_s', \mu_a)/R(\mu_s', 0)$, i.e. the diffuse reflectance with absorber, $R(\mu_s', \mu_a)$, versus without absorber, $R(\mu_s', 0)$.

Theory

Our starting point is the diffusion theory approach of Farrell *et al.* [138] who calculated the diffuse reflectance as a function of radial distance, r , in response to a pencil beam.

$$R(\mu_s', \mu_a, r) = \frac{z_0}{4\pi} \cdot \frac{\mu_s'}{\mu_s' + \mu_a} \cdot \left[\left(\mu + \frac{1}{r_1} \right) \cdot \frac{e^{-\mu r_1}}{r_1^2} + \left(1 + \frac{4}{3}A \right) \cdot \left(\mu + \frac{1}{r_2} \right) \cdot \frac{e^{-\mu r_2}}{r_2^2} \right] \quad (1)$$

In this equation, the following parameters are defined as:

$$\mu = \sqrt{3\mu_a(\mu_a + \mu_s')}, \quad z_0 = 1/(\mu_a + \mu_s'), \quad r_1 = \sqrt{(z_0^2 + r^2)}, \quad r_2 = \sqrt{((1 + 4A/3)^2 z_0^2 + r^2)}$$

Parameter A depends on the refractive index mismatch of the air-tissue boundary [138]. For a phantom reflective index of 1.35, parameter A is equal to 3. To calculate the reflectance ratio in response to an irradiation with radius r_1 as captured by the collection

fiber, one has to integrate reflectances $R(\mu_s', \mu_a)$ and $R(\mu_s', 0)$ over the collection spot size with radius r_c :

$$\frac{R(\mu_s', \mu_a)}{R(\mu_s', 0)} = \frac{\int_0^{r_i} d\rho \int_0^{r_c} dr \cdot R(\mu_s', \mu_a, |\rho - r|) \cdot 2\pi r}{\int_0^{r_i} d\rho \int_0^{r_c} dr \cdot R(\mu_s', 0, |\rho - r|) \cdot 2\pi r} \quad (2)$$

Because Eq. (2) cannot be evaluated analytically, a simple analytical expression for R was derived by Zonios assuming point delivery of light and collection over a circular spot with an effective radius of r_c of the detecting fiber. This resulted in the following equation:

$$\frac{R(\mu_s', \mu_a)}{R(\mu_s', 0)} = \frac{\mu_s'}{\mu_s' + \mu_a} \cdot \frac{\left\{ e^{-\mu \epsilon_0} + e^{-\left(1 + \frac{4}{3}A\right)\mu \epsilon_0} - z_0 \cdot \frac{e^{-\mu r_1}}{r_1} - \left(1 + \frac{4}{3}A\right) \cdot z_0 \cdot \frac{e^{-\mu r_2}}{r_2} \right\}}{2 - \frac{1}{\mu_s'} \cdot \left\{ \frac{1}{r_1'} + \frac{1 + 4A/3}{r_2'} \right\}} \quad (3)$$

Here, r_1 and r_2 have become a function of r_c instead of r , replacing r by r_c . Further, r_1' and r_2' are the values for r_1 and r_2 for $\mu_a=0$. r_c is defined by Zonios *et al.* as the effective spot radius [100]. The geometry setup used in [100] is similar to reflectance measurements in previous chapters, only difference is interchanging of collection and illumination fibers. Therefore, to describe the reflectance measurements r_c has become the effective collection radius. The numerical aperture of our fibers is 0.22; accordingly the acceptance angle is 13°. The fiber radius is 0.20 mm. At a height of 17 mm above the phantom, the collection spot size radius was determined to be, $r_c = 2.7$ mm. The six, equally sized, illumination fibers around the collection fiber will produce an illumination spot size with radius of $r_i = 3.1$ mm.

Equations (2) and (3) will be compared with our experimental phantom measurements. Equation 2 from numerical integration of the $R(\mu_s', \mu_a)$ and $R(\mu_s', 0)$. Equation (3), first, with the physical parameters $A = 3$ and collection area radius $r_c = 2.7$ mm when placing the probe at a height of 17 mm. Second, because the irradiation in our experimental geometry is not by a pencil beam but covers an area with radius r_p , while the detection fiber only covers the diffuse reflectance coming from a smaller area with radius r_c , we also followed Zonios *et al.* [100], and used the parameters A , r_c that best described the phantom measurements using a Levenberg-Marquandt fitting algorithm [139] with error margins represented by the 95% confidence intervals. Table 1 summarizes the various parameters for the three situations.

Table 1. Overview of additional parameters in Eq (2) and Eq (3).

	Symbol	Definition	Physical value	Fitted Value
Exact Diffuse (Eq.2)	ρ	probe position	from 0 to r_i	-
	r_i	Illumination spot radius	3.1 mm	-
	r_c	Collection spot radius	2.7 mm	-
	A	Refractive index parameter	3.1	-
Zonios' Model (Eq. 3)	r_c	Effective collection radius	2.7 mm	6.7 mm
	A	Refractive index parameter	3	2.0

RESULTS

First we have explored the limits of $R(\mu_s', \mu_a)/R(\mu_s', 0)$ for four limits of μ_s' and $\mu_a \rightarrow 0$ and ∞

$$\lim_{\mu_a \rightarrow 0} \frac{R(\mu_s', \mu_a)}{R(\mu_s', 0)} = 1 \quad \lim_{\mu_a \rightarrow \infty} \frac{R(\mu_s', \mu_a)}{R(\mu_s', 0)} = 0 \quad (4)$$

$$\lim_{\mu_s' \rightarrow 0} \frac{R(\mu_s', \mu_a)}{R(\mu_s', 0)} = \infty \quad \lim_{\mu_s' \rightarrow \infty} \frac{R(\mu_s', \mu_a)}{R(\mu_s', 0)} = 1 \quad (5)$$

We found a remarkable result for the limit of the reduced scattering going to zero; the reflectance ratio goes to infinity.

Figure 1 shows the reflectance ratio for varying absorption coefficients and two reduced scattering coefficients (1 and 11.5 mm^{-1}). Figure 2 shows the reflectance ratio for varying reduced scattering coefficients and two absorptions (1 and 10 mm^{-1}). The total reflectance, as shown in Eq (2) collected by the collection fiber with radius $r = 2.7$ mm has been determined. Also, following Zonios' approach, from Eq (3) for both physical parameters $A = 3.1$ and $r_c = 2.7$ mm, as well as for $A = 2.0 \pm 0.4$ and $r_c = 6.7 \pm 0.3$ mm determined from a fit of all phantom experiments. Figures 1 and 2 both show the substantial deviations between these three approaches. Exact diffusion theory, Eq. (2), and Zonios' Eq. (3) with physical A , r_c values show substantial deviations from the experimental results, especially for the low reduced scattering coefficients. However, Zonios' model Eq. (3) with fitted parameters shows good correspondence with the phantom measurements. Agreement between experimental reflectance measurement and diffusion model, determined from integration, $r^2=0.918$, Zonios' approach with physical parameters, $r^2=0.922$, and with fitted parameters can be expressed as, $r^2=0.994$.

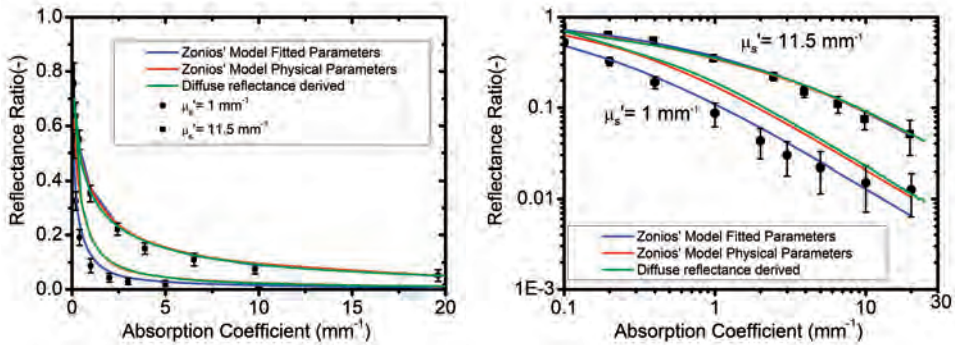


Figure 1. (A) Reflectance Ratio as a function of the absorption coefficient, for high (squares) and low (dots) scattering. Green line represents Eq. (2). The red lines represent Eq. (4) with physical parameters $A = 3.1$, $r_c = 2.7$ mm; the blue lines with fitted parameters $A = 2$, $r_c = 6.7$ mm. (B) Same figure but the reflectance ratio on a logarithmic scale.

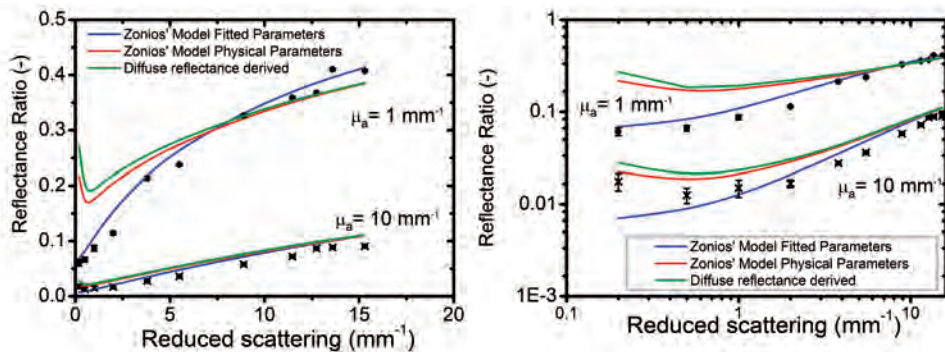


Figure 2. (A) Reflectance Ratio as a function of the reduced scattering coefficient, μ_s' , for high absorption ($\mu_a = 10$ mm⁻¹) and low absorption ($\mu_a = 1$ mm⁻¹). Green line represents Eq. (2). The red lines represent Eq. (4) with physical parameters $A = 3$, $r_c = 2.7$ mm; the blue lines with fitted parameters $A = 2$, $r_c = 6.7$ mm. (B) Same figure but on a logarithmic scale.

DISCUSSION

We have investigated whether the reflectance spectroscopy model derived from diffusion theory, albeit with additional approximations, as given by Eq. (3) of Zonios *et al.* can be used to model the reflectance ratio measurements on phantoms with controlled optical properties.

First, the limit of measuring the reflectance ratio in the situation of the reduced scattering going to zero is purely hypothetical, yet the ratio of $R(\mu_s', \mu_a) / R(\mu_s', 0)$ should not be able to be larger than one, let alone to go infinity. Therefore, the left hand part of Eq. (5) at least implies that Eq. (3) incorrectly describes reflectance ratios for small μ_s' .

Secondly, we showed that Eq. (3) describes the diffuse reflectance ratio of phantom experiments with good agreement, provided that parameters A , r_c are fitted to

experimental results, including cases where $\mu_a \gg \mu_s'$. For large scattering coefficients, Eq. (2) and Eq. (3) with physical A , r_c parameters (table 1) reasonably model the reflectance ratio too. This raises the interesting question why diffuse reflectance spectroscopic experiments under certain conditions allow analysis by equations derived from diffusion theory far beyond the conditions of validity of this theory, in contrast to e.g. fluence rate distributions (see e.g. Figure 6.2 of Star [140]).

When using physical parameters in Eq (3) it only describes the qualitative shape of $R(\mu_s', \mu_a)/R(\mu_s', 0)$ versus absorption, since it correctly describes the limits for $\mu_a = 0$ and μ_a is large, i.e. $R(\mu_s', \mu_a)/R(\mu_s', 0) = 1$ for $\mu_a = 0$ while it tends to zero for $\mu_a = \text{large}$, i.e. Eq. (4) and Eq. (5). Yet, when the two parameters r_c and A are fitted to all experimental results including those with large μ_a , it appears that Eq. (3) with numerically fitted parameters describes the experiments also quantitatively. However, Eq. (3) with fitted parameters has become a semi-empirical model, with no physical meaning of parameters A and r_c .

Additionally, the structure of Eq. (3) is such that the reflectance ratio for larger values of μ_s', μ_a depends less and less on the actual values of A , r_c . This is because then, the third and fourth terms inside the brackets of the nominator, which include A , r_c , become small relative to the first and second terms, while the second term, which includes A , also becomes small relative to the first. Hence, Eq. (3), either with exact or with fitted parameters approaches the same outcome when μ_s' or μ_a become large. Here, it helps that also r_c is relatively large. Thus, diffusion theory described by Eq. (2) and approximated by Eq. (3) with physical parameters A and r_c indeed predicts reflectance ratios accurately for larger values of μ_s' and μ_a , including those far beyond the validity limits of diffusion theory.

In conclusion, by comparison with experimental reflectance measurements, remarkable agreement is observed with the diffusion approximation at high scattering and high absorption properties. When using fitted parameters (A and r_c), the model also showed good agreement at low scattering and high absorption properties. Thus, Zonios' model, expressed by Eq. (3) is able to describe reflectance ratios accurately for a large range of optical properties and is potentially applicable beyond the generally assumed limits of validity of diffusion theory.

CONCLUSION, DISCUSSION AND OUTLOOK



CONCLUSION, DISCUSSION AND OUTLOOK

Concluding remarks

To date, no current techniques are available for crime investigators to determine the age of the bloodstain. All techniques alienated in chapter 1 as well as reflectance spectroscopy discussed in this thesis are still in experimental phase. In this thesis, we have improved age determination with reflectance spectroscopy by exploring the use of spectral analysis of a bloodstain over a large spectral window (450 -800 nm) and to use multi-component fitting algorithm to determine amount of hemoglobin derivatives as a function of the age of the bloodstain. Furthermore, analyzing the bloodstain's reflectance spectra in terms of hemoglobin derivatives reveals the transition of HbO_2 to met-Hb and HC. The fractions of these hemoglobin derivatives as a function of age show the kinetics. These reflectance spectroscopy measurements and analysis are a first exploration of the chemical reaction of hemoglobin oxidation in a bloodstain

In **chapter 1**, all current techniques are summarized. It shows that techniques based on red blood cells, such as oxygen electrodes and reflectance spectroscopy are sensitive for short term ageing. Techniques based on white blood cells, RNA analysis are more sensitive for long term ageing. Therefore, most techniques described in **chapter 1** are complementary to each other. Figure 1 shows the comparison of age determination techniques, including reflectance spectroscopy measurement results shown in **chapter 2**.

Inaccuracy on age determination is an important parameter of age determination techniques, especially when applying the technique to an actual crime case. Figure 1 shows that reflectance spectroscopy has the lowest inaccuracy, based on standard deviation reported on ageing measurements. Figure 1 does incorporate environmental factors, since data points of all four techniques are based on stable laboratory environments. The origin of the inaccuracy in age determination of reflectance spectroscopy as described in chapter 2 is twofold: First, spectroscopic analysis in **chapter 2** is based on Kubelka Munk and is only qualitative. While providing excellent fits for

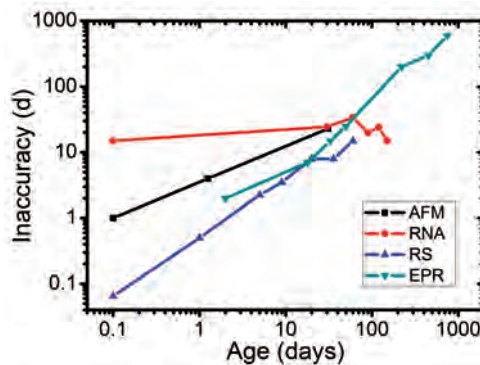


Figure 1. Inaccuracy of age determination as a function of the actual age, determined for four techniques: AFM, black squares, data from [19]; RNA, red circles, data from [36]; reflectance spectroscopy, blue triangles, data from chapter 2; and EPR, green triangles, data from [58].

bloodstains, we could not relate the Kubelka Munk parameters K and S to the optical properties μ_a and μ_s' when measuring the reflectance spectrum of tissue phantoms with well controlled optical properties. This mismatch between K and S on one side and μ_a and μ_s' on the other hampers a quantitative analysis. Therefore we explored different light transport models. The second origin of inaccuracy is measurement error. The measurement protocol of monitoring forty bloodstains simultaneously required displacement of the probe. Therefore, the inaccuracy on age estimation can be reduced when analyzing with a quantitative analysis and when measuring with fixed probe.

Chapter 2 shows the results of analyzing ageing bloodstains for the period of 0-60 days. I have continued monitoring the reflectance spectra of these bloodstains up until today, 600 days after deposition; in total more than 2000 reflectance measurements. The results of the fractions of the hemoglobin derivatives as a function of age is shown in figure 2. After 500 days, the fraction of HbO_2 is 0.09, met-Hb is 0.01 and HC is 0.90. Especially the fraction of met-Hb as a function of age is remarkable. During the first 20 days, the fraction increases linearly, after 20 days the amount decreases exponentially.

We have not yet found an appropriate model to explain the fraction of met-Hb as function of age.

Chapter 3 shows the possibility to use multi-component analysis of bloodstain to discriminate between blood and non-blood samples. The correlation coefficient between the reflectance spectrum and the multi-component fit is an excellent parameter to distinguish blood (high correlation) from non-blood (low correlation).

Chapter 4 shows that a quantitative analysis of non-contact recorded reflectance spectra is possible when developing an empirical photon path length model. This model allows relating the measured reflectance to the absorption coefficient. This model requires knowledge of the reduced scattering coefficient of the phantom, or in

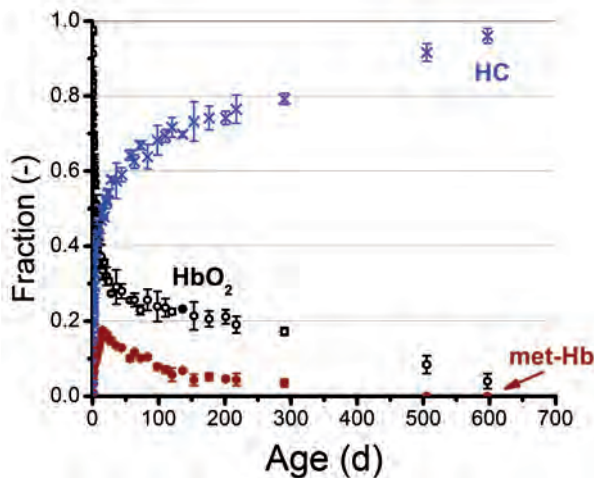


Figure 2. Fraction of HbO_2 (black), met-Hb (red) and HC (blue) in a bloodstain as function of age up to 600 days.

cases of a bloodstain its host material e.g. cotton. At the end of **chapter 4**, we show that the empirical model is applicable on cotton, and reveals the high reduced scattering coefficient of cotton, $\mu_s' > 20 \text{ mm}^{-1}$. At the beginning of **chapter 5**, it is shown that the scattering of bloodstain on cotton is similar to the scattering of cotton itself. This observation with optical coherence tomography allows application of the empirical model as described in **chapter 4** on bloodstains. This observation eliminates the necessity to measure the scattering properties of dried bloodstains itself; this would not have been straight forward. Namely, the reduced scattering coefficient, μ_s' , is product of the scattering coefficient μ_s and $1-g$, with g being the scattering anisotropy parameter. Both parameters, μ_s and g , are difficult to measure for red blood cells, because of the high anisotropy value of red blood cells. To illustrate the difficulty: Mie calculations, in combination with Kramers Kronig analysis at 600 nm show that for fully oxygenated red blood cells $\mu_s = 391 \text{ mm}^{-1}$ and $g = 0.995$, consequently $\mu_s' = 20 \text{ mm}^{-1}$ [140]. On the other hand, do integrating sphere measurements, in combination with inverse Monte Carlo analysis at 600 nm, show that $\mu_s = 70 \text{ mm}^{-1}$ and $g = 0.997$, consequently the reduced scattering is an order of magnitude smaller, $\mu_s' = 2 \text{ mm}^{-1}$ [141]. These observations, both with complicated analysis show disagreement, yet this only about red blood cells in a solution. Scattering of red blood cells in a dried stain is even harder to measure. Luckily, the scattering of cotton is dominant over scattering of the bloodstain.

Figure 7 in **chapter 4** also shows that the chromophores in an aqueous solution redistribute when a stain on cotton is formed. The chromophores dense around the center of the stain, creating a peripheral zone at the edge of the stain without chromophores, see inset of figure 7, chapter 4. This chromatographic effect seems less prominent in bloodstains and therefore we did not have to account for this chromatographic effect in bloodstains. Figure 3 of **chapter 5**, confirms that the empirical path length model is applicable on bloodstains on cotton, without having to account of redistribution of chromophores. This chapter also reveals the biphasic oxidation of oxy-hemoglobin. It shows that the fraction of HbO_2 is temperature dependent, but humidity independent. The influence of temperature of ageing on bloodstains may introduce an additional inaccuracy in age estimation when the temperature under which the bloodstain was stored is not exactly known. This inaccuracy due to lack of knowledge on temperature adds up to the inaccuracy in age determination as shown in figure 1, since inaccuracy due to uncertainty in temperature is not taken into account in this figure.

The observed insensitiveness of ageing HbO_2 on humidity makes the fraction of HbO_2 the most suited candidate for age determination when the humidity is unknown. The fraction of HbO_2 as a function of age decreases faster at higher temperatures. Figure 3 shows the fraction of HbO_2 as a function of age for $T=18 \text{ }^\circ\text{C}$ and $T = 22 \text{ }^\circ\text{C}$. These functions are based on long term measurements shown in figure 2 and the ageing parameters from as function of temperature, as measured in chapter 5. For $T = 22 \text{ }^\circ\text{C}$, these parameters were measured. For $T = 18 \text{ }^\circ\text{C}$, these parameters had to be interpolated at $18 \text{ }^\circ\text{C}$ from measurements at $-20, 4, 22, 29,$ and $37 \text{ }^\circ\text{C}$. The horizontal dashed line shows a hypothetical measurement of HbO_2 fraction of 0.25 in a bloodstain.

The minimal differences in temperature between 18 °C and 22 °C have quite an impact on age estimation: the estimated age is between 58 days for 22 °C and 128 days for 18 °C. Yet the actual age estimation is even worse, since the inaccuracy of biological variation and measurement error is not taken in account in this figure.

Figure 3 shows that long term age estimation with reflectance spectroscopy will remain difficult. Because of the nature of the oxidation of bloodstains, a small uncertainty in temperature already introduces a large uncertainty in age estimation. Figure 1 showed that the inaccuracy increases with age. This inaccuracy is based on measurements presented in **chapter 2**. **Chapter 5** shows a reduction in measurement error on determination of hemoglobin derivatives as a function of age, (chapter 2 figure 6 versus chapter 5 figure 5). This reduction in measurement error and improvement of fitting procedure will reduce the inaccuracy of age estimation. This reduction of measurement error is vital for increasing the forensic relevance of this technique. Focus of future research should therefore be in reducing the measurement error and fully exploring environmental factors on age estimation.

Chapter 6 shows that the reflectance spectrum as a function of absorption is completely determined by the photon path length distribution at zero absorption. The probe specific photon path length distribution is determined by Monte Carlo Simulations. Finally, **Chapter 7** describes the phantom measurement from chapter 4 in terms of the diffusion approximation of light. Three approaches are explored for the diffusion theory, two with physical model parameters and one with empirical determined, fitted parameters. An excellent agreement is observed between phantom measurements and the diffusion approximation, also at large absorption coefficients. This observation is remarkable since diffusion approximation should not be valid, neither for short photon paths nor for large absorption values. These observations indicate possible larger validity of the diffusion approximation, yet conceivably conclusion on this matter requires further investigation of this theory on go beyond the scope of this thesis.

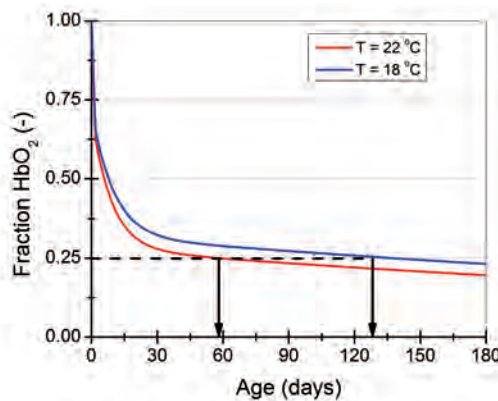


Figure 3. Fraction of HbO₂ as a function of age for T= 18 °C (blue) and T = 22°C (red). The dashed line shows measured HbO₂ fraction in a case report. The estimated age is between 58 days for 22 °C and 128 days for 18 °C.

GETTING STARTED

The next paragraphs describe personal experiences and scientific difficulties during my PhD

Even after four years, it is not hard to remember my first approach in exploring the challenges in ageing bloodstains. Since the color change of an ageing bloodstain is so prominent visible, digital photography was a logical first step. The left parts of figure 4 shows images of an ageing bloodstain. A fresh bloodstain appears bright red and it gradually transits to brown. As described in chapter 1, already in 1907, scientists have related the color change with the age of the bloodstain [42]. However, no study has been performed addressing the quantification of color change. Quantifying color change is effortless when using a digital camera or webcam. I have studied the color change of a bloodstain on cotton with a Logitech webcam. The images recorded with this camera are stored as 8-bit RGB images. The color change of the bloodstain is most prominent in the red pixel value during the first 100 hours of ageing. The red pixel value as function of age is shown in the top right panel of figure 4.

The red pixel value starts around 160 for a fresh bloodstain. It remains around this value during the first hour, thereafter the red pixel decreases in 100 hours to around 80. This change in pixel value is visible as the bloodstain becomes darker. At the bottom of figure 4, the fraction of HbO_2 in a bloodstain is shown. The HbO_2 fraction is determined by multi-component fit of a different bloodstain than shown in the middle panel, but stored under similar circumstances. The fraction of HbO_2 as a function of age in the bottom panel shows a remarkable resemblance with the red pixel value as function of age in the panel above; accordingly the correlation coefficient between the two graphs, $r^2 = 0.918$. During the first hour the HbO_2 fraction remains 1, which is attributed to the reductase proteins present in blood still being active to reduce the

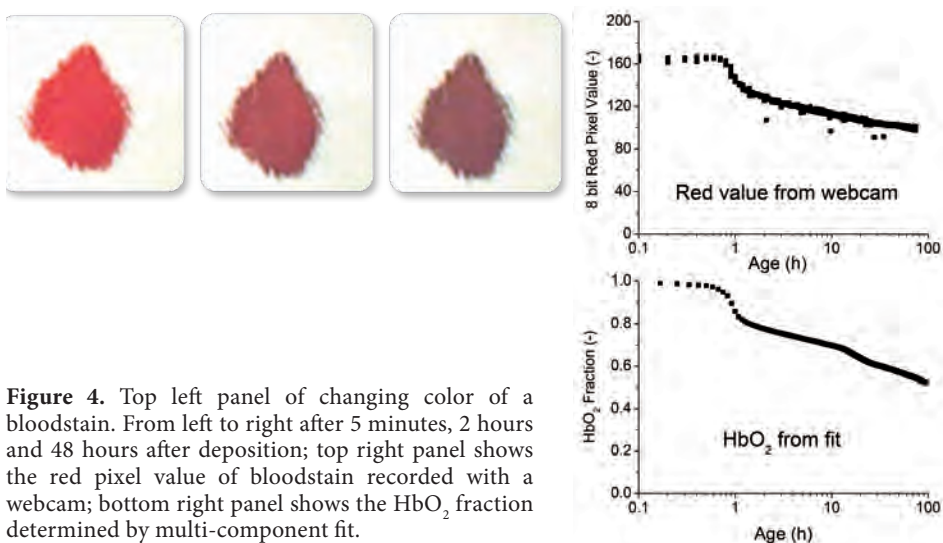


Figure 4. Top left panel of changing color of a bloodstain. From left to right after 5 minutes, 2 hours and 48 hours after deposition; top right panel shows the red pixel value of bloodstain recorded with a webcam; bottom right panel shows the HbO_2 fraction determined by multi-component fit.

formed met-Hb back to hemoglobin. After an hour, the reductase proteins become inactive and the oxidation of HbO_2 into met-Hb and HC becomes irreversible. The use of webcam can be worthwhile monitoring an ageing bloodstain. Yet it is not very applicable for age determination, since the red pixel value also depends on the amount of light and position of the camera. Therefore, the use of a webcam did not receive follow-up.

The most important step during my PhD and in analyzing the reflectance spectra of a bloodstain was the recognition of the presence of hemichrome. It might have come across being obvious to include hemichrome in the analysis, while reading this thesis. Yet for more than two and a half year I have overlooked hemichrome and I was in good company. Many previous studies [5, 52, 57] ignore the presence of this chromophore and it was unknown by my supervisors and colleagues as well. It took until October 20 2009, before I fully realized the presence of hemichrome. Before this realization, I experienced lot of difficulties with the multi-component fitting algorithm of the reflectance of bloodstains. This analysis algorithm is only successful if 1) the light transport is modeled correctly and 2) all chromophores responsible for attenuation of the reflectance signal are included in the multi-component fit. Obviously, during the first two years, I did not meet the second requirement, explaining the origin of the fitting difficulties, while ignoring hemichrome.

Figure 5 shows the difference between a multi-component fit without and with hemichrome included in the fit analysis. For more than two years the features in the residue between the multi-component fit and the reflectance of the bloodstain were attributed to an incorrect light transport model, or incorrect incorporation of the inhomogeneous distribution of the chromophores [74, 119, 142]. Many reflectance spectroscopy models have been explored to analyze the bloodstain measurements, but no model was successful in fitting a bloodstain reflectance without including hemichrome. The mismatch between fit and reflectance is visualized by the residue at the bottom of figure 5. Whereas the left panel shows quite a residue, the residue on the right panel

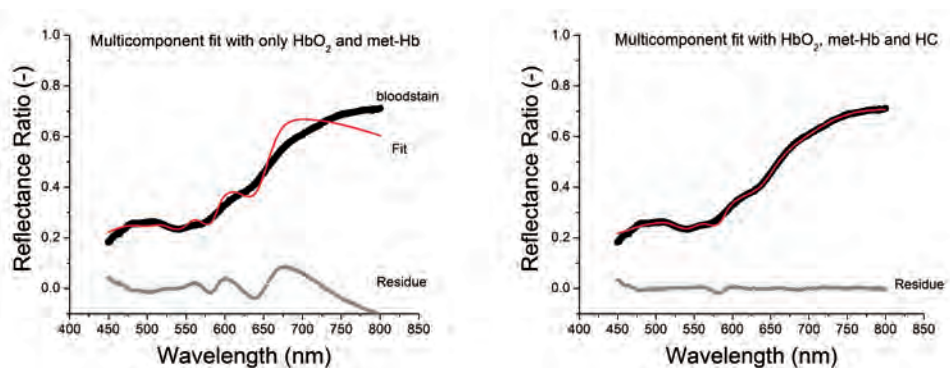


Figure 5. Difference between a multi-component fit with only HbO_2 and met-Hb (left panel) and a multi-component fit with HbO_2 , met-Hb and HC (right panel).

is almost completely flat. The outcome of the multi-component fit algorithm without hemichrome is: $\text{HbO}_2 = 0.34$ and $\text{met-Hb} = 0.66$. While with including hemichrome in the analysis, the fractions are $\text{HbO}_2 = 0.27$, $\text{met-Hb} = 0.15$ and $\text{HC} = 0.58$. Clearly, the absence of including hemichrome in the fitting algorithm causes overestimation of the presence of met-Hb. This overcompensation introduces an error, which makes the outcome of the fitting algorithm unreliable [75].

After exploring almost all available light transport models, and still not finding a fit without flat residue, I hypothesized the presence of an additional, unknown chromophore in the bloodstain. I observed that the mismatch between bloodstain and multi-component fit without HC is most prominent for very old (more than one year old) bloodstains. Would it be possible to isolate the chromophores in an old bloodstain? Yes it is. By placing a two year bloodstain in a funnel and poring distilled water onto the bloodstain, I was able to solute the chromophore into an aqueous solution (see figure 6). The solvent was intercepted into a cuvette, to enable measuring the transmission of light. The determined absorption spectrum showed minimal similarities with the absorption spectrum of met-Hb, and the absorption peak around 630 nm, very typical for the absorption spectrum of met-Hb was not as dominant in the measured chromophore as it is in the absorption spectrum of met-Hb. Apparently, the measured spectrum was from a different, still for me unknown, chromophore. When I included the measured absorption spectrum into the multi-component fit of the reflectance spectrum of a bloodstain, I observed a major improvement of the fit quality and consequent reduction of residue.

It took another few months, before I realized the additional, still unknown chromophore was called hemichrome. In the meantime, I called the newfound chromophore 'XHb'. When analyzing the reflectance of a two year old bloodstain, the fit parameters showed no presence of HbO_2 or met-Hb, but a full fraction of 'XHb'. An observation, which was confirmed in later study and shown in figure 2, where after 500 days almost no HbO_2 and met-Hb are present as well. After an intense literature search, I encountered [23] and [32] to solve the mystery of XHb being hemichrome. In [23] the ageing process of bloodstains is described in terms of HbO_2 , met-Hb and HC; additionally [32] shows an absorption spectrum of HC. This HC absorption spectrum showed almost complete agreement with the absorption spectra I had obtained from the two year old bloodstain, with the funnel procedure. These three observations: improvement of fitting, similar spectra between an old bloodstain and hemichrome from [32], and confirmation from [23] of hemichrome being formed from HbO_2 and met-Hb were key in solving the mystery of XHb being hemichrome.

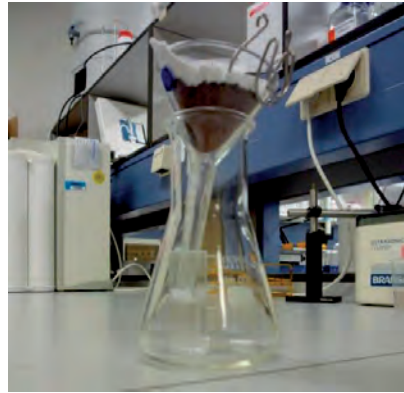


Figure 6. Extraction of hemichrome out of two year old bloodstain.

One final remark on the residue on the right panel of figure 5: The multi-component fit of HbO₂, met-Hb and HC has an almost flat residue. Yet around 574 nm a small feature is visible. This feature is present in almost all bloodstain fits of more than a few days old. This feature is at 574 nm, which is a local absorption peak of HbO₂. One of the assumptions in the multi-component fit algorithm is that the absorption spectra of HbO₂, met-Hb and HC do not change during the ageing process. Possibly, this assumption is not completely true, and the presence of residue between multi-component fit and bloodstain reflectance can be attributed to a change in the absorption spectrum of HbO₂.

REFLECTANCE SPECTROSCOPY

The next paragraphs reflect my personal opinion on reflectance spectroscopy as a clinical measurement technique.

Optical techniques promise non-invasive measurement of clinically relevant quantities such as oxygenation and metabolite (e.g. glucose) levels. Techniques as fluorescence, Raman spectroscopy, in particular reflectance spectroscopy rely heavily on multi-component fitting procedures to infer these from the measured spectra. Amelink *et al.* [75] show that imperfections in the fit model introduce unpredictable, large bias in the fitted parameters. This bias is part of a larger set of pitfalls in reflectance spectroscopy. It is important to understand these pitfalls, since the focus of reflectance spectroscopy is shifting from a more fundamental, optical approach to a more clinical. Reading the reflectance spectroscopy literature, one gets the impression of a modern day Tower of Babel, see figure 7, where everyone builds his own model, instead of harvesting from each other. This current state of affairs makes it difficult to compare work and has kept us from making more progress. In order to meet the expectations, I see three main challenges:

1) Hemoglobin spectra and Packaging Factors

The current situation is that almost every group has developed its own complicated or simplified model for light transport in tissue to describe their own specific experiment. I do not want to argue the quality of any of these models, but it is evident that this situation hampers interdepartmental corporation and clinical effort. There have been some distinguished attempts over the last two decades, like MEDPHOT [143] to propose protocols and more standardization, however most efforts have vanished. It appears that more unity in the form of an applicable standard light model is practically impossible, I do want to stress for more unity on two points: the hemoglobin spectra and packaging factors.

First point is the hemoglobin spectra, the absorption spectrum of hemolyzed hemoglobin has often been measured and its spectrum is used in fitting algorithms to obtain oxygen saturation. These input spectra from Zijlstra [31], Prahl [144] and Friebe [141] differ from each other. Choosing an available hemoglobin data set influences the outcome of the analysis [145], the absorption spectra of Zijlstra *et al* show superior

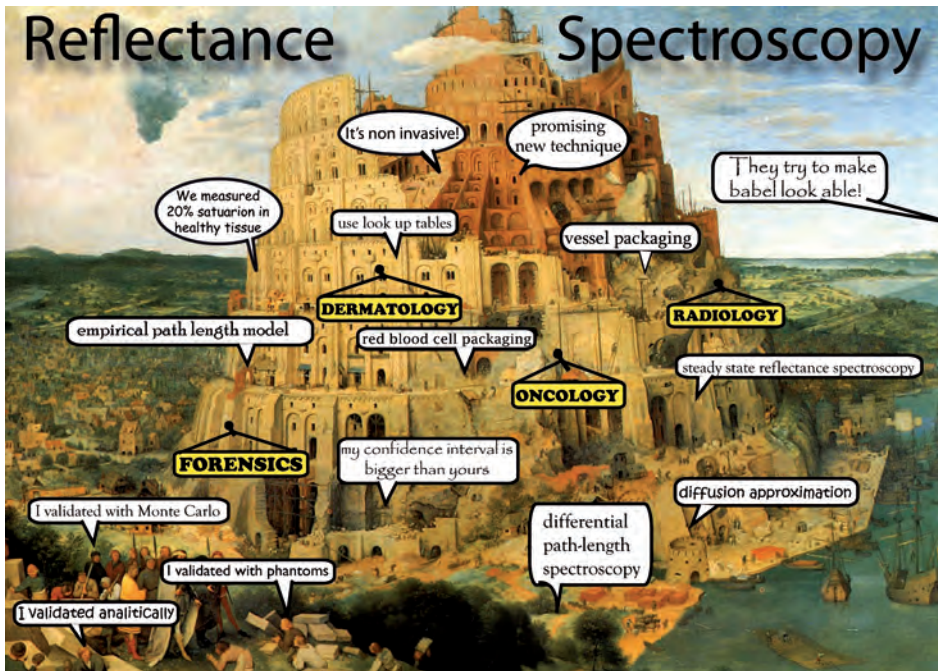


Figure 7. Cartoonist impression of communication among scientists in the field of reflectance spectroscopy.

results in this study. Alike with the various models, people tend to choose that spectrum, or a combination of these spectra, that explains their experiment the best. This is also the case with packaging factors of hemoglobin. Hemoglobin is not spread homogeneous in tissue, but packed in red blood cells, which are on their turn packed in vessels. This heterogeneity of hemoglobin affects the optical path length [142]. Some theories only account for RBC-packaging [74], some only for vessel packaging [119] and some ignore this effect at all.

I would recommend use absorption spectra of Zijlstra *et al.* for HbO₂ and met-Hb as published in whole blood absorption coefficients. Zijlstra provided the absorption spectra in molar extinction coefficients. Multiplying the data from Zijlstra with the typical amount of hemoglobin in blood produces the absorption coefficients for whole blood, as appreciated in table 1. Here spectra in the wavelength region from 450 nm to 800 nm are tabulated of HbO₂ and met-Hb from [31] and HC are from [32]. Translating the molar extinction coefficients to whole blood absorption coefficients has advantages for the multi-component fitting algorithm. By using the whole blood absorption coefficient, the sum of the fit parameters cumulates to the blood volume fraction, as is shown in chapter 4 and 5.

The chromophores in table 1 are specific for age determination of bloodstains. For clinical purposes, deoxy-hemoglobin and bilirubin, should be added, depending on the

nature of the clinical study. Regarding the packaging factor, I would recommend the use of the Verkruyse's approach [119]. The 'Verkruyse' correction factor C_{eff} in Eq (1) can be used simultaneously for hemoglobin packaging in red blood cells and vessels, since the effect of packaging of hemoglobin in vessels is dominant over packaging in red blood cells. The packaging depends on the absorption coefficient, μ_a , and the vessel or red blood cell diameter, D , and is a correction on the actual absorption coefficient.

$$C_{eff} = \frac{1 - \exp(-\mu_a D)}{\mu_a D} \quad (1)$$

2) Fitting Quality

Multi-component fitting algorithms are commonly used to extract chromophore concentrations from measurement results. If the model fits the experimental data correct, one can extract physical or physiological quantities from the fit. The focus of fitting in spectroscopy is more on extracting physiological quantities than on the explaining the nature of the experiment. The step to check whether the model describes the data good enough is crucial, in order to rely on the physiological quantities in the form of fit parameters. A pitfall with fitting algorithms is that no matter the quality of your model, the algorithm will always produces the best possible fit. It remains arbitrary to qualify the goodness of fit, and to value the forthcoming fit parameters. Numbers, such as oxygen saturation are nearly impossible to verify, which makes it difficult to judge the outcome of reflectance spectroscopy, as far as saturation concerns. Additional problem is the calculation of the error margins. The genuine point Amelink et. al. make is that the statistical analysis of error margins can extremely underestimate the error margin [75]. Statistical analysis, such as confidence intervals, assumes a perfect model to describe the data. Imperfections in the model cannot be neglected, but remain difficult to translate to error margins in fit parameters.

I would recommend restraint use of multi-component fit analyses, yet setting limits remains difficult. However, two requirements can assist: one being a minimum correlation coefficient r^2 between data and fit. An empirical found minimum correlation between data and model is 0.98. This is an arbitrary limit to exclude the worst fits; it only works in one direction. If the correlation is higher than 0.98 does not mean the model is correct, since any n^{th} order polynomial will be able to fit the experimental data. Second requirement is the residue, defined being the difference between data and fit. A good fit enhances a pure noisy residue, without any features. Hence, features in the residue suggest imperfections in the model, which can induce overcompensation of one of the fit parameters. If the residue nonetheless show any features, the fit parameters should be considered with great reservation.

3) Tissue Phantoms

The third a final challenge is the production of tissue like phantoms. Phantoms, mimicking the optical properties of tissues, have to be used to characterize biomedical optics systems and to validate their associated theories. Pogue and Patterson listed the 12 properties of an ideal tissue phantom [146]. Some of these properties have higher

Table 1. Tabulated absorption spectra of main chromophores in bloodstains, HbO₂, met-HC and HC. All translated to absorption coefficient values for whole blood with Hct of 0.46.

λ	μ_a	μ_a	μ_a	λ	μ_a	μ_a	μ_a	λ	μ_a	μ_a	μ_a
nm	mm ⁻¹	mm ⁻¹	mm ⁻¹	nm	mm ⁻¹	mm ⁻¹	mm ⁻¹	nm	mm ⁻¹	mm ⁻¹	mm ⁻¹
	HbO ₂	met-Hb	HC		HbO ₂	met-Hb	HC		HbO ₂	met-Hb	HC
450	32.23	23.04	36.38	568	21.01	9.427	13.08	686	0.206	0.595	1.676
451	31.05	22.57	35.31	569	22.13	9.428	12.97	687	0.206	0.585	1.654
452	29.8	22.16	34.24	570	23.37	9.429	12.86	688	0.206	0.576	1.632
453	28.67	21.79	33.47	571	24.73	9.429	12.7	689	0.206	0.567	1.61
454	27.6	21.46	32.69	572	26.1	9.429	12.55	690	0.206	0.56	1.589
455	26.58	21.15	31.95	573	27.44	9.43	12.38	691	0.206	0.553	1.552
456	25.62	20.87	31.21	574	28.72	9.431	12.21	692	0.206	0.548	1.516
457	24.75	20.63	30.59	575	29.74	9.425	12.1	693	0.206	0.543	1.487
458	23.92	20.4	29.97	576	30.5	9.415	12	694	0.206	0.538	1.457
459	23.11	20.18	29.43	577	30.63	9.397	11.81	695	0.207	0.535	1.436
460	22.34	19.98	28.9	578	30.69	9.373	11.62	696	0.208	0.531	1.414
461	21.65	19.8	28.3	579	29.93	9.34	11.51	697	0.208	0.528	1.385
462	21	19.64	27.7	580	28.82	9.297	11.41	698	0.208	0.525	1.355
463	20.36	19.47	27.11	581	27.17	9.239	11.2	699	0.209	0.523	1.334
464	19.75	19.31	26.53	582	25.19	9.171	10.99	700	0.21	0.522	1.312
465	19.19	19.19	25.9	583	22.89	9.091	10.89	701	0.211	0.521	1.29
466	18.67	19.07	25.28	584	20.56	9.003	10.79	702	0.212	0.52	1.268
467	18.15	18.95	24.69	585	18.22	8.907	10.66	703	0.212	0.517	1.246
468	17.67	18.83	24.1	586	15.89	8.804	10.53	704	0.212	0.515	1.224
469	17.22	18.76	23.57	587	13.74	8.697	10.39	705	0.214	0.515	1.202
470	16.8	18.7	23.04	588	11.78	8.587	10.26	706	0.216	0.515	1.181
471	16.38	18.65	22.54	589	10.05	8.476	10.08	707	0.217	0.515	1.159
472	15.99	18.59	22.04	590	8.529	8.364	9.896	708	0.218	0.515	1.137
473	15.62	18.6	21.72	591	7.236	8.258	9.765	709	0.219	0.514	1.115
474	15.27	18.61	21.4	592	6.128	8.155	9.634	710	0.22	0.513	1.093
475	14.93	18.63	21.04	593	5.208	8.056	9.517	711	0.222	0.514	1.071
476	14.61	18.66	20.68	594	4.433	7.962	9.4	712	0.224	0.515	1.049
477	14.3	18.73	20.34	595	3.801	7.88	9.255	713	0.225	0.516	1.035
478	14	18.81	19.99	596	3.27	7.805	9.109	714	0.226	0.517	1.02
479	13.72	18.89	19.63	597	2.834	7.736	9.043	715	0.228	0.518	1.006
480	13.45	18.99	19.27	598	2.469	7.675	8.978	716	0.23	0.52	0.991
481	13.2	19.13	18.94	599	2.173	7.627	8.854	717	0.231	0.52	0.969
482	12.96	19.27	18.61	600	1.922	7.589	8.73	718	0.232	0.52	0.947
483	12.73	19.4	18.36	601	1.714	7.558	8.555	719	0.234	0.521	0.933
484	12.51	19.53	18.12	602	1.534	7.534	8.38	720	0.236	0.522	0.918
485	12.33	19.7	17.91	603	1.379	7.517	8.293	721	0.238	0.524	0.896
486	12.15	19.86	17.7	604	1.249	7.504	8.205	722	0.24	0.527	0.874
487	11.96	20.01	17.48	605	1.16	7.504	8.052	723	0.242	0.528	0.86
488	11.78	20.15	17.26	606	1.078	7.504	7.899	724	0.244	0.529	0.845

λ	μ_a	μ_a	μ_a	λ	μ_a	μ_a	μ_a	λ	μ_a	μ_a	μ_a
nm	mm ⁻¹	mm ⁻¹	mm ⁻¹	nm	mm ⁻¹	mm ⁻¹	mm ⁻¹	nm	mm ⁻¹	mm ⁻¹	mm ⁻¹
	HbO ₂	met-Hb	HC		HbO ₂	met-Hb	HC		HbO ₂	met-Hb	HC
489	11.63	20.32	17.1	607	0.997	7.512	7.783	725	0.245	0.531	0.831
490	11.48	20.5	16.94	608	0.92	7.523	7.666	726	0.246	0.534	0.816
491	11.34	20.63	16.81	609	0.854	7.548	7.542	727	0.248	0.536	0.794
492	11.19	20.76	16.68	610	0.794	7.579	7.418	728	0.25	0.538	0.772
493	11.07	20.9	16.49	611	0.74	7.615	7.316	729	0.252	0.541	0.765
494	10.95	21.04	16.31	612	0.692	7.659	7.214	730	0.254	0.543	0.758
495	10.83	21.12	16.15	613	0.649	7.72	7.127	731	0.256	0.546	0.743
496	10.71	21.21	15.98	614	0.61	7.79	7.039	732	0.258	0.548	0.729
497	10.61	21.29	15.83	615	0.575	7.865	6.945	733	0.26	0.55	0.714
498	10.51	21.37	15.69	616	0.542	7.946	6.85	734	0.262	0.553	0.7
499	10.41	21.39	15.57	617	0.512	8.046	6.733	735	0.264	0.556	0.692
500	10.31	21.41	15.45	618	0.484	8.15	6.617	736	0.266	0.56	0.685
501	10.22	21.4	15.31	619	0.459	8.256	6.507	737	0.268	0.563	0.67
502	10.14	21.39	15.17	620	0.436	8.365	6.398	738	0.27	0.567	0.656
503	10.05	21.32	15.11	621	0.414	8.473	6.289	739	0.272	0.571	0.649
504	9.969	21.24	15.04	622	0.394	8.583	6.18	740	0.274	0.576	0.641
505	9.907	21.15	14.99	623	0.377	8.696	6.121	741	0.276	0.58	0.634
506	9.854	21.04	14.94	624	0.36	8.808	6.063	742	0.278	0.583	0.627
507	9.805	20.88	14.92	625	0.344	8.893	5.917	743	0.28	0.587	0.612
508	9.766	20.72	14.9	626	0.328	8.971	5.771	744	0.282	0.59	0.598
509	9.76	20.56	14.94	627	0.313	9.045	5.662	745	0.284	0.594	0.59
510	9.758	20.4	14.98	628	0.3	9.111	5.553	746	0.286	0.597	0.583
511	9.792	20.18	15.02	629	0.289	9.153	5.414	747	0.288	0.602	0.576
512	9.844	19.97	15.07	630	0.278	9.181	5.276	748	0.29	0.607	0.568
513	9.948	19.76	15.11	631	0.268	9.177	5.232	749	0.303	0.61	0.561
514	10.09	19.56	15.16	632	0.258	9.17	5.188	750	0.315	0.614	0.554
515	10.26	19.32	15.22	633	0.249	9.126	5.065	751	0.308	0.618	0.539
516	10.47	19.09	15.27	634	0.24	9.064	4.941	752	0.3	0.623	0.525
517	10.76	18.87	15.32	635	0.234	8.974	4.831	753	0.302	0.628	0.517
518	11.1	18.65	15.37	636	0.228	8.857	4.722	754	0.304	0.633	0.51
519	11.5	18.41	15.51	637	0.222	8.701	4.627	755	0.306	0.638	0.51
520	11.96	18.18	15.65	638	0.216	8.511	4.533	756	0.308	0.644	0.51
521	12.52	17.97	15.65	639	0.212	8.288	4.438	757	0.311	0.649	0.496
522	13.16	17.75	15.65	640	0.208	8.032	4.343	758	0.314	0.654	0.481
523	13.86	17.54	15.73	641	0.205	7.741	4.234	759	0.316	0.66	0.474
524	14.64	17.32	15.8	642	0.202	7.423	4.125	760	0.318	0.665	0.466
525	15.52	17.14	15.87	643	0.2	7.084	4.03	761	0.32	0.67	0.459
526	16.47	16.96	15.94	644	0.198	6.727	3.935	762	0.322	0.675	0.452
527	17.46	16.79	15.99	645	0.198	6.351	3.862	763	0.324	0.68	0.452
528	18.5	16.62	16.03	646	0.198	5.975	3.789	764	0.326	0.687	0.452
529	19.6	16.47	16.1	647	0.197	5.613	3.709	765	0.329	0.694	0.445

λ	μ_a	μ_a	μ_a	λ	μ_a	μ_a	μ_a	λ	μ_a	μ_a	μ_a
nm	mm ⁻¹	mm ⁻¹	mm ⁻¹	nm	mm ⁻¹	mm ⁻¹	mm ⁻¹	nm	mm ⁻¹	mm ⁻¹	mm ⁻¹
	HbO ₂	met-Hb	HC		HbO ₂	met-Hb	HC		HbO ₂	met-Hb	HC
530	20.7	16.33	16.16	648	0.196	5.266	3.629	766	0.332	0.701	0.437
531	21.78	16.19	16.15	649	0.196	4.949	3.542	767	0.334	0.705	0.43
532	22.84	16.05	16.14	650	0.196	4.635	3.454	768	0.336	0.71	0.423
533	23.85	15.94	16.14	651	0.197	4.32	3.381	769	0.339	0.718	0.415
534	24.8	15.82	16.14	652	0.198	4.008	3.308	770	0.342	0.726	0.408
535	25.66	15.68	16.07	653	0.198	3.729	3.243	771	0.344	0.732	0.408
536	26.44	15.55	15.99	654	0.198	3.452	3.177	772	0.346	0.738	0.408
537	27.16	15.41	15.92	655	0.197	3.168	3.082	773	0.348	0.744	0.401
538	27.8	15.28	15.86	656	0.196	2.891	2.988	774	0.35	0.75	0.394
539	28.27	15.1	15.76	657	0.196	2.713	2.944	775	0.353	0.757	0.386
540	28.64	14.92	15.67	658	0.196	2.547	2.9	776	0.356	0.764	0.379
541	28.87	14.72	15.58	659	0.198	2.384	2.842	777	0.358	0.771	0.379
542	29.03	14.51	15.49	660	0.2	2.222	2.784	778	0.36	0.778	0.379
543	28.89	14.26	15.38	661	0.201	2.06	2.704	779	0.363	0.787	0.372
544	28.67	13.99	15.27	662	0.202	1.901	2.623	780	0.366	0.795	0.364
545	28.24	13.71	15.2	663	0.202	1.755	2.594	781	0.368	0.803	0.364
546	27.66	13.42	15.13	664	0.202	1.623	2.565	782	0.37	0.811	0.364
547	26.87	13.11	14.99	665	0.202	1.506	2.514	783	0.373	0.818	0.357
548	25.98	12.79	14.85	666	0.202	1.402	2.463	784	0.376	0.825	0.35
549	25	12.46	14.74	667	0.203	1.312	2.405	785	0.378	0.832	0.35
550	24.02	12.14	14.63	668	0.204	1.23	2.346	786	0.38	0.84	0.35
551	23.03	11.82	14.54	669	0.204	1.151	2.31	787	0.383	0.848	0.342
552	22.04	11.51	14.46	670	0.204	1.079	2.274	788	0.386	0.856	0.335
553	21.15	11.22	14.38	671	0.204	1.017	2.23	789	0.389	0.864	0.328
554	20.34	10.96	14.31	672	0.204	0.962	2.186	790	0.392	0.872	0.321
555	19.61	10.71	14.22	673	0.205	0.913	2.142	791	0.394	0.879	0.321
556	18.97	10.48	14.14	674	0.206	0.87	2.099	792	0.396	0.887	0.321
557	18.45	10.28	14.09	675	0.206	0.832	2.062	793	0.399	0.896	0.313
558	18.03	10.11	14.05	676	0.206	0.797	2.026	794	0.402	0.905	0.306
559	17.74	9.951	13.93	677	0.206	0.765	1.989	795	0.404	0.914	0.306
560	17.54	9.82	13.82	678	0.206	0.736	1.953	796	0.406	0.922	0.306
561	17.54	9.715	13.76	679	0.206	0.71	1.909	797	0.409	0.929	0.306
562	17.54	9.627	13.7	680	0.206	0.687	1.866	798	0.412	0.936	0.306
563	17.77	9.56	13.58	681	0.206	0.668	1.829	799	0.414	0.945	0.299
564	18.09	9.507	13.45	682	0.206	0.651	1.793	800	0.416	0.954	0.291
565	18.59	9.475	13.38	683	0.206	0.635	1.771				
566	19.23	9.45	13.31	684	0.206	0.621	1.749				
567	20.04	9.437	13.19	685	0.206	0.607	1.712				

priority than others, depending on the specific application. To validate the assessment of chromophore concentration in tissue with reflectance, a phantom must have multiple controllable chromophores and must preferably be multi-layered, mimicking the structure of skin [112]. A single chromophore is insufficient, because many errors arise from overcompensation chromophore concentration in an imperfect fitting model. Making such phantoms is a true challenge itself, but necessary to be able to rely on the outcome of fit parameters in tissue.

In summary, these three points illustrate challenges in analyzing reflectance spectroscopic measurements. Multi-component fit analysis of reflectance spectra seems an improvement compared to analyzing single wavelengths [3, 147], especially when more than two chromophores are unknown. However ignoring the discussed challenges in multi-component fitting may provide inexplicable physiological results [148, 149]. Such results rather indicate insufficient analysis of the reflectance measurements than new insight in clinical issues. To prevent for future inexplicable physiological results requires breaching the current 'Babylonian Confusion' in the field of reflectance spectroscopy. A unified spoken language of reflectance spectroscopy with unification of absorption spectra, reflectance model and requirement of phantom validation is necessary to advance this technique to new clinical and forensic applications.

FORENSIC OUTLOOK

This thesis has shown the potential of spectroscopic age determination of bloodstains. Reflectance spectroscopy is suited very well for age determination on the crime scene. Ideally a reflectance spectroscopy setup would become part of the standard technologies of forensic investigators equipment. Reflectance measurement can become a routine for crime scene investigators when encountering bloodstains on a crime scene. This would not only reduce work load of forensic laboratory, it also assists in reducing inaccuracy, since the inaccuracy increases with the age of the bloodstain.

For the acceptance of reflectance spectroscopy as a standard forensic technology, it is important to explore other potential technique to determine the age of the bloodstain. New opportunities in age determination of bloodstains may occur following after a technical or biomedical invention. The potential for bloodstain age determination based on changes in the state of hemoglobin was already discussed by Leers in 1910 [43], yet hundred years later this still has not been realized into daily forensic practice. Technological improvements though have enabled major steps towards forensic implementation. Spectroscopic measurements in the late 1950s were recorded with a tunable monochromator and a photodiode [150], recording the reflectance spectrum of a single bloodstain over the total visible part of the spectrum would take more than an hour. Nowadays, commercially available portable spectrometers can do this in less than one second. The requirement for technical and biomedical improvement hampers prediction on future technologies addressing the age determination of bloodstains. A possible candidate is degradation of proteins and enzymes. This has already been

investigated by Rajamannar and Tsutsumi *et al* [39, 40], but has not been followed up. Yet, recent developments in cancer protein research open up a variety of opportunities. The techniques that enable microarray tumor classification [151] and prediction of tumor progression based on gene expression [152] can potentially be modified and applied to measure the ageing state of bloodstains. Another potential future age determination technique is Raman Spectroscopy. This non-invasive biomedical technique has already been explored for bloodstain identification [153, 154] and handheld Raman devices are commercially available. Raman spectroscopy is known to produce complicated spectra for every individual biological sample that is studied, including hemoglobin [153]. Often, changes in Raman spectra are analyzed by principal component analysis, yet the real challenge is to relate changes in Raman spectra in ageing bloodstains to changes in hemoglobin derivatives. The latter will allow comparing reaction kinetics measured with Raman to reaction kinetics as discussed in this thesis or measured with oxygen electrodes [57].

Regardless of the advances made during the last years, the influence of temperature and exposure to sunlight cannot be ignored. For reflectance spectroscopy to become standard equipment, future research should focus on mapping all environmental factors and focus on first ten days of ageing, when oxidation is still rapid. Only then, reflectance spectroscopy can become a useful technique to deliver results which will be truly forensically relevant and to be acceptable for court testimony.

ADDENDUM
BIBLIOGRAPHY
PUBLICATION LIST
SUMMARY
SAMENVATTING
DANKWOORD
CURRICULUM VITAE



BIBLIOGRAPHY

1. D. Patterson, Use of reflectance measurements in assessing the colour changes of ageing bloodstains, *Nature* **187** (1960), pp. 688-689.
2. S.S. Kind, D. Patterson and G.W. Owen, Estimation of the age of dried blood stains by spectrophotometric method, *Forensic Science* **1** (1972), pp. 27-54.
3. E.K. Hanson and J. Ballantyne, A Blue Spectral Shift of the Hemoglobin Soret Band Correlates with the Age (Time Since Deposition) of Dried Bloodstains, *PLoS One* **5** (2010), p. e12830.
4. U. Köhler and I. Oepen, On the suitability of spectrophotometric analyses for the estimation of blood stain age *Z Rechtsmed* **18** (1977), p. 5.
5. V. Blazek and G. Lins, Spectroscopic age determination of blood stains: new technical aspects, *Acta Med Leg Soc (Liege)* **32** (1982), pp. 613-616.
6. C. Henssge and B. Madea, Estimation of the time since death, *Forensic Science International* **165** (2007), pp. 182-184.
7. M. Kaliszczan, R. Hauser and G. Kernbach-Wighton, Estimation of the time of death based on the assessment of post mortem processes with emphasis on body cooling, *Legal Medicine* **11** (2009), pp. 111-117.
8. J.L. Smart, Estimation of Time of Death With a Fourier Series Unsteady-State Heat Transfer Model, *Journal of Forensic Sciences* **55** (2010), pp. 1481-1487.
9. C. Meissner and S. Ritz-Timme, Molecular pathology and age estimation, *Forensic Science International* **203** (2010), pp. 34-43.
10. W. Grellner and B. Madea, Demands on scientific studies: Vitality of wounds and wound age estimation, *Forensic Science International* **165** (2007), pp. 150-154.
11. B. Stam, M. van Gemert, T. van Leeuwen and M. Aalders, 3D finite compartment modeling of formation and healing of bruises may identify methods for age determination of bruises, *Medical and Biological Engineering and Computing* **48** (2010), pp. 911-921.
12. N. Langlois, The science behind the quest to determine the age of bruises—a review of the English language literature, *Forensic Science, Medicine, and Pathology* **3** (2007), pp. 241-251.
13. C. Weyermann, C. Roux and C. Champod, Initial Results on the Composition of Fingerprints and its Evolution as a Function of Time by GC/MS Analysis, *Journal of Forensic Sciences* (2010).
14. K. Wertheim, Fingerprint Age Determination: Is There Any Hope?, *Journal of Forensic Identification* **53** (2002), p. 8.
15. M. Ezcurra, J.M.G. Góngora, I. Maguregui and R. Alonso, Analytical methods for dating modern writing instrument inks on paper, *Forensic Science International* **197** (2010), pp. 1-20.
16. X.-F. Wang, J. Yu, M.-X. Xie, Y.-T. Yao and J. Han, Identification and dating of the fountain pen ink entries on documents by ion-pairing high-performance liquid chromatography, *Forensic Science International* **180** (2008), pp. 43-49.
17. S.H. James, *Principles of Bloodstain Pattern Analysis*, CRC Press (2005).
18. P. Hortolà, SEM examination of human erythrocytes in uncoated bloodstains on stone: use of conventional as environmental-like SEM in a soft biological tissue (and hard inorganic material), *Journal of Microscopy* **218** (2005), pp. 94-103.
19. S. Strasser, A. Zink, G. Kada, P. Hinterdorfer, O. Peschel, W.M. Heckl, *et al.*, Age determination of blood spots in forensic medicine by force spectroscopy, *Forensic Science International* **170** (2007), pp. 8-14.
20. H. Chen, M. Ikeda-Saito and S. Shaik, Nature of the Fe-O-2 Bonding in Oxy-Myoglobin: Effect of the Protein, *J. Am. Chem. Soc.* **130** (2008), pp. 14778-14790.
21. J.B. Wittenberg, B.A. Wittenberg, J. Peisach and W.E. Blumberg, On the State of the Iron and the Nature of the Ligand in Oxyhemoglobin, *Proceedings of the National Academy of Sciences of the United States of America* **67** (1970), pp. 1846-1853.
22. A. Borisova, Comparative analysis of various hemoglobins: Autoxidation and spectral properties, *Journal of Evolutionary Biochemistry and Physiology* **44** (2008), pp. 532-534.

23. A. Marrone and J. Ballantyne, Changes in dry state hemoglobin over time do not increase the potential for oxidative DNA damage in dried blood, *PLoS One* **4** (2009), p. e51110.
24. J. Peisach, W.E. Blumberg, B.A. Wittenberg, J.B. Wittenberg and L. Kampa, Hemoglobin A: an Electron Paramagnetic Resonance Study of the Effects of Interchain Contacts on the Heme Symmetry of high-spin and low-spin derivatives of ferric alpha chains, *Proceedings of the National Academy of Sciences of the United States of America* **63** (1969), pp. 934-939.
25. K. Shikama, The molecular mechanism of autoxidation for myoglobin and hemoglobin: A venerable puzzle, *Chemical Reviews* **98** (1998), pp. 1357-1373.
26. J. Umbreit, Methemoglobin - It's not just blue: A concise review, *Am. J. Hematol.* **82** (2007), pp. 134-144.
27. A. Smith, Basic Medical Biochemistry, Lippincott Williams & Wilkins (2004).
28. D.A. Svistunenko, M.A. Sharpe, P. Nicholls, C. Blenkinsop, N.A. Davies, J. Dunne, *et al.*, The pH dependence of naturally occurring low-spin forms of methaemoglobin and metmyoglobin: an EPR study, *Biochem. J.* **351** (2000), pp. 595-605.
29. T. Miki, A. Kai and M. Ikeya, Electron spin resonance of bloodstains and its application to the estimation of time after bleeding, *Forensic Science International* **35** (1987), pp. 149-158.
30. J.M. Rifkind, O. Abugo, A. Levy and J. Heim, Detection, Formation, and Relevance of Hemichromes and Hemochromes, *Methods in Enzymology* **1** (1994), pp. 449-480.
31. W.G. Zijlstra, A. Buursma and W.P. Meeuwse-Van der Roest, Absorption spectra of human fetal and adult oxyhemoglobin, de-oxyhemoglobin, carboxyhemoglobin, and methemoglobin, *Clinical Chemistry* **37** (1991), pp. 1633-1638.
32. T. Asakura, K. Minakata, K. Adachi, M.O. Russell and E. Schwartz, Denatured Hemoglobin in Sick Erythrocytes, *Journal of Clinical Investigation* **59** (1977), pp. 633-640.
33. I. Dulinska, M. Targosz, W. Strojny, M. Lekka, P. Czuba, W. Balwierz, *et al.*, Stiffness of normal and pathological erythrocytes studied by means of atomic force microscopy, *Journal of Biochemical and Biophysical Methods* **66** (2006), pp. 1-11.
34. Y. Wu, Y. Hu, J. Cai, S. Ma, X. Wang, Y. Chen, *et al.*, Time-dependent surface adhesive force and morphology of RBC measured by AFM, *Micron* **40** (2009), pp. 359-364.
35. M. Bauer, S. Polzin and D. Patzelt, Quantification of RNA degradation by semi-quantitative duplex and competitive RT-PCR: a possible indicator of the age of bloodstains?, *Forensic Science International* **138** (2003), pp. 94-103.
36. S. Anderson, B. Howard, G.R. Hobbs and C.P. Bishop, A method for determining the age of a bloodstain, *Forensic Science International* **148** (2005), pp. 37-45.
37. S.E. Anderson, G.R. Hobbs and C.P. Bishop, Multivariate Analysis for Estimating the Age of a Bloodstain, *Journal of Forensic Sciences* **56** (2011), pp. 186-193.
38. J. Dissing, A. Søndervang and S. Lund, Exploring the limits for the survival of DNA in blood stains, *Journal of Forensic and Legal Medicine* **17** (2010), pp. 392-396.
39. K. Rajamannar, Determination of the Age of Bloodstains using Immunoelectrophoresis, *Journal of Forensic Science* **22** (1977).
40. A. Tsutsumi, Y. Yamamoto and H. Ishizu, Determination of the Age Bloodstains by Enzyme Activities in Blood Cells, *Japanese Journal of Legal Medicine* **37** (1983), p. 6.
41. K. Ackermann, K.N. Ballantyne and M. Kayser, Estimating trace deposition time with circadian biomarkers: a prospective and versatile tool for crime scene reconstruction, *Int J Legal Med* (2010).
42. L. Tomellini, De l'emploi d'une table chromatique pour les taches du sang, *Archives d'anthropologie criminelle de Criminologie* **14** (1907), p. 2.
43. O. Leers, Die forensische blutuntersuchung, Berlin (1910).
44. Ziemke and Franz Müller, Beiträge zur Spektroskopie des Blutes, *Arch. f. Anat. u. Physiol.* (1901).
45. Schwarzacher, Determination of the Age of Bloodstains, *American Journal of Police Sciences* **1** (1930).
46. F. Schwarz, Quantitative Untersuchungen der Katalase und Peroxydase im Blutfleck, *International Journal of Legal Medicine* **27** (1937), pp. 1-34.

47. H. Inoue, F. Takabe, M. Iwasa and Y. Maeno, Identification of fetal hemoglobin and simultaneous estimation of bloodstain age by high-performance liquid chromatography, *International Journal of Legal Medicine* **104** (1991), pp. 127-131.
48. H. Inoue, F. Takabe, M. Iwasa, Y. Maeno and Y. Seko, A new marker for estimation of bloodstain age by high performance liquid chromatography, *Forensic Science International* **57** (1992), pp. 17-27.
49. J. Andrasko, The Estimation of the Age of Bloodstains by HPLC Analysis, *Journal of Forensic Science* **42** (1997), p. 7.
50. R. Kumagai, Analysis of hemoglobin in bloodstains using highperformance liquid chromatography, *Nihon Hoigaku Zasshi* **47** (1993), p. 7.
51. V. Blazek and G. Lins, [Spectroscopic age determination of blood stains: new technical aspects], *Acta Med Leg Soc (Liege)* **32** (1982), pp. 613-616.
52. E. Botonjic-Sehic, C.W. Brown, M. Lamontagne and M. Tsaparikos, Forensic Application of Near-Infrared Spectroscopy: Aging of Bloodstains, *Spectroscopy* **24** (2009), pp. 42-48.
53. J.M. McCutcheon, Forensic Discrimination, Age Estimation, and Spectral Optimization for Trace Detection of Blood on Textile Substrates Using Infrared Spectroscopy and Chemometrics, University of South Carolina (2010).
54. H. Brooke, M.R. Baranowski, J.N. McCutcheon, S.L. Morgan and M.L. Myrick, Multimode Imaging in the Thermal Infrared for Chemical Contrast Enhancement. Part 1: Methodology, *Analytical Chemistry* **82** (2010), pp. 8412-8420.
55. H. Brooke, M.R. Baranowski, J.N. McCutcheon, S.L. Morgan and M.L. Myrick, Multimode Imaging in the Thermal Infrared for Chemical Contrast Enhancement. Part 2: Simulation Driven Design, *Analytical Chemistry* **82** (2010), pp. 8421-8426.
56. H. Brooke, M.R. Baranowski, J.N. McCutcheon, S.L. Morgan and M.L. Myrick, Multimode Imaging in the Thermal Infrared for Chemical Contrast Enhancement. Part 3: Visualizing Blood on Fabrics, *Analytical Chemistry* **82** (2010), pp. 8427-8431.
57. T. Matsuoka, T. Taguchi and J. Okuda, Estimation of bloodstain age by rapid determinations of oxyhemoglobin by use of oxygen-electrode and total hemoglobin, *Biological & Pharmaceutical Bulletin* **18** (1995), pp. 1031-1035.
58. Y. Fujita, K. Tsuchiya, S. Abe, Y. Takiguchi, S. Kubo and H. Sakurai, Estimation of the age of human bloodstains by electron paramagnetic resonance spectroscopy: Long-term controlled experiment on the effects of environmental factors, *Forensic Science International* **152** (2005), pp. 39-43.
59. H. Sakurai, K. Tsuchiya, Y. Fujita and K. Okuda, Dating of Human Blood by Electron Spin Resonance Spectroscopy, *Naturwissenschaften* **76** (1989), p. 24.
60. M. Bauer and D. Patzelt, Evaluation of mRNA markers for the identification of menstrual blood, *Journal of Forensic Sciences* **47** (2002), pp. 1278-1282.
61. J. Almog, Forensic Science Does Not Start in the Lab: The Concept of Diagnostic Field Tests*, *Journal of Forensic Sciences* **51** (2006), pp. 1228-1234.
62. K. Virkler and I.K. Lednev, Analysis of body fluids for forensic purposes: From laboratory testing to non-destructive rapid confirmatory identification at a crime scene, *Forensic Science International* **188** (2009), pp. 1-17.
63. D.L. Exline, C. Wallace, C. Roux, C.I. Lennard, M.P. Nelson and P.J. Treado, Forensic applications of chemical imaging: Latent fingerprint detection using visible absorption and luminescence, *Journal of Forensic Sciences* **48** (2003), pp. 1047-1053.
64. S.E. Anderson, G.R. Hobbs and C.P. Bishop, Multivariate Analysis for Estimating the Age of a Bloodstain*, *Journal of Forensic Sciences* (2010).
65. P.G. Hattersley, Activated Coagulation Time of Whole Blood, *Journal of the American Medical Association* **196** (1966), pp. 436-440.
66. N.Y.L. Lam, T.H. Rainer, R.W.K. Chiu and Y.M.D. Lo, EDTA Is a Better Anticoagulant than Heparin or Citrate for Delayed Blood Processing for Plasma DNA Analysis, *Clin Chem* **50** (2004), pp. 256-257.

67. T.L. Laber and B.P. Epstein, Substrate effects on the clotting time of Human Blood, *Can. Soc. Forensic Sci. J.* **34** (2001), pp. 209-214.
68. B.M. Weckhuysen and R.A. Schoonheydt, Recent progress in diffuse reflectance spectroscopy of supported metal oxide catalysts, *Catalysis Today* **49** (1999), pp. 441-451.
69. A.A. Stratonnikov and V.B. Loschenov, Evaluation of blood oxygen saturation in vivo from diffuse reflectance spectra, *Journal of Biomedical Optics* **6** (2001), pp. 457-467.
70. W.G. Zijlstra, A. Buursma and W.P. Meeuwssen-Vanderroest, Absorption spectra of human fetal and adult oxyhemoglobin, de-oxyhemoglobin, carboxyhemoglobin, and methemoglobin, *Clinical Chemistry* **37** (1991), pp. 1633-1638.
71. M.J.C. van Gemert, Star, W.M., Relations between the Kubelka-Munk and the transport equation models for anisotropic scattering, *Lasers Life Sciences* **1** (1987), p. 11.
72. L. Yang and B. Kruse, Revised Kubelka-Munk theory. I. Theory and application, *Journal of the Optical Society of America a-Optics Image Science and Vision* **21** (2004), pp. 1933-1941.
73. D. Yudovsky, Pilon, L., Simple and accurate expressions for diffuse reflectance of semi-infinite and two-layer absorbing and scattering media, *Applied Optics* **48** (2009), p. 13.
74. J.C. Finlay and T.H. Foster, Effect of pigment packaging on diffuse reflectance spectroscopy of samples containing red blood cells, *Optics Letters* **29** (2004), pp. 965-967.
75. A. Amelink, D.J. Robinson and H. Sterenborg, Confidence intervals on fit parameters derived from optical reflectance spectroscopy measurements, *Journal of Biomedical Optics* **13** (2008).
76. B. Efron, Estimating the error rate of a prediction rule - improvement on cross-validation, *J. Am. Stat. Assoc.* **78** (1983), pp. 316-331.
77. M. Tsuruga, A. Matsuoka, A. Hachimori, Y. Sugawara and K. Shikama, The molecular mechanism of autoxidation for human oxyhemoglobin - Tilting of the distal histidine causes nonequivalent oxidation in the beta chain, *Journal of Biological Chemistry* **273** (1998), pp. 8607-8615.
78. R.D. Deegan, O. Bakajin, T.F. Dupont, G. Huber, S.R. Nagel and T.A. Witten, Capillary flow as the cause of ring stains from dried liquid drops, *Nature* **389** (1997), pp. 827-829.
79. L. Randeberg, E. La Puebla Larsen and L. Svaasand, Characterization of vascular structures and skin bruises using hyperspectral imaging, image analysis and diffusion theory, *Journal of Biophotonics* **1** (2009), pp. 53 - 65.
80. B. Lomholt and N. Keiding, Tetrabase, an alternative to benzidine and orthotolidine for detection of hemoglobin in urine, *The Lancet* **1** (1977), pp. 608-609.
81. E. Johnston, C.E. Ames, K.E. Dagnall, J. Foster and B.E. Daniel, Comparison of presumptive blood test kits including Hexagon OBTI, *Journal of Forensic Sciences* **53** (2008), pp. 687-689.
82. L.J. Blum, P. Esperança and S. Rocquefelte, A new high-performance reagent and procedure for latent blood stain detection based on Luminol chemiluminescence, *Can. Soc. Forensic Sci. J.* **39** (2006), p. 20.
83. E.J.M. Kent, D.A. Elliot and G.M. Miskelly, Inhibition of bleach-induced luminol chemiluminescence, *Journal of Forensic Sciences* **48** (2003), pp. 64-67.
84. S.H. James and J.J. Nordby, *Forensic Science*, Taylor&Francis (2005).
85. R. Saferstein, *Criminalistics - An Introduction to Forensic Science* (1981).
86. D. Zubakov, E. Hanekamp, M. Kokshoorn, W. van Ijcken and M. Kayser, Stable RNA markers for identification of blood and saliva stains revealed from whole genome expression analysis of time-wise degraded samples, *International Journal of Legal Medicine* **122** (2008), pp. 135-142.
87. E. Nagababu and J.M. Rifkind, Formation of fluorescent heme degradation products during the oxidation of hemoglobin by hydrogen peroxide, *Biochemical and Biophysical Research Communications* **247** (1998), pp. 592-596.
88. K. Virkler and I.K. Lednev, Raman spectroscopic signature of blood and its potential application to forensic body fluid identification, *Analytical and Bioanalytical Chemistry* **396** (2010), pp. 525-534.

89. K. De Wael, L. Lepot, F. Gason and B. Gilbert, In search of blood - Detection of minute particles using spectroscopic methods, *Forensic Science International* **180** (2008), pp. 37-42.
90. T.M. Kotowski and M.C. Grieve, The use of microspectrophotometry to characterize microscopic amounts of blood, *Journal of Forensic Sciences* **31** (1986), pp. 1079-1085.
91. N.J.D. Nagelkerke, A note on a general definition on the coefficient of determination, *Biometrika* **78** (1991), pp. 691-692.
92. T. Otto, V. Stock, W.-D. Schmidt, K. Liebold, D. Fassler, U. Wollina, *et al.*, Medical applications of VIS/NIR spectroscopy of human tissue surfaces by a novel portable instrumentation In: N. Cam, Editor **vol. 4491**, SPIE (2001), pp. 203-214.
93. I. Charamisinau, K. Keymel, W. Potter and A.R. Oseroff, Handheld dual fluorescence and reflection spectroscopy system for monitoring topical low dose ALA-PDT of actinic keratoses (AK) In: K. David, Editor **vol. 6139**, SPIE (2006), p. 61391E.
94. C.S. Mulvey, C.A. Sherwood and I.J. Bigio, Wavelength-dependent backscattering measurements for quantitative real-time monitoring of apoptosis in living cells, *Journal of Biomedical Optics* **14** (2009).
95. Y.S. Fawzy, M. Petek, M. Terceļj and H.S. Zeng, In vivo assessment and evaluation of lung tissue morphologic and physiological changes from non-contact endoscopic reflectance spectroscopy for improving lung cancer detection, *Journal of Biomedical Optics* **11** (2006).
96. C.C. Yu, C. Lau, G. O'Donoghue, J. Mirkovic, S. McGee, L. Galindo, *et al.*, Quantitative spectroscopic imaging for non-invasive early cancer detection, *Optics Express* **16** (2008), pp. 16227-16239.
97. R.B. Saager, D.J. Cuccia and A.J. Durkin, Determination of optical properties of turbid media spanning visible and near-infrared regimes via spatially modulated quantitative spectroscopy, *J. Biomed. Opt.* **15** (2010), p. 017012.
98. S.C. Gebhart, S.K. Majumder and A. Mahadevan-Jansen, Comparison of spectral variation from spectroscopy to spectral imaging, *Appl. Opt.* **46** (2007), pp. 1343-1360.
99. L.L. Randeberg, O.A. Haugen, R. Haaverstad and L.O. Svaasand, A novel approach to age determination of traumatic injuries by reflectance spectroscopy, *Lasers Surg. Med.* **38** (2006), pp. 277-289.
100. G. Zonios, L.T. Perelman, V.M. Backman, R. Manoharan, M. Fitzmaurice, J. Van Dam, *et al.*, Diffuse reflectance spectroscopy of human adenomatous colon polyps in vivo, *Applied Optics* **38** (1999), pp. 6628-6637.
101. R. Reif, O. A'amar and I.J. Bigio, Analytical model of light reflectance for extraction of the optical properties in small volumes of turbid media, *Appl. Optics* **46** (2007), pp. 7317-7328.
102. G. Zonios, I. Bassukas and A. Dimou, Comparative evaluation of two simple diffuse reflectance models for biological tissue applications, *Appl. Optics* **47** (2008), pp. 4965-4973.
103. J.E. Phelps, K. Vishwanath, V.T.C. Chang and N. Ramanujam, Rapid ratiometric determination of hemoglobin concentration using UV-VIS diffuse reflectance at isobestic wavelengths, *Opt. Express* **18** (2010), pp. 18779-18792.
104. N. Rajaram, T.H. Nguyen and J.W. Tunnell, Lookup table--based inverse model for determining optical properties of turbid media, *J. Biomed. Opt.* **13** (2008), pp. 050501-050503.
105. S.C. Kanick, H. Sterenborg and A. Amelink, Empirical model of the photon path length for a single fiber reflectance spectroscopy device, *Opt. Express* **17** (2009), pp. 860-871.
106. S.C. Kanick, H. Sterenborg and A. Amelink, Empirical model description of photon path length for differential path length spectroscopy: combined effect of scattering and absorption, *J. Biomed. Opt.* **13** (2008), p. 8.
107. S.E. Hernandez, V.D. Rodriguez, J. Perez, F.A. Martin, M.A. Castellano and J.L. Gonzalez-Mora, Diffuse reflectance spectroscopy characterization of hemoglobin and intralipid solutions: in vitro measurements with continuous variation of absorption and scattering, *J. Biomed. Opt.* **14** (2009), p. 6.

108. H.J. Van Staveren, C.J.M. Moes, J. Van Marle, S.A. Prahl and M.J.C. Van Gemert, Light-scattering in Intralipid-10-percent in the wavelength range of 400-1100 nm, *Appl. Optics* **30** (1991), pp. 4507-4514.
109. G. Zaccanti, S. Del Bianco and F. Martelli, Measurements of optical properties of high-density media, *Appl. Optics* **42** (2003), pp. 4023-4030.
110. M.C.P. Van Beekvelt, W.N.J.M. Colier, R.A. Wevers and B.G.M. Van Engelen, Performance of near-infrared spectroscopy in measuring local O₂ consumption and blood flow in skeletal muscle, *J. Appl. Physiol.* **90** (2001), pp. 511-519.
111. M. Friebel, J. Helfmann, U. Netz and M. Meinke, Influence of oxygen saturation on the optical scattering properties of human red blood cells in the spectral range 250 to 2000 nm, *J. Biomed. Opt.* **14** (2009), p. 6.
112. D.M. de Bruin, R.H. Bremmer, V.M. Kodach, R. de Kinkelder, J. van Marle, T.G. van Leeuwen, *et al.*, Optical phantoms of varying geometry based on thin building blocks with controlled optical properties, *Journal of Biomedical Optics* **15** (2010), pp. 025001-025010.
113. R. Reif, M.S. Amoroso, K.W. Calabro, O. A'Amar, S.K. Singh and I.J. Bigio, Analysis of changes in reflectance measurements on biological tissues subjected to different probe pressures, *J. Biomed. Opt.* **13** (2008).
114. D. Huang, E. Swanson, C. Lin, J. Schuman, W. Stinson, W. Chang, *et al.*, Optical coherence tomography, *Science* **254** (1991), pp. 1178-1181.
115. M.C.G. Aalders, M. Triesscheijn, M. Ruevekamp, M.d. Bruin, P. Baas, D.J. Faber, *et al.*, Doppler optical coherence tomography to monitor the effect of photodynamic therapy on tissue morphology and perfusion, *J. Biomed. Opt.* **11** (2006), p. 044011.
116. D.M. de Bruin, D.L. Burnes, J. Loewenstein, Y. Chen, S. Chang, T.C. Chen, *et al.*, In Vivo Three-Dimensional Imaging of Neovascular Age-Related Macular Degeneration Using Optical Frequency Domain Imaging at 1050 nm, *Invest. Ophthalmol. Vis. Sci.* **49** (2008), pp. 4545-4552.
117. D. Faber, F. van der Meer, M. Aalders and T. van Leeuwen, Quantitative measurement of attenuation coefficients of weakly scattering media using optical coherence tomography, *Opt. Express* **12** (2004), pp. 4353-4365.
118. Y. Sugawara, E. Kadono, A. Suzuki, Y. Yukuta, Y. Shibasaki, N. Nishimura, *et al.*, Hemichrome formation observed in human haemoglobin A under various buffer conditions, *Acta Physiologica Scandinavica* **179** (2003), pp. 49-59.
119. W. Verkruyse, G.W. Lucassen, J.F. deBoer, D.J. Smithies, J.S. Nelson and M.J.C. vanGemert, Modelling light distributions of homogeneous versus discrete absorbers in light irradiated turbid media, *Physics in Medicine and Biology* **42** (1997), pp. 51-65.
120. B. Venkatesh, S. Ramasamy, M. Mylrajan, R. Asokan, P.T. Manoharan and J. M. Rifkind, Fourier transform Raman approach to structural correlation in hemoglobin derivatives, *Spectrochimica Acta Part A: Molecular and Biomolecular Spectroscopy* **55** (1999), pp. 1691-1697.
121. H. Motulsky and A. Christopoulos. Fitting models to biological data using linear and nonlinear regression a practical guide to curve fitting. <http://www.myilibrary.com?id=84377>. 2004.
122. J.A. Kellum, Determinants of blood pH in health and disease, *Critical Care* **4** (2000), pp. 6 - 14.
123. R. Wever, B. Oudega and B.F. Van Gelder, Generation of superoxide radicals during the autoxidation of mammalian oxyhemoglobin, *Biochimica et Biophysica Acta (BBA) - Enzymology* **302** (1973), pp. 475-478.
124. R.H. Bremmer, A. Nadort, M.J.C. van Gemert, T.G. van Leeuwen and M.C. Aalders, Age estimation of blood stains by hemoglobin derivative determination using reflection spectroscopy, *Forensic Science International* **206** (2011), pp. 166-171.
125. G.M. Palmer and N. Ramanujam, Monte Carlo-based inverse model for calculating tissue optical properties. Part I: Theory and validation on synthetic phantoms, *Appl. Opt.* **45** (2006), pp. 1062-1071.

126. S.C. Kanick, D.J. Robinson, H.J.C.M. Sterenborg and A. Amelink, Monte Carlo analysis of single fiber reflectance spectroscopy: photon path length and sampling depth *Phys. Med. Biol.* **54** (2009).
127. B. Varghese, V. Rajan, T.G. Van Leeuwen and W. Steenbergen, Path-length-resolved measurements of multiple scattered photons in static and dynamic turbid media using phase-modulated low-coherence interferometry, *Journal of Biomedical Optics* **12** (2007), pp. 024020-024027.
128. A. Pifferi, A. Torricelli, L. Spinelli, D. Contini, R. Cubeddu, F. Martelli, *et al.*, Time-Resolved Diffuse Reflectance Using Small Source-Detector Separation and Fast Single-Photon Gating, *Phys. Rev. Lett.* **100** (2008), p. 138101.
129. A.L. Petoukhova, W. Steenbergen, T.G. van Leeuwen and F.F.M. de Mul, Effects of absorption on coherence domain path length resolved dynamic light scattering in the diffuse regime, *Applied Physics Letters* **81** (2002), pp. 595-597.
130. E. Alerstam, S. Andersson-Engels and T. Svensson, White Monte Carlo for time-resolved photon migration, *Journal of Biomedical Optics* **13** (2008), pp. 041304-041310.
131. R.H. Bremmer, S.C. Kanick, N. Laan, A. Amelink, T.G. van Leeuwen and M.C.G. Aalders, Non-contact spectroscopic determination of large blood volume fractions in turbid media, *Biomed. Opt. Express* **2** (2011), pp. 396-407.
132. F.F.M. de Mul, M.H. Koelink, M.L. Kok, P.J. Harmsma, J. Greve, R. Graaff, *et al.*, Laser Doppler velocimetry and Monte Carlo simulations on models for blood perfusion in tissue, *Appl. Opt.* **34** (1995), pp. 6595-6611.
133. F. Martelli, S.D. Bianco, A. Ismaelli and G. Zaccanti, Light propagation through biological tissue, SPIE (2010).
134. G. Popescu and A. Dogariu, Optical path-length spectroscopy of wave propagation in random media, *Opt. Lett.* **24** (1999), pp. 442-444.
135. C.M.A.M. van der Horst, P.H.L. Koster, C.A.J.M. de Borgie, P.M.M. Bossuyt and M.J.C. van Gemert, Effect of the Timing of Treatment of Port-Wine Stains with the Flash-Lamp-Pumped Pulsed-Dye Laser, *New England Journal of Medicine* **338** (1998), pp. 1028-1033.
136. N. Bosschaart, D.J. Faber, T.G. van Leeuwen and M.C.G. Aalders, Measurements of wavelength dependent scattering and backscattering coefficients by low-coherence spectroscopy, *Journal of Biomedical Optics* **16** (2011), pp. 030503-030503.
137. V.M. Kodach, D.J. Faber, J. van Marle, T.G. van Leeuwen and J. Kalkman, Determination of the scattering anisotropy with optical coherence tomography, *Opt. Express* **19** (2011), pp. 6131-6140.
138. T.J. Farrell, M.S. Patterson and B. Wilson, A diffusion-theory model of spatially resolved, steady-state diffuse reflectance for noninvasive determination of tissue optical properties in vivo, *Med. Phys.* **19** (1992), pp. 879-888.
139. K. Levenberg, A method for the solution of certain problems in least squares, *Quarterly of Applied Mathematics* **2** (1944), pp. 164-168.
140. D.J. Faber, M.C.G. Aalders, E.G. Mik, B.A. Hooper, M.J.C. van Gemert and T.G. van Leeuwen, Oxygen saturation-dependent absorption and scattering of blood, *Phys. Rev. Lett.* **93** (2004), p. 4.
141. M. Friebel, A. Roggan, G. Muller and M. Meinke, Determination of optical properties of human blood in the spectral range 250 to 1100 nm using Monte Carlo simulations with hematocrit-dependent effective scattering phase functions, *Journal of Biomedical Optics* **11** (2006), pp. 034021-034010.
142. C. Bustamante and M.F. Maestre, Statistical effects in the absorption and optical activity of particulate suspensions, *Proceedings of the National Academy of Sciences* **85** (1988), pp. 8482-8486.
143. A. Pifferi, A. Torricelli, A. Bassi, P. Taroni, R. Cubeddu, H. Wabnitz, *et al.*, Performance assessment of photon migration instruments: the MEDPHOT protocol, *Appl. Opt.* **44** (2005), pp. 2104-2114.

144. S.A. Prahl, <http://omlc.ogi.edu/spectra/hemoglobin>, retrieved March 2011.
145. A. Amelink, T. Christiaanse and H.J.C.M. Sterenborg, Effect of hemoglobin extinction spectra on optical spectroscopic measurements of blood oxygen saturation, *Opt. Lett.* **34** (2009), pp. 1525-1527.
146. B.W. Pogue and M.S. Patterson, Review of tissue simulating phantoms for optical spectroscopy, imaging and dosimetry, *Journal of Biomedical Optics* **11** (2006), p. 041102.
147. V. Hughes and N. Langlois, Use of reflectance spectrophotometry and colorimetry in a general linear model for the determination of the age of bruises, *Forensic Science, Medicine, and Pathology* **6** (2010), pp. 275-281.
148. G. Zonios and et al., Probing skin interaction with hydrogen peroxide using diffuse reflectance spectroscopy, *Physics in Medicine and Biology* **53** (2008), p. 269.
149. G.N. Stamatias, B.Z. Zmudzka, N. Kollias and J.Z. Beer, In vivo measurement of skin erythema and pigmentation: new means of implementation of diffuse reflectance spectroscopy with a commercial instrument, *British Journal of Dermatology* **159** (2008), pp. 683-690.
150. E.J. van Kampen and W.G. Zijlstra, Standardization of hemoglobinometry II. The hemiglobincyanide method, *Clinica Chimica Acta* **6** (1961), pp. 538-544.
151. J. Quackenbush, Microarray Analysis and Tumor Classification, *New England Journal of Medicine* **354** (2006), pp. 2463-2472.
152. L.J. van 't Veer, H. Dai, M.J. van de Vijver, Y.D. He, A.A.M. Hart, M. Mao, *et al.*, Gene expression profiling predicts clinical outcome of breast cancer, *Nature* **415** (2002), pp. 530-536.
153. M. Asghari-Khiavi, A. Mechler, K.R. Bamberg, D. McNaughton and B.R. Wood, A resonance Raman spectroscopic investigation into the effects of fixation and dehydration on heme environment of hemoglobin, *Journal of Raman Spectroscopy* **40** (2009), pp. 1668-1674.
154. R. Dasgupta, S. Ahlawat, R.S. Verma, A. Uppal and P.K. Gupta, Hemoglobin degradation in human erythrocytes with long-duration near-infrared laser exposure in Raman optical tweezers, *Journal of Biomedical Optics* **15** (2010), p. 055009.

PUBLICATION LIST

Forensic Quest for Age Determination of Bloodstains, A Review.

Rolf H Bremmer, Karla G de Bruin, Martin JC van Gemert, Ton G van Leeuwen and Maurice CG Aalders

Forensic Science International, submitted.

Age estimation of bloodstains by hemoglobin derivative determination using reflectance spectroscopy.

Rolf H Bremmer, Annemarie Nadort, Martin JC van Gemert, Ton G van Leeuwen and Maurice CG Aalders

Forensic Science International, **206** 166-171 (2011).

Remote Spectroscopic Identification of bloodstains.

Rolf H Bremmer, Gerda Edelman, Tessa Dijn Vegter, Ted Bijvoets, Maurice CG Aalders
Journal of Forensic Science, in print (2011).

Non-contact spectroscopic determination of large blood volume fractions in turbid media.

Rolf H Bremmer, Stephan C Kanick, Nick Laan, Arjen Amelink, Ton G van Leeuwen, Maurice CG Aalders

Biomedical Optics Express, **2** 2 396-407 (2011).

Biphasic Oxidation of oxy-hemoglobin in bloodstains.

Rolf H Bremmer, Daniel M de Bruin, Maarten de Joode, Wybren Jan Buma, Ton G van Leeuwen, Maurice CG Aalders

PLoS One, submitted.

Photon path length distribution model for reflectance spectroscopy.

Rolf H Bremmer, Wouter Smeets, Martin JC van Gemert, Ton G van Leeuwen, Maurice CG Aalders

Optics Letters, submitted.

Can diffusion approximation be valid beyond its assumed borders?

Rolf H Bremmer, Martin JC van Gemert, Ton G van Leeuwen, Maurice CG Aalders
In preparation.

Co-authored publications, not described in this thesis

Optical phantoms of varying geometry based on thin building blocks with controlled optical properties.

Daniel M de Bruin, Rolf H Bremmer, Vitali M Kodach, Roy de Kinkelder, Jan van Marle, Ton G van Leeuwen, Dirk J Faber

Journal of Biomedical Optics **15** (2010).

Heat conduction from the exceedingly hot fiber tip contributes to the endovenous laser ablation of varicose veins.

Renate R. van den Bos, Michale A Kockaert, Martino HA Neumann, Rolf H Bremmer, Tamar Nijsten, Martin JC van Gemert

Lasers in Medical Science 2009 **24**(2) 247-251.

Volume determination of bloodstains with Optical Coherence Tomography and implications for Bloodstain Pattern Analysis.

Nick Laan, Rolf H Bremmer, Maurice CG Aalders, Karla G de Bruin

Forensic Science International, in preparation.

SUMMARY

Bloodstains are among the most encountered traces on crime scenes. Estimation of the age of a bloodstain can be a first indication for forensic investigators to establish when the crime was committed. Or, if the time of perpetration is evidenced otherwise, bloodstain age determination may either confirm or exclude a bloodstain as being relevant to the crime. Age determination of bloodstain can be measured by reflectance spectroscopy and its forensic relevance is huge. Reflectance spectroscopy is a technique to measure color quantitatively. This technique is routinely used in clinic to determine oxygen saturation in blood, and is being explored to differentiate between healthy tissue and tumors. Already in the 1960s this technique was suggested as a candidate for measuring the age of a bloodstain. So far, analysis of reflectance measurements has been limited to a single wavelength. However, the key to success of this thesis proved to be analyzing the reflectance spectrum over a large spectral window (450-800 nm) simultaneously. Large spectral window analysis of the reflectance spectrum of a bloodstain allows for determination of relative amounts of hemoglobin derivatives: oxy-hemoglobin (HbO_2), met-hemoglobin (met-Hb) and hemichrome (HC) in bloodstains. Accordingly, these hemoglobin amounts can be related to the age of the bloodstain.

Chapter 1 summarizes an extensive literature search and describes research on age determination of bloodstains in general. This chapter starts with an overview of the physical and chemical properties of red and white blood cells during the ageing process in a bloodstain. The main part is a summary of all the techniques that have been explored to determine the age of a bloodstain. For instance, with atomic force microscopy an increase in elasticity of the red blood cell after deposition has been observed. Another technique, Electron Spin Resonance has been used to map the magnetic properties of hemoglobin in bloodstains during ageing. And RNA analysis has successfully been explored to measure changes in RNA proteins, up to 15 years after deposition of the bloodstain. All these techniques are compared with reflectance spectroscopy, which measured changing color of a bloodstain. The color of a bloodstain changes because of an oxidation process of the hemoglobin present. It is found that reflectance spectroscopy is most accurate, especially for bloodstains up to one month old. Additional advantage of reflectance spectroscopy is the non-destructive nature of this technique and, as a result, its great applicability on the crime scene.

Chapter 2 describes reflectance spectroscopic measurements on 40 bloodstains by analyzing the reflectance spectrum over the spectral range of 450-800 nm simultaneously. The relative amounts of the hemoglobin derivatives are determined by comparing the reflectance of a bloodstain with the spectra of HbO_2 , met-Hb and HC with a non-linear least square fit. Initially in a bloodstain, all hemoglobin is HbO_2 , but thereafter $\text{HbO}_2 \rightarrow \text{met-Hb} \rightarrow \text{HC}$. This transition has been determined for 20 bloodstains on cotton at room temperature during 60 days. The determined transition rate is employed for age determination on a second group of 20 bloodstains. Age

determination is possible: for one-day-old bloodstains with accuracy of a few hours; for ten-days-old bloodstains with accuracy of a few days.

An important step in age determination of bloodstains proved a quality check of the linear squares fit algorithm. In case of low agreement between reflectance of the bloodstain and hemoglobin fit, the outcome of the fit will become unreliable. The amount of agreement can be expressed in a correlation coefficient, r^2 . The minimal correlation for a reliable fit analysis has (arbitrarily) been determined to be $r^2=0.98$. In **chapter 3**, the correlation coefficient is used to discriminate bloodstains from non-bloodstains. The reflectance spectrum of 35 blood-mimicking stains have been measured, including, wine, ketchup and fake blood. All 35 stains had an r^2 lower than 0.97, while 98% of 2000 measurements on 40 bloodstain showed an r^2 higher than 0.97. Fitting of hemoglobin spectra to the reflectance of bloodstains appears to be an almost perfect method to discriminate blood from non-blood on white cotton. A remarkable result was found that, from all non-blood stains, the stain created with lip gloss from a local pharmacy showed the highest correlation coefficient.

In chapter 2, the Kubelka Munk model for light transport has been used to translate absorption spectra into reflectance spectra. It appeared impossible to relate Kubelka Munk's parameters to the optical properties, when measuring on phantoms. The relation between optical properties – scattering and absorption – is necessary for quantitative reflectance measurements. For that reason, the effective photon path length approach is explored in **chapter 4**. It proved possible to determine the relation between reflectance and absorption could be determined for a large range of scattering and absorption coefficients by measuring the reflectance signal on phantoms containing a controlled amount of water, fat and a chromophore. The wide range of absorption and scattering coefficients represents the large variety of optical properties in bloodstains. It was found that the effective photon path length decreases with absorption, whereas it remains constant with scattering, if scattering is high – which is the case for cotton. At the end of this chapter it is shown that the effective photon path length model can also been applied for stains on cotton.

Chapter 5 describes that the effective photon path length model can also be used for measuring the blood volume fraction of diluted bloodstains on cotton. Additional evidence for the effective photon path length approach is given by optical coherence tomography analysis at 1300 nm, a non-absorbing wavelength. When analyzing the reflectance spectrum of a bloodstain in terms of the hemoglobin derivatives, it is observed that the transition of HbO_2 into met-Hb is biphasic. Initially, the transition rate is high, but after a few hours, the rate drops dramatically. The biphasic nature of the transition was already observed for hemoglobin in an aqueous solution by Tsuruga *et al.*, but never before in bloodstains. Additionally, the transition rate as a function of temperature and humidity has been measured. The transition rate strongly depends on temperature, but only partly so on humidity. The first part of the transition, $\text{HbO}_2 \rightarrow \text{met-Hb}$ is humidity independent, but, on the contrary, the second part met-Hb

→ HC depends on humidity. The discovery of a humidity independent transition of HbO₂ to met-Hb is important for translating laboratory results into forensic practice. Lack of information on the humidity on the crime scene needs no longer hamper age determination of the bloodstain.

At the end of this thesis an analysis of the reflectance spectrum of blood mimicking phantoms is presented in great detail. In **chapter 6**, the photon transport has been simulated by Monte Carlo computations. It was found that the reflectance signal as a function of absorption is completely determined by the photon path length distribution at zero absorption. In **chapter 7**, the reflectance signal is analyzed by the diffusion approximation. It was possible to describe phantom measurements, as presented in earlier chapters, by this approximation even for measurements that do not meet the conditions this approximation – yet only when model parameters were fitted.

SAMENVATTING PROEFSCHRIFT

Dit proefschrift beschrijft het onderzoek naar de leeftijdsbepaling van bloedvlekken door middel van reflectiespectroscopie. Leeftijdsbepaling van bloedvlekken kan rechercheurs helpen bij forensisch onderzoek om zicht te krijgen op het tijdsverloop van een zaak. Reflectiespectroscopie, een contactloze kleurmeting, is een technologie die in het ziekenhuis al wordt toegepast voor het meten van zuurstofsaturatie in bloed, of het voor het detecteren van oppervlakkige tumoren. De mogelijkheid om deze techniek toe te passen voor forensisch onderzoek was eerder al verkend; tot nu toe echter zonder succes. Eerdere pogingen om met behulp van reflectiespectroscopie de leeftijd van bloedvlekken te meten, beperkten zich tot analyse van enkele golflengtes. Het vernieuwende element van dit onderzoek is dat de analyse van het reflectiespectrum zich niet beperkt tot enkele golflengtes, maar dat het gehele spectrum van 450-800 nm simultaan wordt geanalyseerd. Deze analysemethode heeft als voordeel dat relatieve hoeveelheden hemoglobineproducten in een bloedvlek kunnen worden bepaald. De verhouding van de hemoglobines, te weten, oxy-hemoglobine (HbO_2), met-hemoglobine (met-Hb) en hemichrome (HC) is dan een goede maat voor de leeftijd van de bloedvlek.

Dus door de precieze kleur van een bloedvlek te meten, kan je nagaan hoe oud een bloedvlek is. Deze informatie kan voor een rechercheur van onschatbare waarde zijn in bijvoorbeeld een moordzaak.

Hoofdstuk 1 is een samenvatting van de literatuur naar bloedvlekveroudering in het algemeen tot nu toe verschenen. Het begint met een overzicht van de fysische eigenschappen van rode en witte bloedcellen tijdens het verouderingsproces in een bloedvlek. Voorts staat er een opsomming beschreven van diverse technologieën die eerder al verkend zijn voor de leeftijdsbepaling van bloedvlekken. Zo is door middel van de *atoomkrachtmicroscoop* de toenemende elasticiteit van rode bloedcellen gedurende het verouderingsproces in kaart gebracht. Verder is met *elektronspinresonantie* de veranderende magnetische eigenschappen van het hemoglobinemolecuul verkend; en is met *RNA-analyse* de verandering van RNA-eiwitten in witte bloedcellen onderzocht. Al deze technologieën zijn vergeleken met de in deze thesis beschreven onderzoeksmethode, reflectiespectroscopie. Deze methode maakt gebruik van de veranderende optische eigenschappen, als gevolg van een roestingsproces waarbij HbO_2 wordt omgezet in met-Hb en HC. Reflectiespectroscopie blijkt de meest nauwkeurige techniek voor het bepalen van de ouderdom van een bloedvlek, en bovendien het minst invasief en daarvoor het beste toepasbaar op een plaats delict.

Hoofdstuk 2 gaat over verkennende metingen op verouderende bloedvlekken, waarbij het reflectiespectrum over het spectrum van 450-800 nm wordt geanalyseerd. Door het reflectiespectrum van een bloedvlek te vergelijken met de spectra HbO_2 , met-Hb en HC door middel van een kleinstekwadratenanalyse kan de verhouding van deze drie hemoglobinevarianten worden bepaald. Een verse bloedvlek bestaat voor 100% uit HbO_2 . Daarna wordt $\text{HbO}_2 \rightarrow \text{met-Hb} \rightarrow \text{HC}$. Deze omzetting is in kaart gebracht

voor 20 bloedvlekken op katoen bij kamertemperatuur. Bij 20 andere bloedvlekken is de leeftijd bepaald aan de hand van de typische omzetting van eerste 20 bloedvlekken.

Een belangrijke stap in de leeftijdsbepaling van bloedvlekken is een kwaliteitscontrole van de kleinste-kwadratenanalyse. Wanneer de combinatie van de drie hemoglobine spectra onvoldoende overeenkomen met het reflectiespectrum van de bloedvlek, is de analyse onbetrouwbaar. De mate van overeenkomst tussen de kleinste-kwadratenanalyse en het reflectiespectrum van de bloedvlek kan worden uitgedrukt in een correlatiecoëfficiënt, r^2 . De minimale correlatiecoëfficiënt voor een betrouwbare kleinste-kwadratenanalyse is (arbitrair) gesteld op $r^2 = 0.98$. Deze correlatiecoëfficiënt kan ook worden gebruikt om onderscheid te maken tussen bloed en niet-bloed. In **hoofdstuk 3** staat beschreven dat het reflectiespectrum van 35 op bloed lijkende vlekken, zoals ketchup, wijn en nep-bloed allen een correlatiecoëfficiënt hebben die kleiner is dan 0.97. Dit is vergeleken met 2000 metingen op 40 bloedvlekken, waarvan 98% van de metingen op bloedvlekken een correlatiecoëfficiënt van groter dan 0.97 hebben. De kleinste-kwadratenanalyse met hemoglobine en een grens van 0.97 kan met een perfecte specificiteit en een bijna perfecte sensitiviteit onderscheid worden gemaakt tussen bloed en niet-bloedvlekken op wit katoen. Een opmerkelijk resultaat was dat de niet-bloedvlek met de hoogste r^2 waarde de lip-gloss van de Etos bleek te zijn.

Het lichttransportmodel dat in hoofdstuk 2 gebruikt wordt voor de analyse van het reflectiespectrum van bloedvlekken is de *Kubelka Munk* theorie. Het bleek echter niet mogelijk om deze theorie te gebruiken voor kwantitatieve reflectiemetingen. In **hoofdstuk 4** is daarom overgestapt op de effectieve-padlengteanalyse. Met behulp van reflectiespectroscopische metingen op fantomen met gecontroleerde optische eigenschappen, gemaakt door een mengsel van water, vet (Intralipid) en kleurstof, is het verband tussen absorptie en verstrooiing aan de ene kant en het reflectiesignaal aan de andere kant in kaart gebracht. De hoeveelheid vet bepaalt de mate van verstrooiing, en de hoeveelheid kleurstof de mate van absorptie. Door hoeveelheid vet en kleurstof te variëren kon de effectieve weglengte die de fotonen door het fantoom afleggen worden vastgesteld en gebruikt voor een absolute bepaling van de hoeveelheid kleurstof in een fantoom. Deze methode van de effectieve padlengte blijkt ook toepasbaar voor kleurstoffen op katoen.

Hoofdstuk 5 beschrijft hoe de methode van de effectieve padlengte gebruikt kan worden voor het bepalen van de fractie HbO_2 , met-Hb en HC in bloedvlekken. Ondersteunend bewijs voor aannames die ten grondslag liggen aan de effectieve-padlengtemethode wordt geleverd door middel van *optische coherentie tomografie* analyse. De effectieve-padlengtemethode laat zien dat in bloedvlekken de omzetting van HbO_2 in met-Hb in twee fases verloopt. Aanvankelijk is de omzetsnelheid hoog, maar na een aantal uur daalt de snelheid aanzienlijk. Deze twee-fase-omzetting was eerder al geconstateerd in een hemoglobineoplossing door Tsuruga *et al.* en nu voor het eerst ook waargenomen in bloedvlekken. Voorts staat in dit hoofdstuk beschreven hoe de omzettingssnelheid afhangt van de omgevingstemperatuur en de luchtvochtigheid.

Een opmerkelijk resultaat is, dat de omzetting van HbO_2 naar met-Hb niet afhangt van de luchtvochtigheid en de omzetting van met-Hb naar HC wél afhangt van de luchtvochtigheid. Dat de overgang van HbO_2 naar met-Hb onafhankelijk is van de luchtvochtigheid is een belangrijke ontdekking voor de implementatie van leeftijdsbepaling in het forensisch veld. Immers hoeft de luchtvochtigheid niet bekend te zijn, om de leeftijd van de bloedvlek te kunnen bepalen.

Tot slot wordt nog dieper ingegaan op het lichttransport door bloedvlekken en door de fantomen die de optische eigenschappen van bloedvlekken nabootsen. In **hoofdstuk 6** wordt het fotontransport gesimuleerd met Monte Carlo-berekeningen. Een belangrijke bevinding, is dat het verband tussen het reflectiesignaal en de mate van absorptie volledig bepaald wordt door de fotonpadlengtedistributie. In **hoofdstuk 7** wordt uitgelegd dat de diffusiebenadering voor lichttransport formeel niet mag worden toegepast op deze metingen, maar dat deze diffusiebenadering toch een goede beschrijving geeft van het reflectiesignaal als functie van absorptie. Dit laatste geeft mogelijk nieuw inzicht in de diffusiebenadering.

DANKWOORD

Wow, mijn proefschrift is af... Vier jaar onderzoek samengevat in een klein boekwerk. Hoewel het grootste deel van deze tijd bestaat uit eenzaam programmeren, schrijven en experimenteren, had dit eindresultaat er niet kunnen zijn zonder de hulp van velen.

Allereerst wil ik graag Maurice bedanken. Zonder jou was dit resultaat er niet geweest want jij stond als creatieve bedenker aan de wieg van het bloedvlekkenonderzoek en hebt er vanaf de start veel vertrouwen in gehad en dit ook regelmatig uitgesproken. In het begin was jouw vrije vorm van begeleiding even wennen, maar richting de finish van het proefschrift werd de samenwerking steeds intensiever en plezieriger. Naast jou voelde ik me vaak een cowboy op de braakliggende terreinen van het forensisch onderzoek.

Ton wil ik graag bedanken voor stimulerende discussies en het richting geven aan de vele artikelen die we samen schreven. Altijd stond jouw deur open en maakte je tijd voor het bespreken van nieuwe resultaten. Jij bleef me verbazen met scherpe observaties en nieuwe inzichten.

Martin, veel dank voor de vele uren van jouw pensioen die je hebt opgeofferd aan het maken van kleine sommetjes. Met veel geduld en groot enthousiasme polijste jij de ruwe verhalen tot gladde, leesbare tekst, waarbij altijd het resultaat voorop stond.

Ook de overige collega's van de groep Biomedical Engineering & Physics van het AMC ben ik ertentelijk. Fijn om met zoveel jonge, enthousiaste mensen te werken. Twee mensen wil ik er graag even uitlichten: Jelmer, altijd stond jij klaar als mijn opstelling moest worden aangepast of als ik iets moest bestellen en steeds met een talent voor goed humeur! Jeroen, dank voor vele kleine momenten van reflectie, jouw kritische natuurkundige inzichten hebben mij vaak op scherp gezet.

Een groot aantal van de experimenten heb ik samen met een aantal studenten gedaan. Annemarie, Sebastiaan, Eline, Rob, Tessa Dijn, Jojanneke, Nick, Maarten en Wouter, dank voor al jullie hulp en vele discussies over de interpretatie van de metingen die mij vaak ook nieuwe inzichten gaven.

Graag wil ik ook een aantal mensen van buiten het AMC noemen. Ten eerste, bedank ik de collega's van het Erasmus MC, Arjen Amelink en Chad Kanick. Jullie hebben mij kritisch leren kijken naar mijn spectroscopie data, daarvan heb ik veel geleerd. Deze samenwerking heeft niet alleen geleid tot hoofdstuk 4, maar was een basis voor de rest van dit proefschrift.

Ten tweede, van het Nederlands Forensisch Instituut wil ik graag Karla bedanken. Jouw enthousiasme en nuchterheid zijn een prettige combinatie. Maar vooral jouw forensische kennis en grote behulpzaamheid hebben het eerste hoofdstuk van dit proefschrift naar een hoger niveau gebracht.

Ten derde Ted Bijvoets van politiebureau Kennermerland. Jouw nieuwsgierigheid naar nieuwe technieken werkten zeer aanstekelijk en hebben er voor gezorgd dat ik mijn onderzoek al in een vroeg stadium kon toepassen in de praktijk.

Mijn paranimfen Roy en Martijn, ik kan mij geen mooier duo wensen om mij te laten bijstaan tijdens de komende verdediging. Jullie zijn niet alleen fijne, bevlogen collega's, maar ook goede vrienden geworden. Bijna vier jaar samenwerken hebben mooie herinneringen opgeleverd in Amsterdam, München en Hawaii. It was legendary.

Tot slot, de mensen in mijn omgeving die mij hebben ondersteund. Michiel, om samen een huis te verbouwen, terwijl jij 70 uur in de week werkt en ik mijn proefschrift aan het afronden ben, is geen gemakkelijke klus. Dankzij jouw visie, goede humeur en inzet hebben wij dit niet alleen tot fraai succes gemaakt, maar ook tot een vriendschap voor het leven.

Mijn ouders, Rolf en Wineke en boer en zussen, Ate, Eeuwke, Linde en Annewil wil ik noemen voor hun vertrouwde en vanzelfsprekende manier van steun.

Als laatste, Marjolein, sinds ik jou heb ontmoet, lijkt alles vanzelf te gaan. Bedankt voor heel veel liefde en alle fijne momenten samen.

-Rolf

CURRICULUM VITAE

Rolf Bremmer was born on January 24th 1982 in Nijmegen, The Netherlands. After finishing the Athenaeum in Rotterdam in 2000 he attended Leiden University to study physics. During his study, he followed a traineeship at the Office for Science and Technology at the Netherlands embassy in the United States. His graduation project was measuring the quantum conductance of monatomic gold wires under the influence of oxygen and hydrogen. After his graduation he performed his PhD research at the Academic Medical Center / University of Amsterdam at the Biomedical Engineering & Physics department where he worked on age determination of bloodstains with reflectance spectroscopy. His work was to expand current clinical techniques to forensic applications, which resulted in this thesis. For this work he received the Emerging Forensic Scientist Award from the American Academy of Forensic Sciences in 2011.



